# ODMR of PBQ

Optically Detected Magnetic Resonance of

para-benzoquinone in its lowest $n\pi^*$ triplet state

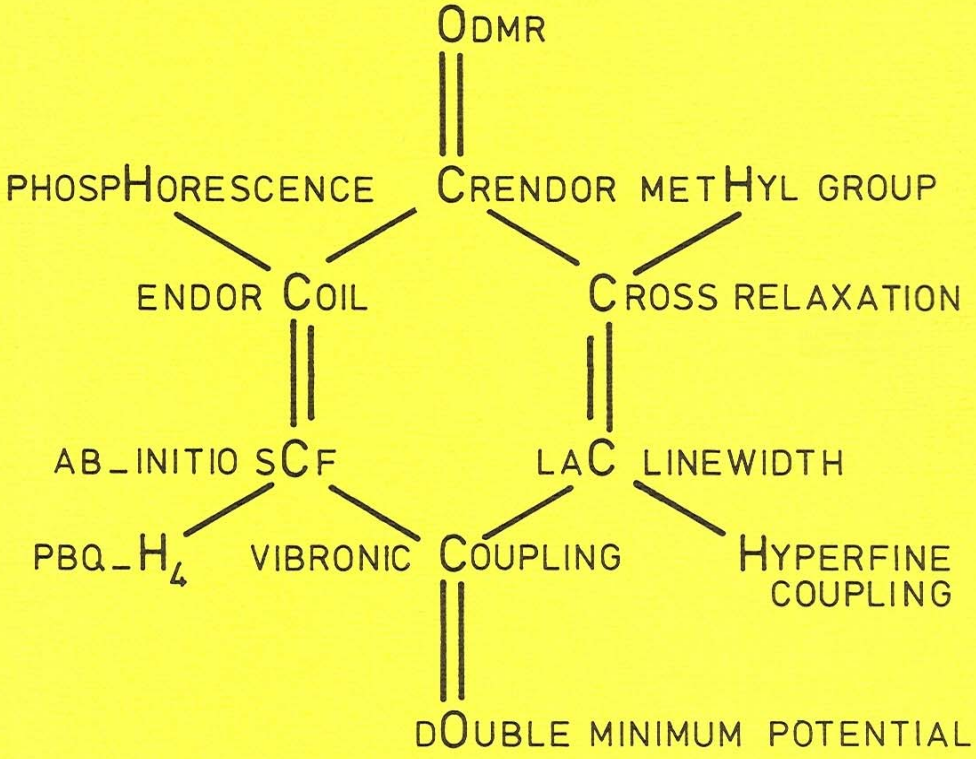


Jan H. Lichtenbelt

RIJKSUNIVERSITEIT GRONINGEN

# ODMR of PBQ

Optically Detected Magnetic Resonance of
para-benzoquinone in its lowest $n\pi^*$ triplet state

proefschrift

ter verkrijging van het doctoraat
in de wiskunde en natuurwetenschappen
aan de Rijksuniversiteit te Groningen
op gezag van de
Rector Magnificus Dr. L.J. Engels
in het openbaar te verdedigen op
vrijdag 13 mei 1983
des namiddags te 2.45 uur precies

door

Jan Hendrik Lichtenbelt
geboren te Utrecht

Promotor : Prof.dr. D.A. Wiersma

Coreferent: Prof.dr. J. Kommandeur

Aan Andrea, Barthold en Frits.

Ter nagedachtenis aan mijn grootvader H.R.Kruyt
in leven hoogleraar in de Fysische Chemie.

"Een proefschrift is een werkstuk van de hand van de promovendus, waarmee deze blijk geeft tot zelfstandig wetenschappelijk onderzoek in staat te zijn".
(artikel 11, Promotie regelement van de Rijks Universiteit te Groningen, 1.9.81)

*Graag wil ik hierbij allen bedanken, die met hun persoonlijke inzet dit promotie onderzoek mogelijk hebben gemaakt. Velen hebben tot het onderzoek en dit proefschrift bijgedragen. Enkelen wil ik hierbij persoonlijk noemen.*
*Allereerst mijn promotor Douwe Wiersma, die uit Amerika terugkwam met een goed promotie onderwerp, wat aansloot bij mijn werkzaamheden op dat moment. Zijn enthousiasme en goede kijk op o.a. de optische metingen, zorgde ervoor dat de grote brei informatie goed en vlot tot een model verwerkt kon worden.*
*Jan Kommandeur had de ondankbare taak mij te helpen bij voorbereidende ruisige ENDOR experimenten. Wat zagen we vaak mooie signalen in die ruis! Dat je als coreferent wilde optreden toen eindelijk de leuke resultaten begonnen te komen, waardeer ik ten zeerste.*
*Studenten Joop Bouman en Ko Roelfsema hielpen mij enorm in het begin van het onderzoek. Jammer genoeg zagen jullie ook geen ENDOR signalen. Toch de ervaringen opgedaan in die tijd maakte dat daarna alles veel vlotter verliep. In de tijd daarna hebben Jan Fremeijer en Bert Benthem hard meegeholpen aan experimenten, die vaak van 's morgens vroeg tot 's avonds laat duurden. Bovendien groeiden jullie alle éénkristallen. De hierbij gebruikte stoffen, met nagenoeg alle mogelijke isotoop kombinaties, werden met zeer veel vakmanschap door Berend Kwant gesynthetiseerd. Geert Geertsema voerde ons idee uit van "Quantum Beats". Misschien werkte het wel, maar zagen we niets!*
*Gerrit van der Velde en Harry Jonkman hadden reeds mooie theoretische berekeningen aan para-benzochinon verricht. Onze prettige samenwerking resulteerde in het opsplitsen van getallen in fysisch interpreteerbare grootheden.*

De metingen bij lage temperatuur geschiedden met een vierdubbele dewar die, met een hoog staaltje van glasblaaskunst, door Piet Lasker werd geblazen en door L.J. van der Holst met technische kennis van zaken werd begeleid. Het verzilveren van deze dewar gaf heel wat problemen en werd zelfs op de vrije zaterdag uitgevoerd door o.a. Aalderik Meulema. Tenslotte heeft Joop Huisman † nog veel mooi en goed werk voor mij verricht o.a. als de dewar weer eens kapot was of, door de koude, lekte.
Voor de ENDOR metingen was veel extra elektronika nodig zoals aktieve nauwbandige filters, fase gevoelige detektoren, coaxkabels enz. Voor al deze problemen wist Bernard van Meurs, op zijn eigen rustige manier, tenslotte een oplossing te vinden. Al mijn huidige kennis van de elektronika heb ik van hem verkegen.
Ik zou bladzijden vol kunnen schrijven over de mooie en nauwkeurige instrumenten die Willem Zevenberg voor mij maakte. In het bijzonder wil ik hier noemen de ESR cavity's die je elektrolytisch groeide met koper om een verzilverde perspex mal. Ook Henk Bruinenberg en Bert van Dammen hielpen vaak mee technische problemen op te lossen.
Door grote warmtelekken in de dewar was ik lange tijd de grootste gebruiker van vloeibaar helium. Ubel Linstra en J.C. Boonstra wil ik hierbij danken voor het feit dat zij zeer rustig en altijd op redelijk korte termijn de gevraagde hoeveelheden vloeibaar helium konden leveren en het teruggeblazen heliumgas konden opvangen.
Naast de experimenten werd er veel gerekend op het Rekencentrum. Hierbij wil ik enkele mensen van het Rekencentrum bedanken voor het menselijk gezicht dat zij gaven aan zo'n doodse machine. L.T. van der Weele voor de vele Algol-problemen ondervonden op de TR4, zelfs op de late avonduren. Kees van der Laan voor het oplossen van de numerieke problemen en de bereidheid zich te verdiepen in gebruikersproblemen. Doeke de Vries had altijd de tijd voor Algol-problemen op de CDC en Jan Kraak veranderde het bewerkelijke PLOTUP en PLOTD voor grafieken in een maakelijk te verwerken KOMPLOT procedure.

Popko Dijkema behield een vaste hand bij de vele tekeningen, die hij voor mij maakte en Klaas Gilissen verzorgde de foto's als we weer eens iets snel klaar moesten hebben, zoals meestal het geval bleek te zijn.
Tenslotte zijn er altijd een aantal mensen die indirekt bijdragen tot dit succes. Frits Elzinga bedankt voor de vele prettige avondjes praten. Ellen Niemeijer-Geers bedankt voor de stimulerende aanzet tot het terugdringen van anticipatie-angst, zodat het leven een stuk prettiger werd. Zie hier het resultaat! Bart Drinkenburg bedankt dat je de laatste tijd tot de promotie zonder meer hebt willen begeleiden, maar ook voor de fijne samenwerking bij de experimenten, die ik op het Technisch Chemisch Laboratorium verrichtte.
Het in begrijpelijk Nederlands formuleren van het promotie-onderwerp vind ik één van de moeilijkste onderdelen. In de samenvatting heb ik tenslotte toch een poging gewaagd. Mijn vrouw Andrea heeft dan ook vaak niet begrepen waarom wij zo laat nog door moeten werken, wat voor problemen daarbij optraden en welke mensen daar wel of niet aan te pas kwamen, om maar niet te spreken wat al die moeilijke vaktermen betekenden. Daarom Andrea, hartelijk dank voor het geduld dat je had en het vertrouwen dat jij mij gaf, waardoor de afronding van dit proefschrift mogelijk werd.

CONTENTS

With permission of the North-Holland Publishing Company, Amsterdam, the following articles are included in this thesis:

Chem. Phys., 10 (1975) 107 - Chapter 3.
Chem. Phys., 18 (1976) 93 - Chapter 4.
Chem. Phys., 22 (1977) 297 - Chapter 5.
Chem. Phys., 29 (1978) 367 - Chapter 7.
Chem. Phys., 34 (1978) 47 - Chapter 6.
Chem. Phys., 39 (1979) 37 - Chapter 8.

# CHAPTER 1 INTRODUCTION AND SUMMARY

Many interesting optical measurements [1-9] were made in the past two decennia on the aromatic diketone p-benzoquinone PBQ (fig. 1). By a symmetric and asymmetric combination of the two n-orbitals in PBQ there are two electronic $n\pi^*$ states with $B_{1g}$- and $A_u$-symmetry (with $D_{2h}$ symmetry for PBQ). Trommsdorff [2] was the first to propose that the lower $n\pi^*$ (singlet) states in PBQ crystals, contrary to the accepted view at that time [3], were near-degenerate. There are nowadays two different interpretations of the observed close lying states of opposite parity.

The first one is proposed by Dunn and Francis [4] and more recently by Goodman and Brus [5]. They interpret the two states to be purely electronic without any interacting nuclear motion. The fact that the electronic levels are close ($\lesssim 20\ cm^{-1}$) is caused by the localized nature of the $n\pi^*$ excitations.

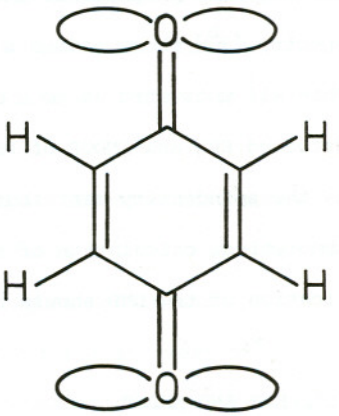


*Fig. 1. p-Benzoquinone*

The second interpretation was proposed by Hochstrasser et al. [6] and independently by Veenvliet and Wiersma [7]. They include a vibronic coupling between the two electronic $B_{1g}$ and $A_u$ $n\pi^*$ (triplet) states. This coupling is so strong that the potential energy surface of the lowest $B_{1g}$ state contains a double minimum potential (DMP) well along a $b_{1u}$ type nuclear motion. Such a DMP can be shown to be formed under conditions where the electronic and nuclear motion are strongly correlated [8]. The g- and u-vibronic inversion states of the DMP of the lowest $n\pi^*$ $B_{1g}$ state have $B_{1g}$- and a little higher in energy ($\lesssim 20\ cm^{-1}$),

$A_u$-symmetry.

Merienne-Lafore and Trommsdorff [9] performed a theoretical calculation which showed that for the description of the two nearly degenerate $n\pi^*$ $B_{1g}$ and $A_u$ states the molecule could approximately be considered as a dimer. Ter Horst et al. [10] confirmed this recently with a supersonic jet experiment.

In this vibronic picture a small symmetry disturbance, by e.g. asymmetric isotope substitution, will have a large influence on the DMP. It will be accompanied with a relative large change in the optical spectra [1-10] and the magnetic properties. The Optically Detected Magnetic Resonance (ODMR) spectra [7b] shows indeed a large isotope dependence.

This all motivated us to a detailed magnetic resonance study, like optically detected EPR and ENDOR of PBQ in its lowest $n\pi^*$ triplet state, which gives us the spindensity distribution in this state. In combination with a theoretical calculation of the ab-initio molecular orbitals further identification of the DMP should be possible.

## 1.1. EPR AND ENDOR

Isotopic species of PBQ like: PBQ-$h_4$, -$dh_3$, -2,6 $d_2h_2$, -$d_3h$, -$CH_3$, -$^{13}C$ and -$^{17}O$ using PBQ-$d_4$ as a host crystal were used in the study of the zero-point (g-inversion) level of the lowest triplet state in PBQ at 1.8 K. Primarily the optically detected EPR and ENDOR of the protons and $^{13}C$ were performed. The EPR shows the zero field splitting- or fine structure parameter D to be very sensititve to deuterium and $^{13}C$ isotope substitution but *not* to $^{17}O$- or $^{18}O$-substitutions. Our interpretation of this isotope effect is that the oxygen atom is at rest in the $b_{1u}$ mode that vibronically mixes the near

degenerate $n\pi^*$ triplet states. This is in contrast with the assumptions of an asymmetric C=O $b_{1u}$ vibronic mode proposed by other authors [7,10].
At 4.2 K a second, larger fine structure parameter D was determined from the EPR spectra. This could be from the other $A_u$ inversion level. This was confirmed by optical experiments by Veenvliet and Wiersma [7] and lateron by rotary spin echo experiments by van 't Hof and Schmidt [11].
The crystal site has $C_i$ inversion symmetry and the proton- and $^{13}C$-ENDOR experiments showed that the $n\pi^*$ triplet state of PBQ-$h_4$ as guest in PBQ-$d_4$ has a *chairform* with the carbonyl group in the crystal cleavage plane.
V. Bolhuis and Kiers [12] improved the earlier crystal structure measurements [13] at 77 K and showed the ground state structure to be a chair form too. Such a chair form was not found in the $n\pi^*$ singlet state as studied in a supersonic beam by Ter Horst et al. [10].
The ENDOR data of the isotope- and $CH_3$-substitutions in PBQ show that mono-substitution leaves the $C_{2v}$ symmetry of the unsubstituted half of the molecule virutally intact. This favours the hypothesis of Merienne-Lafore and Trommsdorff [9] that PBQ may be considered as a dimer for its lowest $n\pi^*$ singlet and triplet states. The hyperfine data, in combination with ab-initio calculations, can be explained by assuming a slight "localization" of the $n\pi^*$ excitation on the oxygen at the substituted fragment.

## 1.2. HYPERFINE CALCULATIONS

The calculated ab-initio molecular orbitals [14] for the unpaired n- and $\pi$-orbitals yield hyperfine interaction constants that compare very nicely with the experimentally observed ones. These ab-initio results were further

analyzed in terms of atomic contributions which give insight into the limitations of the semi-empirical analysis of the ENDOR data. Especially the different spin distribution of the n- and π-orbitals will lead to different atomic interaction constants for the anisotropic hyperfine interaction for e.g. oxygen and carbon of the carbonyl group in PBQ.

The semi-empirical calculation of the isotropic proton hyperfine data, however, fails completely. It lacks completely the large (extra) contribution of the neighbouring carbon 2s orbital.

The π-unpaired electron is almost equally divided among the carbonyl groups and the central ring system in contrast with the unpaired n-electron density which is largely confined (75%) to the oxygen atoms.

### 1.3. CRENDOR

A high degree of nuclear spin polarization can be achieved at a magnetic field where cross-relaxation occurs between a triplet excited PBQ molecule and a doublet spin system (which is photochemically induced). By a radio frequency this polarization can induce a phosphorescence change which we call Cross RElaxation Nuclear Double Resonance (CRENDOR).

In principle this, newly found, phenomenon gives the same information as the "high field" ENDOR experiments except that the CRENDOR is detected at lower magnetic fields and also possible from a different electronic state (e.g. $m_s = -1$ for ENDOR and $m_s = +1$ for CRENDOR).

For some crystal orientations detection of the ENDOR signal was not possible because of a too low signal to noise ratio but, by the larger polarization, CRENDOR detection was still possible. This made a better inter- and extra-

polation possible of the hyperfine data at crystal orientations where neither ENDOR nor CRENDOR was possible.

## 1.4. LAC

The level-anti-crossing (LAC) of the lowest $n\pi^*$ triplet state of PBQ only shows a broad line. This is the result of a combination of a number of LAC's of the mixing of electronic-nuclear states through the hyperfine interaction and/or magnetig field misorientations.
A combination of a low frequency EPR (up to 100 MHz) and a prediction of the LAC signal, by an exact calculation with the known (hyper-)fine structure parameters, shows a disorder of $0.9^{\circ}$ of the PBQ's of the molecular plane.

## 1.5. METHYL TUNNELING ROTATION

In experiments on toluquinone (TOL, which is a mono methyl substituted PBQ) a methyl tunneling rotation is seen in the ENDOR experiments. This phenomenon was previously extensively studied in doublet radicals with methyl groups by Clough et al. [15].
A tunneling frequency 3J of 2.9 GHz was derived from the TOL ENDOR spectra, corresponding to a torsional oscillator barrier of 2.77 kJ/mol, which shows that rotation of the methyl group at 1.8 K is strongly hindered.
A special optically detected triplet methylgroup tunneling phenomenon are the LAC side bands which are interpreted by a cross-relaxation between the lowest rotational $|A\rangle$ states with the higher $|E\rangle$ states (with local methyl $C_3$ symmetry) of translationally equivalent molecules.

## 1.6. MAGNETIC RESONANCE THEORY AND EXPERIMENTAL

To complete this thesis an extended chapter on magnetic resonance theory is given. Exact equations for the triplet EPR-, LAC- and cross relaxation are derived. First order- and exact calculations of ENDOR- and CRENDOR transitions are given. And the $24^{th}$ order spin hamiltonian matrix of the methyl group rotation in the tiplet system is derived. This hamiltonian is used for the second order perturbation energies from which the tunneling frequency 3J and the methyl group hyperfine data are derived.

In the experimental part, the NMR coil impedance matching conditions are theoretically derived for the frequency dependent ENDOR experiments. This leads to the conclusion, after all, that the best way to confirm ENDOR experiments is to use a few-winding-coil and a resistance in serie with an impedance equal to the impedance of the power amplifier. A new detail is that the length of the coaxial cables used *has to* be changed outside a special frequency range to avoid to much power reflections, and to optimize NMR field strength.

## 1.7. CONCLUSION

The optically detected EPR data of para-benzoquinone (PBQ) in its lowest $n\pi^*$ triplet state at 1.8 K showed the fine structure parameter D to be very sensitive to mild substitutions, but insensitive to $^{17}O$- or $^{18}O$-substitutions. This shows that the $b_{1u}$ vibronic coupling mode, which mixes the near degenerate $n\pi^*$ triplet states is not the asymmetric carbonyl mode, but more

likely one of the four other (mixed) $b_{1u}$ modes.

The ENDOR data of PBQ showed that a mild substitution leaves the $C_{2v}$ symmetry at the unsubstituted half of the molecule intact, which favours the dimer or Double Minimum Potential (DMP) model of PBQ.

Hyperfine constants calculated by ab-initio are comparable with the experimental ENDOR hyperfine constants and showed the $\pi^*$-unpaird electron to be spread over the molecule, while the unpaired n-electron is largely localized on the oxygen atoms.

The newly discoverd Cross RElaxation Double Resonance (CRENDOR) technique makes the inversion of an electronic into nuclear polarization possible, by a cross relaxation between a triplet and a doublet system. This electronic polarization enlarges the sensitivity of the optically detected nuclear transition. And this results in an improvement of the ENDOR data.

The low frequency EPR near the Level Anti Cross (LAC) signal exhibits a lineform which could be simulated by assuming a disorder of $0.9^{\circ}$ in the tilt of the PBQ molecular planes.

The relatively strong dependence of the EPR and ENDOR spectra on mild substitutions favour the interpretation of the DMP of the lowest $n\pi^*$ $B_{1g}$ triplet state of PBQ as guest in PBQ-$d_4$ at 1.8 K. The final conclusion is that the magnetic resonance data in the lowest $n\pi^*$ triplet state in PBQ favour the interpretation of this level as a vibronic strongly pertubated state.

## 1.8. REFERENCES


1. J.M. Hollas, Spectrochim. Acta 20 (1964) 1563.

   J.W. Sisman, J. Am. Chem. Soc. 78 (1956) 2363.

   J.W. Sidman, J. Chem. Phys. 27 (1957) 820.

2. H.P. Trommsdorff, Chem. Phys. Lett. 10 (1971) 176.

3. D.O. Cowan, R. Gleiter, J.A. Hahsmall, E. Heibronner and V. Hornung, Angew. Chemie 83 (1971) 405.

4. T.M. Dunn and A.H. Francis, J. Mol. Spectry. 50 (1974) 14.

5. J. Goodman and L.E. Brus, J. Chem. Phys. 69 (1978) 1604.

6. R.M. Hochstrasser, L.W. Johnson and H.P. Trommsdorff, Chem. Phys. Lett. 21 (1973) 251.

7. H. Veenvliet and D.A. Wiersma, Chem. Phys. 2 (1973) 69.
H. Veenvliet and D.A. Wiersma, Chem. Phys. Lett. 22 (1973) 87.
H. Veenvliet and D.A. Wiersma, Chem. Phys. 8 (1975) 432.

8. G. Herzberg and E. Teller, Z. Physik. Chemie B21 (1933) 410.

9. M.F. Merienne-Lafore and H.P. Trommsdorff, J. Chem. Phys. 64 (1976) 3791.

10. G. ter Horst and J. Kommandeur, Chem Phys. 44 (1979) 278
G. ter Horst, J. Kommandeur and D.A. Wiersma, to be published.

11. C.A. van 't Hof and J. Schmidt, Chem Phys. Lett. 36 (1975) 457.
C.A. van 't Hof and J. Schmidt, Chem Phys. Lett. 36 (1975) 460.
C.A. van 't Hof and J. Schmidt, Chem Phys. Lett. 42 (1976) 73.

12. F. van Bolhuis and C.T. Kiers, Acta Cryst. 34B (1978) 1015.

13. J. Trotter, Acta Cryst. 13 (1960) 86.

14. H.T. Jonkman, Thesis, University of Groningen (1975).
H.T. Jonkman, G.A. van der Velde and W.C. Nieuwpoort, Quantum Chemistry The State of the Art, Proceedings of S.C.R. Atlas Symposium, 4 (1974) 245.

15. S. Clough and F. Poldy, J. Chem. Phys. 51 (1969) 2076.
S. Clough, J. Hill and F. Poldy, J. Phys. C.: Solid State Phys. 5 (1972) 518.
S. Clough and F. Poldy, J. Phys. C: Solid State Phys. 6 (1973) 1953.

CHAPTER 2

# THEORY OF OPTICALLY DETECTED MAGNETIC RESONANCE SPECTRA

## 1. INTRODUCTION

The theory of optically detected magnetic resonance (ODMR) for an organic molecule in its lowest excited triplet state, is summarized in this chapter. Also short derivations of some equations are given for the interpretation of angular dependent EPR, -ENDOR, -cross-relaxation (CR), -cross-relaxation-nuclear-double-resonance (CRENDOR) and level-anti-cross (LAC) spectra of p-benzoquinone (PBQ) and toluquinone (TQ).

The functions, operators and hamiltonian adapted to the local $C_3$ symmetry of a hindered rotated methyl group in TQ are given, which forms the background of the equations given in the chapter on this subject.

The hamiltonian of a system of a paramagnetic center with electron spin S and nuclei with nuclear spins $I^i$ is:

$$\mathcal{H} = \beta\, \underline{H}.\underline{\underline{g}}.\underline{S} + \underline{S}.\underline{\underline{D}}.\underline{S} + \sum_i \left( \underline{S}.\underline{\underline{A}}^i.\underline{I}^i - \beta_N\, \underline{H}.\underline{\underline{g}}_N.\underline{I}^i + \sum_j \underline{I}^i.\underline{\underline{Q}}^{ij}.\underline{I}^j \right) \qquad (1)$$

$$\mathcal{H} = \mathcal{H}_1 + \mathcal{H}_2 + \mathcal{H}_3 + \mathcal{H}_4 + \mathcal{H}_5$$

with the usual meaning [1] of the electron Zeeman interaction $\mathcal{H}_1$, fine-structure interaction $\mathcal{H}_2$, hyperfine structure interaction $\mathcal{H}_3$, nuclear Zeeman interaction $\mathcal{H}_4$ and nuclear dipole-dipole and quadrupole interaction $\mathcal{H}_5$.

To calculate EPR and ENDOR transition frequencies for an organic molecule in its (lowest $n\pi^*$) triplet state, some simplifications of the hamiltonian are allowed. First we neglect the nuclear-nuclear interaction $\mathcal{H}_5$, because the quadrupole and/or dipole-dipole interactions are zero or small compared to all other terms and will be mostly smaller than the ENDOR linewidth of 10-50 kHz.

In all other cases the influence of the quantisation direction of one nuclear spin on all other will be small so we can consider each nucleus by itself and the summation over the nuclei in equation (1) can be ignored. The nuclear $\underline{\underline{g}}_N$ tensor will be assumed to be isotropic. The simplified EPR- and ENDOR hamiltonians therefore reduce to:

$$\mathcal{H}_{EPR} = \beta\, \underline{H}.\underline{\underline{g}}.\underline{S} + \underline{S}.\underline{\underline{D}}.\underline{S} \qquad (2a)$$

$$\mathcal{H}_{ENDOR} = \underline{S}.\underline{\underline{A}}.\underline{I} - \beta_N g_N\, \underline{H}.\underline{I} \qquad (2b)$$

With in general the $\underline{\underline{g}}$- and $\underline{\underline{A}}$-tensors being asymmetric [2] and the $\underline{\underline{D}}$-tensor symmetric [1].

To find the hyperfine tensor from the ENDOR data (given in section 3) the $\underline{\underline{g}}$- and $\underline{\underline{D}}$-tensors first have to be extracted from EPR experiments (given in section 2). Finally in section 4 the $C_3$-group adapted nuclear interactions are given for a hindered rotating methyl group.

## 2. THE ELECTRONIC TRIPLET SYSTEM

### 2.1. EPR THEORY

Because the fine structure interaction ($\mathcal{H}_2$) will be of the same order as the electron Zeeman interaction ($\mathcal{H}_1$) in X-band EPR experiments for organic molecul in their lowest excited triplet state, we have to solve the Schrödinger equatio for the triplet system exactly, as done e.g. by Kottis [3].

For e.g. the zero-field functions $|T_x\rangle$, $|T'_y\rangle$ and $|T_z\rangle$ (with $|T'_y\rangle = \frac{1}{2}\sqrt{2}(|\alpha\alpha\rangle + |\beta\beta\rangle$ see also the appendix) the hamiltonian matrix is:

$$\begin{array}{c} \\ \langle T_x| \\ \langle T'_y| \\ \langle T_z| \end{array} \begin{array}{c} \begin{array}{ccc} |T_x\rangle & |T'_y\rangle & |T_z\rangle \end{array} \\ \begin{pmatrix} X & -H'_z & iH'_y \\ -H'_z & Y & -iH'_x \\ -iH'_y & iH'_x & Z \end{pmatrix} \end{array} \qquad (3)$$

with $\underline{H}' = \beta\, \underline{H}.\underline{\underline{g}}$ and $\underline{H} = H\, \underline{l}$ where $\underline{l}$ is the unit vector with respect to the z-axis and $X = -D_{xx}$ , $Y = -D_{yy}$ and $Z = -D_{zz}$ the eigenvalues of the fine-structure $\underline{\underline{D}}'$-tensor. Note $\underline{\underline{D}}' = -\underline{\underline{D}}$.

The secular equation gives:

$$E^3 - M.E + N = 0 \qquad (4a)$$

with $M \equiv (\beta^2H^2)g^2 - A$ and $N \equiv (\beta^2H^2)D'' - B$ where $g \equiv \sqrt{\underline{l}^T.\underline{\underline{g}}.\underline{\underline{g}}^T.\underline{l}}$ , $A \equiv XY + XZ + YZ$, $D'' \equiv \underline{l}^T.\underline{\underline{g}}.\underline{\underline{D}}'.\underline{\underline{g}}^T.\underline{l}$ and $B \equiv XYZ$. The eigenvalues are found by substitution:

$$E = E_0 \cos[\tfrac{1}{3}(\varphi + 2n\pi)] \quad \text{with} \quad E_0 = 2\sqrt{(M/3)} \ , \quad \cos\varphi = -\frac{N}{2}\sqrt{(3/M)^3} \qquad (4b)$$

$$\text{and} \quad n = 1,2 \text{ or } 3.$$

More important in an EPR experiment is the resonance magnetic field at which the energy difference between two states is equal to the EPR energy $\delta \equiv h\nu = \Delta E$. After some rearrangements a cubic equation in $(\beta^2H^2)$ is found which gives us the two $\Delta m_s = 1$ and one $\Delta m_s = 2$ resonance magnetic fields:

$$4\, g^6\, (\beta^2H^2)^3 - 3[g^4(4A + 3\delta^2) + 9D''^2](\beta^2H^2)^2 + 3[g^2(4A + 2\delta^2)(A + \delta^2) + 18BD''] \beta^2H^2 - [(4A + \delta^2)(A + \delta^2)^2 + 27B^2] = 0 \qquad (5)$$

By rotation of the molecule in three (nearly) perpendicular planes the $\underline{\underline{g}}$- and $\underline{\underline{D}}$-tensors can be found by a least square fitting procedure of the transition frequencies.

When the principal axes of the $\underline{\underline{g}}$- and $\underline{\underline{D}}$-tensor *coincide* it can be shown that the angular dependent elements g and D'' of equation (5) can always be written as a function of the square elements $l_x^2$, $l_y^2$ and $l_z^2$ (in a special coordinate system). This means that in each rotation plane there will be a principal axis with a *symmetrical* angular magnetic field dependence. Thus the angular dependence function (even *or* arbitrary) in a rotation plane shows us whether the $\underline{\underline{g}}$- and $\underline{\underline{D}}$-tensors coincide or not. If they do and with the magnetic field exactly

parallel to a principal fine-structure axis, then it is possible to derive an analytical equation for the magnetic field as a function of the principal tensor element(s).

For $\underline{H}'$ parallel to the dipolar z-axis [3], only a 2x2 matrix of the hamiltonian of equation (3) has to be diagonalised. By solving the quadratic equation *or* by a rotation of $45^{\circ}-\theta$ the eigenvalues are found to be:

$$E_0 = Z \tag{6a}$$

$$E_{\pm} = \tfrac{1}{2}\sqrt{4H_z'^2 + (X-Y)^2} - \tfrac{1}{2}Z \tag{6b}$$

$$\text{or} \quad E_{\pm} = \pm[H_z' + \tfrac{1}{2}(X-Y)\,tg\theta] - \tfrac{1}{2}Z \tag{6c}$$

The off-diagonal elements after rotation have to be zero, so $tg\,2\theta = (X-Y)/2H_z'$. For $\theta = 0^{\circ}$ the zero field functions $|T_x\rangle, |T_y'\rangle$ and $|T_z\rangle$ are rotated to the high field functions $|1\rangle, |0\rangle$ and $|-1\rangle$. So $tg\theta$ is the quotient of the mixing coefficients of the $|1\rangle$ and $|-1\rangle$ states. The reason for the use of the rotation is that in the equations derived, the terms with $\theta$ form the exact corrections with respect to the "high" field first order terms. For nearly $|m_s\rangle$ states is: $tg\theta \approx \tfrac{1}{2}tg2\theta = (X-Y)/4H_z'$.

The $\Delta m_s = 1$ transition resonance fields are exact:

$$H'_{z\pm} = \sqrt{(\delta \pm \frac{3}{2}Z)^2 - \tfrac{1}{4}(X-Y)^2} \tag{7a}$$

$$= \delta \pm \frac{3}{2}Z - \tfrac{1}{2}(X-Y)\,tg\theta_{\pm} \tag{7b}$$

When the principal axes of the $\underline{g}$- and $\underline{D}$-tensor coincide, the sum and the difference of the two magnetic resonance fields give us respectively the principal values $g_{zz}$ and $|Z|$ (for $\delta > 2|D|$):

$$g_{zz} = \frac{2h\nu}{\beta(H_{z+} + H_{z-})} - \frac{(X-Y)(tg\theta_+ + tg\theta_-)}{2\,\beta(H_{z+} + H_{z-})} \tag{8a}$$

$$\text{and} \quad |Z| = \left|\frac{1}{3}\beta\, g_{zz}\,(H_{z-} - H_{z+}) + \frac{1}{6}(X-Y)(tg\theta_+ - tg\theta_-)\right| \tag{8b}$$

The second correction terms in the equations (8) are always *negative*.

For the EPR field $H_1$ exactly perpendicular to the permanent magnetic field H *and* H parallel to a fine-structure axis, the $\Delta m_s = 2$ transition is not allowed. The resonance field can be found by interpolation in an angular dependent measurement or in an experiment with $H_1 // H$. This field gives us some extra information about the other dipolar principal values $|X-Y|$:

$$H'_z = \tfrac{1}{2}h\nu - \tfrac{1}{2}(X-Y)\ tg\theta \qquad (8c)$$

The calculated value of $|X-Y|$ however will relatively be sensitive to small errors in the measurements. Note that the second correction term in equation (8c) will always be negative.

## 2.2. LEVEL-(ANTI)-CROSSING

For the magnetic field parallel to the dipolar z-axis level crossing (LC) is possible. When the energies of equation (6a) and (6b) are equal the states $|\psi_a\rangle$ and $|\psi_b\rangle$ will cross at the magnetic field strength $H'_z$:

$$|\psi_a\rangle = |T_z\rangle \qquad (9a)$$

$$|\psi_b\rangle = \sqrt{\frac{Z-Y}{3Z}}\,|T_x\rangle + \mathrm{sign}(D.E)\sqrt{\frac{Z-X}{3Z}}\,|T_y\rangle \qquad (9b)$$

and $$H'_z = \sqrt{(Z-X)(Z-Y)} \qquad (10)$$

For D.E <0 or >0 there will be another LC for the magnetic field parallel to respectively the fine-structure x- or y-axis.

This LC mixes two states [4], which can manifest itself in a change in the phosphorescence from the excited triplet state [5] or by the optical nuclear spin polarization (ONP) of the ground state [6]. However, by a very small rotation [5] ($10^{-5}$ degrees) the LC is changed into a level-anti-crossing (LAC) by mixing the states by the off-diagonal Zeeman elements $H'_x$ and/or $H'_y$. Also a hyperfine interaction will change the LC in a LAC *even* for the magnetic field direction *exactly* parallel to the principal axis [5,6].

## 2.3. CROSS-RELAXATION BETWEEN A TRIPLET- AND DOUBLET SYSTEM

Cross-relaxation (CR) between an electronic triplet- and doublet system can occur when the energy differences in both systems are equal so energy exchange is possible while the total energy remains constant [5,7].

The CR magnetic field is found by substitution in equation (5) for the triplet energy difference $\delta_{triplet} = \beta\, g_{doublet} \cdot \underline{H}$ . This gives us a cubic equation in $(\beta^2 H^2)$:

$$(\beta^2H^2)^3\,(4g_t^2 - g_d^2)(g_t^2 - g_d^2)^2 - (\beta^2H^2)^2\,3[A(4g_t^2 - 2g_d^2)(g_t^2 - g_d^2) + 9D''^2] +$$
$$(\beta^2H^2)\,3[A^2(4g_t^2 - 3g_d^2) + 18BD''] - [4A^3 + 27B^2] = 0 \qquad (11)$$

with index t=triplet and d=doublet and g,A,B and D" defined as in equation (4a). For $g_t \approx g_d$ there is one solution at very high magnetic field (with $H \rightarrow \infty$ for $g_t \rightarrow g_d$), one solution at a low magnetic field ($\approx$ 0-1000 Gauss) and one imaginary solution.

## 2.4. CROSS-RELAXATION BETWEEN TRIPLET SYSTEMS

Energy exchange between two translationally *equivalent* triplet molecules is e.g. possible at the same magnetic field as the LAC occurs, for e.g. D<0 between the states $|0\rangle \leftrightarrow |-1\rangle$ and $|1\rangle \leftrightarrow |-1\rangle$.

There is another CR between translationally *equivalent* triplet molecules possible. For H//z-axis this will occur at:

$$H'_z = \sqrt{XY} = \sqrt{\tfrac{1}{9}D^2 - E^2} \qquad (12)$$

For other magnetic field directions and for CR between translationally *inequivalent* molecules no analytical solution can be derived and only a "trial and error" method can be used to calculate the magnetic field strengths at which CR's occur.

## 3. HYPERFINE INTERACTIONS

### 3.1. ENDOR

To calculate the nuclear energy levels, it is necessary to know the quantisation direction of the nuclear spin operator I in the hamiltonian of equation (2b). Through the hyperfine interaction(s), this direction will depend on the quantisation of the electron spin S. If we assume as a first order approximation that the quantisation direction of S does *not* depend on that of I, then the energies will be:

$$E = E_{EPR} + |\langle \underline{S} \rangle . \underline{\underline{A}} - g_N \beta_N \underline{H}| \langle I'_z \rangle \qquad (13)$$

with $E_{EPR}$ given in section 2 and $\langle I'_z \rangle = m_I$.

In the case of relatively large hyperfine interactions the second order terms like $I_x S_y$ etc. are responsible for a change in the energy, which are given in the next section 3.2.

The *first* order ENDOR frequencies are derived from equation (13):

$$\nu_{ENDOR} = \sqrt{\sum_{i=x,y,z} (\langle S_x \rangle A_{xi} + \langle S_y \rangle A_{yi} + \langle S_z \rangle A_{zi} - l_i \nu_N)^2} \qquad (14)$$

with $A_{ij}$ in frequency units and $A_{ij} \neq A_{ji}$ by spin-orbit coupling [1]. This asymmetry can easily be shown by writting $\underline{S}.\underline{\underline{A}}.\underline{I} = \beta_e \beta_N \, \underline{S}.\underline{\underline{g}}_e.\underline{\underline{A}}'.\underline{\underline{g}}_N.\underline{I} + A_{iso} \underline{S}.\underline{I}$ with $\underline{\underline{A}}'$ the pure "radial" tensor. The product of the three tensors gives in general an asymmetric $\underline{\underline{A}}$-tensor. For organic molecules and special for PBQ and TQ, the $\underline{\underline{g}}_e$- and $\underline{\underline{g}}_N$-tensors are (nearly) isotropic, so we assume further the hyperfine tensor $\underline{\underline{A}}$ to be symmetric.

In equation (14) the free nuclear frequency is $\nu_N = g_N \beta_N \, H/h = 2\pi \gamma H$. The expectation values $\langle S_i \rangle$ are in the "high field" limit:

$$\langle S_x \rangle = l_x m_s \quad , \quad \langle S_y \rangle = l_y m_s \quad \text{and} \quad \langle S_z \rangle = l_z m_s \qquad (15)$$

The expectation values for a general magnetic field direction are calculated after diagonalisation of the EPR hamiltonian of equation (2a), from the eigenvectors by the equations:

$$\left.\begin{aligned} \langle S_x\rangle &= \tfrac{1}{2}\sqrt{2}\,[(C_1+C_{-1})\,C_0^* + C_0(C_1^*+C_{-1}^*)] \\ \langle S_y\rangle &= \tfrac{i}{2}\sqrt{2}\,[(C_1-C_{-1})\,C_0^* - C_0(C_1^*-C_{-1}^*)] \\ \langle S_z\rangle &= C_1\,C_1^* - C_{-1}C_{-1}^* \end{aligned}\right\} \text{ for } |m_s\rangle \text{ start-functions} \qquad (16$$

or:

$$\langle S_x\rangle = i\,(C_y\,C_z^* - C_z\,C_y^*) \text{ and cyclic permutations} \qquad (17)$$

for pure zero-field start-functions $|T_x\rangle$, $|T_y\rangle$ and $|T_z\rangle$.

By an angular dependent ENDOR experiment in three (nearly) perpendicular planes the hyperfine tensor can be determined by a least square fitting procedure. Although the ENDOR frequencies in *each* plane depend on *all* hyperfine elements, they will e.g. in the xy-plane, mainly depend on $A_{xx}$, $A_{yy}$ and $A_{xy}$.

In contrast with the EPR magnetic field dependence, the ENDOR frequency as a function of the rotation angle will *not* be symmetric with respect to any principal axis. The sign of the rotation angle has therefore to be determined in an unique way. This can be done by:

1) Performing all experiments using *one* crystal.
2) Using the asymmetric EPR angular dependence of one molecule, in the case that the $\underline{g}$- and $\underline{D}$-tensors do not coincide.
3) Using the asymmetric EPR angular dependence of two translationally *inequivalent* molecules in the case of $\underline{g}$- and $\underline{D}$-tensors which coincide.

In all these cases it is possible to distinguish between left- and right handed rotation. Consult also reference 8.

### 3.2. CRENDOR

The cross-relaxation nuclear double resonance (CRENDOR) can be detected by a change of the phosphorescence of the CR of a triplet- and doublet system,

introducted by a nuclear transition. The CRENDOR frequency is, in principle, the same as the ENDOR frequency, except that in general the CR magnetic fields are much lower than the EPR magnetic fields. At this CR field the quantisation direction of the proton nuclear spin has an influence on the quantisation direction of the electron spin. It is possible to derive second order corrections for CRENDOR frequencies in the same way as was done for the ENDOR frequencies (e.g. [9 through 13]). In practice a better way is to fit the experimental CRENDOR frequencies to the calculated nuclear transition frequencies, found by a diagonalisation of the total hamiltonian, by changing (some of) the hyperfine elements.

The easiest, *general* way to find the hamiltonian matrix is to expand the electron- and nuclear functionspace to the total interaction space by a direct product method, very nicely described by Poole and Farach [14].

So e.g. for the electronic triplet system and one proton, the nuclear spin matrices are equal to the Pauli matrices:

$$\underline{\underline{I}}_x = \tfrac{1}{2}\begin{pmatrix} 0 & 1 \\ 1 & 0 \end{pmatrix}, \qquad \underline{\underline{I}}_y = \tfrac{1}{2}\begin{pmatrix} 0 & -i \\ i & 0 \end{pmatrix} \qquad \text{and} \qquad \underline{\underline{I}}_z = \tfrac{1}{2}\begin{pmatrix} 1 & 0 \\ 0 & -1 \end{pmatrix} \qquad (18)$$

and the electron spin matrices are:

$$\underline{\underline{S}}_x = \tfrac{1}{2}\sqrt{2}\begin{pmatrix} 0 & 1 & 0 \\ 1 & 0 & 1 \\ 0 & 1 & 0 \end{pmatrix}, \quad \underline{\underline{S}}_y = \tfrac{1}{2}\sqrt{2}\begin{pmatrix} 0 & -i & 0 \\ i & 0 & -i \\ 0 & i & 0 \end{pmatrix} \quad \text{and} \quad \underline{\underline{S}}_z = \begin{pmatrix} 1 & 0 & 0 \\ 0 & 0 & 0 \\ 0 & 0 & -1 \end{pmatrix} \qquad (19)$$

These last equations (19) can be found by a direct product of two Pauli matrices and followed by a "rotation" to the appropiate function space (from $|\alpha\alpha\rangle, |\beta\beta\rangle, |\alpha\beta\rangle$ and $|\beta\alpha\rangle$ to $|\alpha\alpha\rangle, |\beta\beta\rangle, \tfrac{1}{2}\sqrt{2}(|\alpha\beta\rangle+|\beta\alpha\rangle)$ and $\tfrac{1}{2}\sqrt{2}(|\alpha\beta\rangle-|\beta\alpha\rangle)$). All other spin matrices can be found by matrix summation and multiplication.

If the interaction is e.g. a pure electron spin interaction, the direct product with the *unit* nuclear spin matrix has to be executed. E.g. $H'_x \; \underline{\underline{S}}_x \otimes \underline{\underline{U}}_N$ with

$\underline{\underline{U}}_N = \begin{pmatrix} 1 & 0 \\ 0 & 1 \end{pmatrix}$ or for a pure nuclear spin interaction: $-g_N\beta_N H_y \underline{\underline{U}}_E \otimes \underline{\underline{I}}_y$ with

$\underline{\underline{U}}_E = \begin{pmatrix} 1 & 0 & 0 \\ 0 & 1 & 0 \\ 0 & 0 & 1 \end{pmatrix}$ .

The hamiltonian of equation (1) forms the basis of the direct product equation of the electron spin matrices $\underline{\underline{S}}_{x,y,z}$ and the nuclear spin matrices $\underline{\underline{I}}_{x,y,z}$ with their connected interaction sizes. The result gives us the total hamiltonian matrix. In our example of S= 1 and I= ½, this hamiltonian will be of the $6^{th}$ order. A computer program was written for the total hamiltonian matrix of equation (1) for the interaction of an electron spin S with more nuclear spins $I_i$ including the quadrupole and/or nuclear dipole-dipole interaction hamiltonian matrix $\mathcal{H}_5$ [15].

The sign of the hyperfine elements can be determined easily for an electronic triplet system in contrast with a doublet system. Let us assume a first order treatment to be allowed for H//z-axis and $|A_{zz}| < \nu_N$. In this case the ENDOR frequency is: $\nu_{ENDOR} = \nu_N - m_s A_{zz}$. For a doublet EPR transition $\langle -½ | \leftrightarrow | ½ \rangle$ there are always two ENDOR frequencies at $\pm ½ A_{zz}$ around $\nu_N$, *independent* of the sign of $A_{zz}$! In a triplet system however there are two EPR transitions possible. One $\langle -1 | \leftrightarrow | 0 \rangle$ , which gives two ENDOR frequencies $\nu_N$ and $\nu_N + A_{zz}$ which will be $< \nu_N$ or $> \nu_N$ *depending* on the sign of $A_{zz}$. The other EPR transition $\langle 0 | \leftrightarrow | 1 \rangle$ gives the same information except that the ENDOR frequency will be at the "opposite side" $(\nu_N - A_{zz})$ compared to $\nu_N$ as in the first case.

If the sign of this principal value is known, then the sign of the other off-diagonal elements are found by solving equation (14) more exactly for some angles or by a least square fitting procedure.

## 4. METHYL GROUP ROTATION

One of the most important original papers of the methyl group rotation is from Clough and Poldy [16]. Unfortunately they never improved wrong equations therein. This motivated us to give here a more extended theoretical treatment of the methyl group rotation.

At lower temperatures the methyl group of a molecule, like TQ, will be in its lowest vibronic torsional oscillator state. It is shown e.g. by Clough [16,17] that the nuclear spins $\sum_{i=1,2,3} I_i$ can be better described in the local $C_3$ methyl group symmetry.

A quartet I = 3/2 with A-symmetry has the lowest energy and two degenerated doublets I= 1/2 states with E-symmetry, which are 3J (=tunneling frequency) higher in energy and which are given here as $E^a$ and $E^b$. With the definitions:

$$\left.\begin{aligned} A &\equiv R_1 + R_2 + R_3 \\ E^a &\equiv R_1 + \varepsilon R_2 + \varepsilon^* R_3 \\ E^b &\equiv R_1 + \varepsilon^* R_2 + \varepsilon R_3 \end{aligned}\right\} \quad \varepsilon = e^{2\pi i/3} \tag{20}$$

and with R for operators or tensors and with index 1,2 and 3 for the three protons.

The results are given elsewhere e.g. by Lichtenbelt and Wiersma [18], but we will given here the operators, functions and matrices which form the basis of the equations derived.

The eigenfunctions of $I_z$ are:

$|A_{3/2}\rangle = |\alpha\alpha\alpha\rangle$ and $|A_{1/2}\rangle, |E^a_{1/2}\rangle$ and $|E^b_{1/2}\rangle$ are given by equation (20) with $R_1 = \frac{1}{\sqrt{3}}|\beta\alpha\alpha\rangle$, $R_2 = \frac{1}{\sqrt{3}}|\alpha\beta\alpha\rangle$ and $R_3 = \frac{1}{\sqrt{3}}|\alpha\alpha\beta\rangle$. The functions for negative $m_I$-values are found by exchanging $\alpha$ and $\beta$.

The non-zero expectation values are found with the following product rules: $A\,E^a = E^a$, $E^a\,E^b = A$, $E^a\,E^a = E^b$, $E^{a*} = E^b$ and $E^{b*} = E^a$:

$$\begin{array}{c|ccc} & |A\rangle & |E^a\rangle & |E^b\rangle \\ \langle A| & A & E^b & E^a \\ \langle E^a| & E^a & A & E^b \\ \langle E^b| & E^b & E^a & A \end{array} \qquad (21)$$

The expectation values are:

$$\langle Y_m|\, I_z^A\, |X_m\rangle = m \qquad (22a)$$

$$\langle Y_m|\, I_z^{E_a,E_b}\, |X_m\rangle = -2m \text{ for } m = \pm\tfrac{1}{2} \text{ and } 0 \text{ for } m = \pm\tfrac{3}{2} \qquad (22b)$$

with $m = m_I$ and $|X_m\rangle$ and $|Y_m\rangle$ the functions $|A\rangle, |E^a\rangle$ or $|E^b\rangle$ connected by equation (21).

$$\langle A_{m+1}|\, I_+^A\, |A_m\rangle = \langle A_m|\, I_-^A\, |A_{m+1}\rangle = \sqrt{15/4 - m(m+1)} \qquad (23a)$$

$$\langle E^{b,a}_{m+1}|\, I_+^A\, |E^{a,b}_m\rangle = \langle E^{b,a}_m|\, I_-^A\, |E^{a,b}_{m+1}\rangle = 2m = -1 \qquad (23b)$$

and

$$\langle Y_{m+1}|\, I_+^{E_a,E_b}\, |X_m\rangle = \langle Y_m|\, I_-^{E_a,E_b}\, |X_{m+1}\rangle = \sqrt{15/4 - m(m+1)} \qquad (24a)$$

except!

and

$$\begin{aligned} &\langle A_{\frac{1}{2}}|\, I_+^{E_a,E_b}\, |E^{b,a}_{-\frac{1}{2}}\rangle = \langle A_{-\frac{1}{2}}|\, I_-^{E_a,E_b}\, |E^{b,a}_{\frac{1}{2}}\rangle = -1 \\ &\langle E^{a,b}_{\frac{1}{2}}|\, I_+^{E_a,E_b}\, |A_{-\frac{1}{2}}\rangle = \langle E^{a,b}_{-\frac{1}{2}}|\, I_-^{E_a,E_b}\, |A_{\frac{1}{2}}\rangle = -1 \end{aligned} \qquad (24b)$$

The hamiltonian in symmetry adapted form will be:

$$\begin{aligned} \mathcal{H} = {} & g\,\beta\,H\,S_z + \underline{S}.\underline{\underline{D}}.\underline{S} + \tfrac{1}{3}\,\underline{S}.(\underline{\underline{A}}^A.\underline{I}^A + \underline{\underline{A}}^{E_a}.\underline{I}^{E_b} + \underline{\underline{A}}^{E_b}.\underline{I}^{E_a}) - g_N\beta_N H\, I_z^A \\ & -J(\underline{I}^A.\underline{I}^A - \tfrac{9}{4}) - \tfrac{1}{3}(Q^{A}P^{A} + Q^{E_a}P^{E_b} + Q^{E_b}P^{E_a}) \end{aligned} \qquad (25)$$

with the last term the nucler dipole-dipole and/or quadrupole interaction term which we first assume to be negligible small (see for this correction e.g. Allen [19]).

The zero-order energy for H parallel to the dipolar z-axis will be:

$$E^{(0)} = g\,\beta\,H\,m_s - (\tfrac{3}{2}m_s^2 - 1)Z - g_N\beta_N H\,m_I \pm \tfrac{3}{2}J + \tfrac{1}{3}m_s\,m_I\,A^A_{zz} \qquad (26)$$

with the plus sign for the E-states and the minus sign for the A-states.

The hyperfine- and electron dipolar(see table 1) interaction will give off-diagonal elements in the hamiltonian. For the $S_z$-elements the hyperfine hamiltonian matrix will be:

| | $\lvert A_{3/2}\rangle$ | $\lvert A_{1/2}\rangle$ | $\lvert A_{-1/2}\rangle$ | $\lvert A_{-3/2}\rangle$ | $\lvert E^a_{1/2}\rangle$ | $\lvert E^b_{1/2}\rangle$ | $\lvert E^a_{-1/2}\rangle$ | $\lvert E^b_{-1/2}\rangle$ |
|---|---|---|---|---|---|---|---|---|
| $\langle A_{3/2}\rvert$ | $\frac{1}{2}A_{zz}$ | $\frac{\sqrt{3}}{6}A_{z-}$ | 0 | 0 | $\frac{\sqrt{3}}{6}E_{a\,z-}$ | $\frac{\sqrt{3}}{6}E_{b\,z-}$ | 0 | 0 |
| $\langle A_{1/2}\rvert$ | $\frac{\sqrt{3}}{6}A_{z+}$ | $\frac{1}{6}A_{zz}$ | $\frac{1}{3}A_{z-}$ | 0 | $-\frac{1}{3}E_{a\,zz}$ | $-\frac{1}{3}E_{b\,zz}$ | $-\frac{1}{6}E_{a\,z-}$ | $-\frac{1}{6}E_{b\,z-}$ |
| $\langle A_{-1/2}\rvert$ | 0 | $\frac{1}{3}A_{z+}$ | $-\frac{1}{6}A_{zz}$ | $\frac{\sqrt{3}}{6}A_{z-}$ | $-\frac{1}{6}E_{a\,z+}$ | $-\frac{1}{6}E_{b\,z+}$ | $\frac{1}{3}E_{a\,zz}$ | $\frac{1}{3}E_{b\,zz}$ |
| $\langle A_{-3/2}\rvert$ | 0 | 0 | $\frac{\sqrt{3}}{6}A_{z+}$ | $-\frac{1}{2}A_{zz}$ | 0 | 0 | $\frac{\sqrt{3}}{6}E_{a\,z+}$ | $\frac{\sqrt{3}}{6}E_{b\,z+}$ |
| $\langle E^a_{1/2}\rvert$ | $\frac{\sqrt{3}}{6}E_{b\,z+}$ | $-\frac{1}{3}E_{b\,zz}$ | $-\frac{1}{6}E_{b\,z-}$ | 0 | $\frac{1}{6}A_{zz}$ | $-\frac{1}{3}E_{a\,zz}$ | $-\frac{1}{6}A_{z-}$ | $\frac{1}{3}E_{a\,z-}$ |
| $\langle E^b_{1/2}\rvert$ | $\frac{\sqrt{3}}{6}E_{a\,z+}$ | $-\frac{1}{3}E_{a\,zz}$ | $-\frac{1}{6}E_{a\,z-}$ | 0 | $-\frac{1}{3}E_{b\,zz}$ | $\frac{1}{6}A_{zz}$ | $\frac{1}{3}E_{b\,z-}$ | $-\frac{1}{6}A_{z-}$ |
| $\langle E^a_{-1/2}\rvert$ | 0 | $-\frac{1}{6}E_{b\,z+}$ | $\frac{1}{3}E_{b\,zz}$ | $\frac{\sqrt{3}}{6}E_{b\,z-}$ | $-\frac{1}{6}A_{z+}$ | $\frac{1}{3}E_{a\,z+}$ | $-\frac{1}{6}A_{zz}$ | $\frac{1}{3}E_{a\,zz}$ |
| $\langle E^b_{-1/2}\rvert$ | 0 | $-\frac{1}{6}E_{a\,z+}$ | $\frac{1}{3}E_{a\,zz}$ | $\frac{\sqrt{3}}{6}E_{a\,z-}$ | $\frac{1}{3}E_{b\,z+}$ | $-\frac{1}{6}A_{z+}$ | $\frac{1}{3}E_{b\,zz}$ | $-\frac{1}{6}A_{zz}$ |

with the index definition: $\pm \equiv x \pm iy$. (27)

All elements have to be multiplied by the electronic expectation value $\langle m_s|\,S_z\,|m_s\rangle = m_s$. For the $S^+$ and $S^-$ operators the matrix elements are found by substitution respectively of $\frac{1}{2}A_{-i}$ and $\frac{1}{2}A_{+i}$ for $A_{zi}$ and have to be multiplied by the electronic expectation value $\langle m_s+1|S^+|m_s\rangle = \langle m_s|S^-|m_s+1\rangle = \sqrt{S(S+1)-m_s(m_s+1)}$.

It is seen directly in equation (26) that the zeroth order eigenvalues of $E^a_m$ are equal to the of $E^b_m$. This degeneracy has to be removed and will depend on the product-off-diagonal elements: $A^{Ea}_{zz}.A^{Eb}_{zz}$ .

Clough and Poldy [16] could solve this further for an electronic doublet system, by assuming:

$A_{zz}^{1,2,3} \approx A_{iso}^{1,2,3} \approx B_2 \cos^2\varphi_{1,2,3} >> |A_{ij}|$, with $\varphi$ the angle between the $\pi$-orbital and the methyl C-H projection on the $H_3$-plane.

For the lowest $n\pi^*$ triplet system of TQ this angular dependence will be differer and we can perform this diagonalisation in an analytical way only if we assume a mirror plane through the methyl group for the hyperfine interaction descriptior Then $A_{zz}^1 = A_{zz}^2 \neq A_{zz}^3$ and $A_{zx}^1 = -A_{zx}^2$ etc.

After diagonalisation the following new functions are found:

$$|E'_m> = \tfrac{1}{2}\sqrt{2}\ (\varepsilon|E_m^a> + \varepsilon^*|E_m^b>) \text{ with eigenvalue } \frac{1}{3} m_s m_I (A_{zz}^A - 2A_{zz}^\Delta) \quad (28a)$$

$$|E''_m> = \tfrac{1}{2}\sqrt{2}\ (\varepsilon|E_m^a> - \varepsilon^*|E_m^b>) \text{ with eigenvalue } \frac{1}{3} m_s m_I (A_{zz}^A + 2A_{zz}^\Delta) \quad (28b)$$

with $A_{ij}^\Delta \equiv A_{ij}^3 - \tfrac{1}{2}(A_{ij}^1 + A_{ij}^2)$.

The new matrix elements of equation (27) are found by a rotation using the rotation matrix formed by elements which are equal with coefficients in equation (28). After this diagonalisation the following definition turns out to be useful

$$A_{ij}^\eta \equiv A_{ij}^1 - A_{ij}^2 \quad \text{with } A_{iso}^\eta = 0.$$

In the case of TQ in its lowest $n\pi^*$ triplet state, it was found (experimentally that $|A_{iso}^\Delta|$ exceeds all other hyperfine elements and therefore the hamiltonian matrix becomes like table 1. Herein small- and zero-element values are not given This table forms the basis for the second order equations given by Lichtenbelt and Wiersma [18].

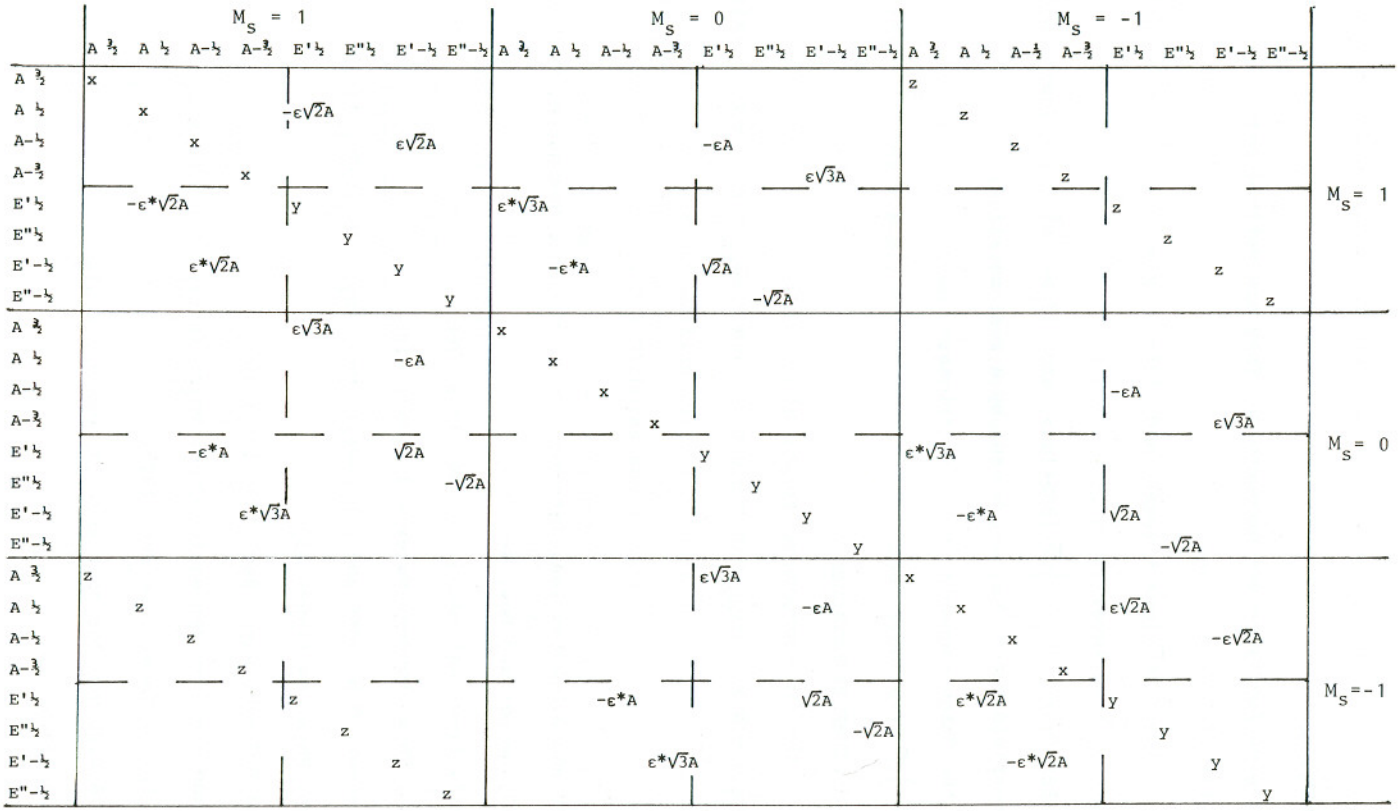


Table 1. The hamiltonian matrix of an electronic triplet system with a rotating methyl group. A mirror plane is assumed for the hyperfine interaction description and $A^{\Delta}_{iso}$ is the largest hyperfine interaction. $\varepsilon = e^{2\pi i/3}$, $A = A^{\Delta}_{iso}$, $z = (Y-X)/2$ and x and y are the first-order eigenvalues as given by a combination of equations (26) and (28).

## 5. APPENDIX

### 5.1. TRIPLET FUNCTIONS

Three kind of triplet functions are encountered. They are defined as:

"High magnetic field" functions:

$$|1\rangle = |\alpha\alpha\rangle \ , \quad |0\rangle = \tfrac{1}{2}\sqrt{2}(|\alpha\beta\rangle + |\beta\alpha\rangle) \quad \text{and} \quad |-1\rangle = |\beta\beta\rangle \tag{A1}$$

The "zero-field" functions:

$$|T_x\rangle = \frac{1}{2}\sqrt{2}(|\beta\beta\rangle - |\alpha\alpha\rangle), \ |T_y\rangle = \frac{i}{2}\sqrt{2}(|\beta\beta\rangle + |\alpha\alpha\rangle) \text{ and } |T_z\rangle = \frac{1}{2}\sqrt{2}(|\alpha\beta\rangle + |\beta\alpha\rangle) \tag{A2}$$

and the real zero-field functions, which can, by a real rotation,

be changed into the "high magnetic field" functions:

$$|T_x\rangle, \ |T'_y\rangle = \frac{1}{2}\sqrt{2}(|\beta\beta\rangle + |\alpha\alpha\rangle) \quad \text{and} \quad |T_z\rangle \tag{A3}$$

### 5.2. THE FINE-STRUCTURE EIGENVALUES

The eigenvalues of the fine-structure tensor $\underline{\underline{D}}'$ are defined as:

$$-D_{xx} = X = \frac{1}{3}D - E \ , \quad -D_{yy} = Y = \frac{1}{3}D + E \quad \text{and} \quad -D_{zz} = Z = -\frac{2}{3}D \tag{A4}$$

## REFERENCES


1. A.Carrington and A.D.McLachlan, Introduction to Magnetic Resonance. 1st ed. 1967, Harper and Row, New York.
2. H.M.McConnell, Proc. Nat. Acad. Sc. 44 (1958) 766.
   F.K.Kneubühl, Phys. Kondens Materie 1 (1963) 410.
   R.M.Hochstrasser, G.W.Scott and A.H.Zewail, Mol. Phys. 36 (1978) 475.
3. P.Kottis,Ann. Phys. t4 (1969) 459.
4. H.Wieder and T.G.Eck, Phys. Rev. 153 (1967) 103.
5. W.S.Veeman and J.H. van der Waals, Chem. Phys. letters 7 (1970) 65.
   W.S.Veeman, Ph. D. Thesis, Leiden (1972).
   W.S.Veeman, A.L.J. van der Poel and J.H. van der Waals,
   Mol. Phys. 29 (1975) 225.

6. J.C.Colpa and D.Stehlik, Chem. Phys. 21 (1977) 273.
D.Stehlik and J.C.Colpa, Chem. Phys. 21 (1977) 289.
D.Stehlik, P.Rösch, P.Lau, H.Zimmermann and K.H.Hauser,
Chem. Phys. 21 (1977) 301.
J.P.Colpa, F.Seiff and D.Stehlik, Chem. Phys. 33 (1978) 79.
7. J.H.Lichtenbelt, J.G.F.M.Fremeijer, H.Veenvliet and D.A.Wiersma,
Chem. Phys. 10 (1975) 107.
8. J.H.Lichtenbelt and D.A.Wiersma, Chem. Phys. 34 (1978) 47.
9. A.L.Kwiram, J. Chem. Phys. 55 (1971) 2484.
10. B.Bleaney F.R.S., Philosophical Mag., 42 (1951) 441.
A.Abragram and B.Bleaney. Electron Paramagnetic Resonance of Transition Ions.
1970 Oxford University Press, Ely House,London.
11. G.E.Pake and T.L.Estle, The physical principles of Electron Paramagnetic
Resonance. Second edition 1973, W.A.Benjamin Inc. Reading, Mass.
12. C.A.Hutchison Jr, J.V.Nicholas and G.W.Scott, J. Chem. Phys. 53 (1970) 1906.
13. J.A.Weil, J. Magn. Res. 18 (1975) 113.
K.A.Thuomas and A.Lund, J. Magn. Res. 18 (1975) 12.
And references therein.
14. C.P.Poole and H.A.Farach. The theory of Magnetic Resonance. 1972,
Wiley-Interscience, New York.
15. L.Benthem, J.H.Lichtenbelt and D.A.Wiersma, Chem. Phys. 29 (1978) 367.
16. S.Clough and F.Poldy, J.Chem. Phys. 51 (1969) 2076.
17. S.Clough, J.Hill and F.Poldy, J. Phys. C: Solid State Phys. 5 (1972) 518.
S.Clough and F.Poldy, J. Phys. C: Solid State Phys. 6 (1973) 1953.
18. J.H.Lichtenbelt and D.A.Wiersma, Chem. Phys. 39 (1979) 37.
19. P.J.Allen, J. Chem. Phys. 48 (1968) 3031.

"Theory is not all that matters".

## STRUCTURE AND DYNAMICS OF THE LOWEST TRIPLET STATE IN p-BENZOQUINONE

### II. An optically detected EPR and proton ENDOR study

Jan H. LICHTENBELT, Jan G.F.M. FREMEYER, Hendrik VEENVLIET and Douwe A. WIERSMA
*Laboratory for Physical Chemistry, University of Groningen, Groningen, The Netherlands*

Optically detected high field EPR and proton ENDOR experiments on the zero-point (*g*-inversion) level of the lowest triplet state in *p*-benzoquinone-$h_4$ as guest in *p*-benzoquinone-$d_4$ are reported. The results are used to obtain the parameters of the molecular spin hamiltonian and the following results are obtained at 1.8 K: The fine-structure principal values are $X = -798.2 \pm 0.6$ MHz, $Y = -569.1 \pm 0.6$ MHz, and $Z = 1367.3 \pm 0.6$ MHz; while the molecular *g*-values are found to be $g_{xx} = 2.0045 \pm 0.0005$, $g_{yy} = 2.0035 \pm 0.0005$, and $g_{zz} = 2.00994 \pm 0.00008$.

The principal *z* axes of both the fine-structure and *g*-tensor are found to coincide with the carbonyl bond direction of the *p*-benzoquinone ground state structure.

The orientation of the *x* and *y* axes of the fine-structure and proton hyperfine-structure tensor however indicates that the molecule in the excited state is distorted into a centrosymmetric chair-form, which also implies that the symmetry of this state is only $A_g$. The $\frac{1}{3}$ trace of the proton hyperfine interaction tensor is found to be 9.6 MHz and from this we calculate that 1.8% of the unpaired n-electron density is at each proton.

We further report the effect of mono deuteration on the fine-structure and *g*-tensor principal values and these data are used to calculate the fine-structure parameter *Z* of the u-inversion level (20 $cm^{-1}$ above the zero-point level) in the triplet state of *p*-benzoquinone-$h_4$. This method yields $Z = 5.8$ GHz which is to be compared with the value $6 \pm 1.3$ GHz obtained from the temperature dependence of the corresponding fine-structure parameter of the zero-point level.

Finally, a new effect – the observation of radio-frequency induced changes in the phosphorescence cross relaxation signal – is reported and used to identify the electron spin state, in which the (ENDOR) proton spin flips take place.

### 1. Introduction

The spectroscopic interesting properties of aromatic diketones mainly stem from the near degeneracy of the lowest $n\pi^*$ excitations in these molecules. As a result of this near degeneracy, vibronic coupling strongly mixes these electronic excitations and the potential energy surface of the lower state may then acquire a double minimum potential (DMP) well along a vibronic coupling mode [1,2].

The pseudo Jahn–Teller character of the lowest excited triplet state in the prototype aromatic diketone *p*-benzoquinone was recently demonstrated through a series of experiments [3,4] of which the observed large isotope effects on the fine-structure parameter *D* [5] was most intriguing. In *p*-benzoquinone (PBQ ($L = z$, $M = y$)) vibronic coupling between the $B_{1g}$and $A_u$ $n\pi^*$ triplet states is so strong that the potential energy surface of the lowest ($B_{1g}$) triplet state indeed contains a DMP well along a $b_{1u}$ type nuclear motion.

Much of our effort in the past was devoted to an optical study aimed at further identification of the lowest inversion levels in the DMP well of the lowest triplet state in PBQ and in part I of the series [6] we reported results of an isotope effect study on the absorption, emission and ODMR spectra of the lowest triplet state. Next to a detailed optical study, we are also engaged in an EPR and ENDOR study of the lowest triplet state in PBQ of several isotopic species such as: PBQ-$h_4$, -$dh_3$, -2,6-$d_2h_2$, -$d_3h$, -$^{13}$C and -$^{17}$O using PBQ-$d_4$ as a host crystal. In the present paper we are primarily concerned with the results of an EPR and proton ENDOR study of the zero-point (g-inversion) level of the lowest triplet state in PBQ-$h_4$ as guest in PBQ-$d_4$ at 1.8 K.

The preliminary results of EPR experiments at 4.2 K on the u-inversion level of the DMP well in PBQ-$h_4$ will also be presented and discussed.

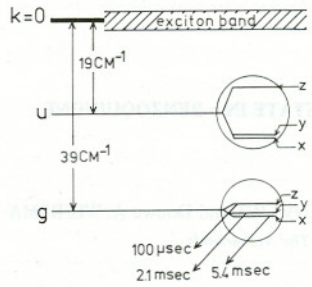


Fig. 1. Location of the inversion levels in the lowest triplet state of *p*-benzoquinone-$h_4$ with respect to the lowest triplet exciton band of *p*-benzoquinone-$d_4$. The data in this figure have been taken from ref. [6]. It should be further noted that the zero field splitting of the inversion levels has been expanded (about 120 times) and that the ordering of the *x* and *y* spin sublevels in the u-inversion level is unknown.

Finally we demonstrate the usage of a new phenomenon: the observation of r.f. induced changes in the cross relaxation effect, which is used to determine the absolute sign of the proton hyperfine coupling constants in the lowest $n\pi^*$ triplet state of PBQ-$h_4$.

## 2. EPR measurements

Fig. 1 schematically shows the energy level diagram of the PBQ-$h_4$ molecular trap inside the PBQ-$d_4$ host crystal. The zero-point (g-inversion) level of the PBQ-$h_4$ trap is 39 $cm^{-1}$ and the u-inversion (vibronic) level is only 19 $cm^{-1}$ below the host triplet exciton band [6]. In part I we have shown that the dynamics of this system is very much temperature dependent, however detailed knowledge of the communication process among the inversion levels is lacking at present. In case of Boltzmann equilibrium among the inversion levels at all temperatures, only at very low temperature, e.g., 1.8 K, the g-inversion level, for its magnetic properties, may be considered isolated [consult also eq. (2)]. At, e.g., 4.2 K however, EPR and ENDOR measurements on the g-inversion level indirectly probe magnetic properties of the u-inversion level and vice versa.

In a recent communication [5] we reported the fine-structure parameters and *g*-tensor principal values of the zero-point level of the lowest $n\pi^*$ triplet state of PBQ-$h_4$ and PBQ-$dh_3$ as guest in a PBQ-$d_4$ host crystal at 1.8 K. In the meantime we have been able to considerably improve the accuracy of these data, especially the *g*-tensor principal values, by using much more accurate magnetic field measurements then in the previous report. The parameters in table 1 were calculated from angular dependent EPR measurements at 1.8 K performed in orthogonal crystal planes, whereby the resonance field positions of both inequivalent molecules in the unit cell were accurately determined. They were further adjusted such that the magnetic resonance data of the symmetry related molecules in the unit cell [7] were simultaneously optimal fitted to the following well known spin hamiltonian:

$$H = |\beta_e|(S_x g_{xx} H_x + S_y g_{yy} H_y + S_z g_{zz} H_z) - h(XS_x^2 + YS_y^2 + ZS_z^2). \quad (1)$$

Herein are $g_{xx}$, $g_{yy}$ and $g_{zz}$ the principal values of the *g*-tensor of the triplet spin system, *X*, *Y* and *Z* the principal values of the fine-structure tensor with zero trace, $S_x$, $S_y$ and $S_z$ components of the spin angular

Table 1
Fine-structure parameters and *g*-tensor principal values in the lowest triplet state of PBQ-$h_4$ and PBQ-$dh_3$ as guest (1 mol%) in PBQ-$d_4$ at 1.8 K as obtained from high field EPR measurements. The numbers in parentheses are obtained from zero-field ODMR experiments [6]

| | PBQ-$h_4$ | | PBQ-$dh_3$ |
|---|---|---|---|
| *X* (MHz) | −798.2 ± 0.6 | (−797.3 ± 0.8) | −915.5 ± 0.6 |
| *Y* (MHz) | −569.1 ± 0.6 | (−569.3 ± 0.8) | −705.5 ± 0.6 |
| *Z* (MHz) | 1367.3 ± 0.6 | (1366.6 ± 0.8) | 1621.0 ± 0.6 |
| $g_{xx}$ | 2.0045 ± 0.0005 | | 2.0045 ± 0.0005 |
| $g_{yy}$ | 2.0035 ± 0.0005 | | 2.0038 ± 0.0005 |
| $g_{zz}$ | 2.00994 ± 0.00008 | | 2.01038 ± 0.00008 |

momentum in the molecular axes system and $|\beta_e|/h$ a constant which in this paper is taken from ref. [8]. ($|\beta_e|/h$ = 1.3996109 GHz/kG.)

We have further assumed in the treatment of our data that the principal axes system of the fine-structure- and $g$-tensor coincide. Our experiments indeed show this to be the case for the $z$ axes, but positive evidence that this is also the case for the $x$ and $y$ axes could not be produced.

This is primarily due to the fact that the splitting between the $X$ and $Y$ spin substates is very small, which makes the fitting procedure rather insensitive to a small rotation around the $z$-axis of the $g$-tensor versus the fine-structure tensor.

It is gratifying to see in table 1, that the fine-structure parameters obtained in this manner very nicely agree with the refined ODMR data obtained in zero field.

We would like to point out that, although the spread in the reported $g_{zz}$ values is rather large, the absolute difference in these parameters for PBQ-$h_4$ and PBQ-$dh_3$ can be determined quite accurately as all EPR measurements were made on crystals that simultaneously contained these species. The observed isotope effect on the $g$- and fine-structure tensor reported here are unprecedented and it is interesting to note that $g_{zz}$ and $|D|$ both significantly increase on mono deuteration.

In part I of these series we have shown that this can be explained as a change in spin–orbit contribution to these parameters. When we compare the $g$-tensor principal values of PBQ-$h_4$ with those of benzophenone-$h_{10}$ [9] we note that $g_{zz}$ is of similar magnitude in both compounds, while $g_{xx}$ and $g_{yy}$ in benzophenone-$h_{10}$ both are smaller than the free electron $g$-value, but in PBQ-$h_4$ they are both larger. This most likely illustrates the fact that $g_{zz}$ values in $n\pi^*$ triplet states of aromatic carbonyls are mainly determined by spin–orbit coupling with the nearest higher $\pi\pi^*$ triplet state of the correct symmetry [10]. The $g_{xx}$ and $g_{yy}$ values however probably result from many such interfering spin–orbit coupling terms and a simple interpretation of these parameters therefore seems impossible.

Our EPR results for PBQ-$h_4$ further show that the $z$-axis of the fine-structure tensor in the zero-point level coincides with the oxygen–oxygen ($L$) direction of the PBQ-$h_4$ ground state structure [7]. The $x(N)$ and $y(M)$ axes of this tensor however deviate slightly ($5 \pm 2°$) from the ground state molecular axes system. We conclude that the lowest triplet state in PBQ-$h_4$ is no longer planar and this is confirmed by the proton ENDOR experiments (vide infra).

Fig. 2 shows a typical tracing of the optically detected EPR spectrum of PBQ-$h_4$ in a PBQ-$d_4$ host crystal at 1.8 K for the magnetic field parallel to the $z$-axis of one of the two molecules ($\alpha$) in the unit cell. The figure also shows the cross relaxation (CR) and level anti-cross (LAC) signals observed in this crystal. The CR signal at $362 \pm 1$ gauss[‡] is due to cross relaxation between an unknown doublet ($S = \frac{1}{2}$) and a PBQ-$h_4$ ($\alpha$) excited triplet species. We will show in section 5 that the CR signal can be used to probe hyperfine interactions in the triplet excited state of PBQ-$h_4$. The LAC signal observed at $726 \pm 2$ gauss[‡] (minimum line-width observed 60 MHz) is due to LAC between the $Z$ and $Y$ spin substates of the $\alpha$-species and its position is in good agreement with the one calculated (727.7 gauss) from the parameters in table 1.

Sofar the experiments discussed here refer to the isolated zero-point level of the lowest triplet state of PBQ-$h_4$ in a PBQ-$d_4$ host crystal at 1.8 K. When the temperature is raised to 4.2 K and assuming Boltzmann equilibrium among the inversion levels we expect to measure a change in $D_g$ (the fine-structure parameter of the zero-point (g-inversion) level) according to the following expression:

$$D_g(T) = Z^{-1}\,[D_g(0) + D_u(0)\,e^{-\Delta E/kT}], \qquad (2)$$

wherein $D_g(0)$ and $D_u(0)$ are the fine-structure parameters of the g- and u-level under isolated conditions, $\Delta E$ the gap between the inversion levels (20 $cm^{-1}$) and $Z^{-1}$ the partition function of the system. We can write $Z^{-1}$ to a very good approximation as $(1 + e^{-\Delta E/kT})^{-1}$. Eq. (2) shows that for identical $D_g(0)$ and $D_u(0)$ we expect $D_g(T)$ to be temperature independent. We have measured $|D_g(T)|$ at 4.2 K and found an average increase of $8 \pm 2$ MHz versus the value measured at 1.8 K.

From eq. (2) we then calculate the fine-structure parameter $D$ of the vibronic (u-inversion) level and find $D_u(0) = -9 \pm 2$ GHz. There are two other pieces of information that support such a large value of the

‡ The accuracy of our field measurements below 750 gauss is low due to the fact that our AEG probes do not cover this area.

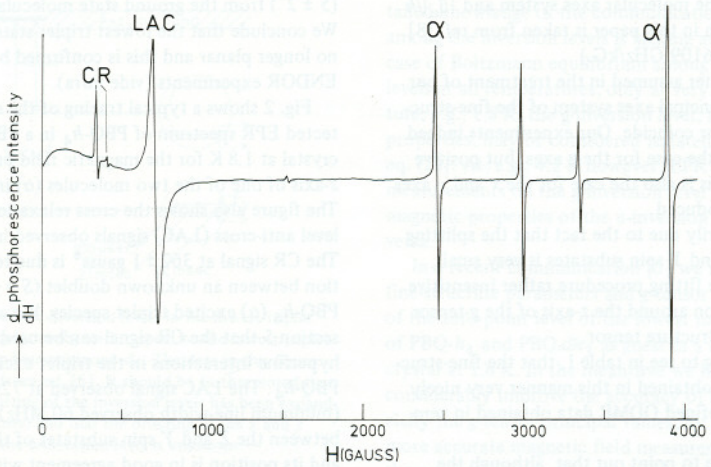


Fig. 2. Optically detected EPR spectrum of the lowest triplet state in *p*-benzoquinone-$h_4$ as guest in *p*-benzoquinone-$d_4$ at 1.8 K. The signals are taken for the magnetic field parallel to the *z*-axis of one of the molecules ($\alpha$) in the unit cell. The signal denoted by LAC is due to level anticrossing between the *z* and *y* spin sublevels of the $\alpha$-species and the signals denoted by CR are due to cross relaxation between a triplet species (the most intense one $\alpha$) and a doublet spin system. Note that the CR and LAC signals are persistent in the absence of a microwave field.

fine-structure parameter $D$ in the u-inversion level of the lowest triplet state in PBQ-$h_4$.

First, from integrated oscillator strength intensity measurements on the inversion levels in pure PBQ-$h_4$ and PBQ-$dh_3$ crystals [6] one concludes that, in a two-state model, the zero-point level of the lowest triplet state in PBQ-$dh_3$ (compared to PBQ-$h_4$) should be described as

$$|g'\rangle = 0.97\,|g\rangle + 0.24\,|u\rangle. \qquad (3)$$

Herein is $|g\rangle$ the wave function of the zero-point and $|u\rangle$ the wave function of the u-inversion level in PBQ-$h_4$. From eq. (3) and the magnetic resonance data of table 1 we calculate the fine-structure parameter $D$ of the u-inversion level to be $-8.7 \pm 1.0$ GHz.

Secondly, direct polarized Zeeman absorption experiments on pure PBQ-$d_4$ crystals [4] show the fine-structure parameter $D$ of the u-inversion level in this molecule to be $-10 \pm 3$ GHz.

These results stimulated us to search for EPR signals that could be attributed to microwave transitions in the spin system of the u-inversion level. And indeed in a 1 mol% PBQ-$h_4$ in PBQ-$d_4$ isotopic mixed crystal at 4.2 K intense EPR, CR and LAC signals (the latter at 3635 gauss for $H \| z$ of one of the PBQ-molecules in the unit cell) were observed that must be due to a triplet species with $D = -10.2 \pm 0.1$ GHz.

We are however, at this point, not able to exclude the possibility of other transients (like photochemically produced carbenes) to be responsible for the signals observed at 4.2 K. This is a point of further investigation in our laboratory.

We have further in mind to probe the fine-structure parameters of the u-inversion level indirectly by an electric field effect study on the ODMR spectra of the g-inversion level at 1.8 K.

### 3. EPR hyperfine structure

In only the best PBQ-$h_4$ in PBQ-$d_4$ host mixed crystals that were grown, we have been able to observe at 1.8 K hyperfine structure for the magnetic field approximately parallel to the short ($y$) molecular axis. A five line pattern, with a splitting of $\sim 14$ MHz and intensity distribution characteristic to four equivalent protons, was observed. Along other magnetic field directions, under the same conditions, no such

well resolved splittings were obtained. This indicates that the hyperfine interaction constants along the $x$ ($A_{xx}$) and $z$ ($A_{zz}$) molecular axes apparently are smaller than the one along the $y$ ($A_{yy}$) molecular axis. Usually the optically detected EPR lines were 30–45 MHz wide and it soon became clear that the EPR hyperfine structure would not yield us the hyperfine interaction constants nor principal axes system to an acurracy we wanted. We therefore decided to try to obtain these data from optical detected ENDOR measurements. $p$-Benzoquinone seemed quite a good candidate for optical detection of ENDOR transitions, since the phosphorescence lifetime is very short ($\tau_z = 100\,\mu s$) and the optically detected EPR signals quite often showed a signal to noise ratio of 500 or even better. Fig. 3 shows an optically detected ENDOR spectrum of PBQ-$h_4$ in a PBQ-$d_4$ mixed crystal at 1.8 K for a magnetic field parallel to the long ($z$) molecular axis of one of the molecules in the unit cell.

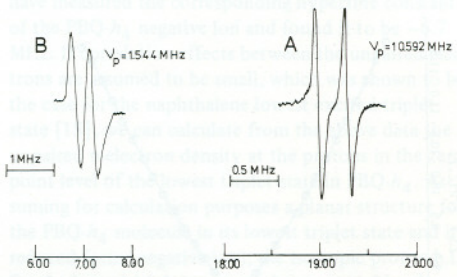


Fig. 3. Optically detected ENDOR(A) and CRENDOR(B) transitions in the lowest triplet state of $p$-benzoquinone-$h_4$ as guest in $p$-benzoquinone-$d_4$ at 1.8 K. The magnetic field in both cases is oriented along the long molecular (z) axis of one of the inequivalent PBQ molecules in the unit cell. The ENDOR signals are observed on the low field $\langle 0| \leftrightarrow |-1\rangle$ EPR transition and the CRENDOR signals on the cross relaxation $\langle 0| \leftrightarrow |+1\rangle$ transition.

## 4. Proton ENDOR measurements

The basic principles underlying the electron nuclear double resonance (ENDOR) technique are well established [11]. Nuclear spinflips, induced by a tuned r.f. source are used to (de)saturate a partly saturated EPR transition. We are thus interested in a calculation of the nuclear spin energy levels in a triplet state electron spin system. These energy levels are determined by the following well-known spin hamiltonian:

$$\underbrace{H = |\beta_e|\, S \cdot g_e \cdot H_0}_{H_1} \underbrace{-h(XS_x^2 + YS_y^2 + ZS_z^2)}_{H_2} \underbrace{-|\beta_n|\, g_n H_0 \cdot \sum_k I_k}_{H_3} + \underbrace{S \cdot \sum_k A_k \cdot I_k}_{H_4}, \qquad (4)$$

where $S = 1$; $I_k = \frac{1}{2}$, for protons and $k$ sums over all nuclei.

Hutchison and Pearson [12] have shown that, to a very good approximation, the nuclear eigenvalues may be calculated from a first-order perturbation treatment of $H$. In this approximation, the exact eigenfunctions of $H_1 + H_2$ are used to calculate the diagonal contributions of $H_3 + H_4$ to the energy of the compound electron–nuclear spin state. A calculation of the off-diagonal elements of $H_3 + H_4$ for the case of PBQ-$h_4$ shows that the maximum error in the nuclear eigenvalues is expected to be $(A_{yy})^2/\nu_{EPR} \approx 20$ kHz. It does not seem unreasonable then to neglect these second order contributions as the narrowest ENDOR lines observed had a linewidth of 50 kHz. Using the above outlined procedure one calculates for the ENDOR shift of the $k$th proton [12]:

$$\Delta\nu_k = h^{-1}[(\langle S_x\rangle A_{xx}^k + \langle S_y\rangle A_{xy}^k + \langle S_z\rangle A_{xz}^k - lh\,\nu_p)^2 + (\langle S_x\rangle A_{yx}^k + \langle S_y\rangle A_{yy}^k + \langle S_z\rangle A_{yz}^k - mh\,\nu_p)^2 + (\langle S_x\rangle A_{zx}^k + \langle S_y\rangle A_{zy}^k + \langle S_z\rangle A_{zz}^k - nh\,\nu_p)^2]^{1/2} - \nu_p, \qquad (5)$$

in which $l$, $m$ and $n$ are the direction cosines of $H_0$ in the molecular axes system. $A_{ij}^k$ are the elements of the hyperfine tensor of the $k$th proton in the molecular axes system. The $A_{ij}^k$ tensor is only symmetric for an isotropic $g_e$ tensor. In PBQ-$h_4$ this is not the case but the largest difference between $A_{ij}^k$ and $A_{ji}^k$ $(i \neq j)$ is only expected to be $(1 - g_{yy}/g_{zz}) \times 100\% = 0.3\%$. In our present treatment of the ENDOR data we have ignored these differences and taken the $A_{ij}^k$ tensor to be symmetric. The expectation values of $\langle S_x\rangle$, $\langle S_y\rangle$ and $\langle S_z\rangle$ were calculated by computer, using the parameters of table 1.

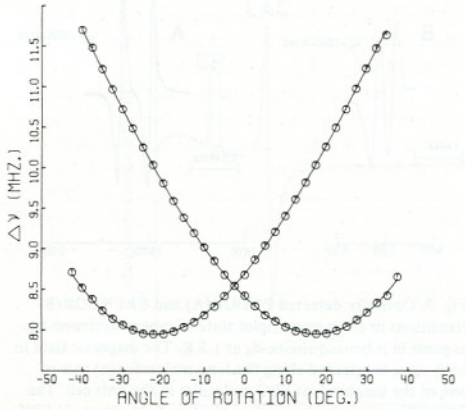


Fig. 4. Experimental proton ENDOR data (circles) and computer fitted curves for the lowest triplet state in *p*-benzoquinone-$h_4$ at 1.8 K. The magnetic field is rotated in the $(20\bar{1})$ cleavage plane (nearly *yz* molecular plane) and at zero degrees is parallel to the long molecular (*z*) axis. $\Delta\nu$ represents the difference between the measured proton ENDOR frequency and the free proton frequency at the EPR transition studied.

Table 2 *

Hyperfine tensors (in MHz) of the two inequivalent protons in the lowest triplet state of PBQ-$h_4$ as guest in PBQ-$d_4$ at 1.8 K. The tensors are assumed to be symmetric and described in the molecular ground state principal axes system [7].

The principal values ($A^P$) together with the direction cosines of the principal axes system are also given.

The numbers in parentheses represent standard deviations (in MHz) of the computer fittings of the ENDOR data

| | | | | | | |
|---|---|---|---|---|---|---|
| $A_1$ = | 6.5 | (0.2) | | | | |
| | 0.8 | (0.3) | 13.6 | (0.2) | | |
| | −0.21 | (0.02) | −1.87 | (0.01) | 8.6 | (0.1) |
| $A_1^P$ | 6.4 | (0.3) | 14.3 | (0.2) | 8.0 | (0.2) |
| *L* | 0.005 | | −0.312 | | 0.950 | |
| *M* | −0.105 | | 0.945 | | 0.311 | |
| *N* | 0.994 | | 0.101 | | 0.028 | |
| $A_2$ = | 6.7 | (0.2) | | | | |
| | −0.5 | (0.3) | 13.7 | (0.2) | | |
| | −0.11 | (0.02) | 1.50 | (0.01) | 8.4 | (0.1) |
| $A_2^P$ | 6.7 | (0.2) | 14.1 | (0.2) | 8.0 | (0.1) |
| *L* | 0.003 | | 0.252 | | 0.968 | |
| *M* | 0.071 | | 0.965 | | −0.252 | |
| *N* | 0.997 | | −0.069 | | 0.015 | |

In the case of PBQ-$h_4$, with the magnetic field in the neighbourhood of the *y*-axis, we were only able to observe ENDOR transitions occurring in the $|0\rangle$ electron spin state (strong field approximation). For magnetic fields in the neighbourhood of the *z*-axis, ENDOR transitions occurring in the $|-1\rangle$ electron spin state were most intense. This feature is probably due to the fact that $T_z$ is the most radiative level in PBQ-$h_4$ and that ENDOR transitions are dominant in those electron spin states for which longitudinal relaxation is slowest. We have also been able to measure ENDOR transitions on the "$\Delta m = 2$" (half field) EPR signal and again only ENDOR transitions that could be correlated with the $|-1\rangle$ electron spin state were observed. The ENDOR data obtained were in a self-consistent manner, least-squares fitted to expression (5) with $\nu_p$ being the free proton frequency measured during each ENDOR scan. The plane of rotation was in each experiment determined by fitting the observed EPR magnetic field data to a spin hamiltonian $[(H_1 + H_2)$ of eq. (4)] using the parameters of table 1. Figs. 4 and 5 show some of the experimental ENDOR data and the computer fitted curves for the zero-point level of PBQ-$h_4$ as trap in PBQ-$d_4$ at 1.8 K. Table 2 contains all the hyperfine coupling data that were obtained from the present proton ENDOR study.

There are two important structural features of the

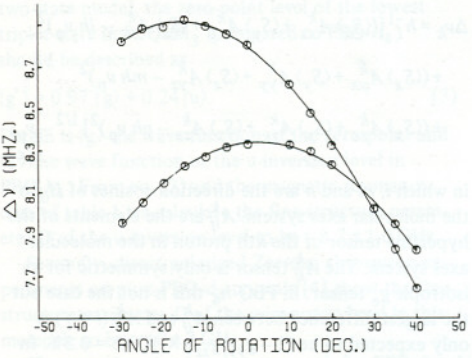


Fig. 5. Experimental proton ENDOR data (circles) and computer fitted curves for the lowest triplet state in *p*-benzoquinone-$h_4$ at 1.8 K. The magnetic field is rotated in the (nearly) *xz* molecular plane and at zero degrees is parallel to the long molecular (*z*) axis. See also the caption of fig. 4.

* note: A correction of the proton hyperfine data is given in Chapter 6.

PBQ-$h_4$ molecule in its zero-point level of the lowest triplet state that are immediately obvious from this proton ENDOR study.

First, fig. 3 already shows that for $H \| z$ of one of the molecules in the unit cell there are 2 proton ENDOR signals, instead of 1 expected for a $D_{2h}$ symmetric molecule.

Secondly, fig. 5 and table 2 clearly show that the $z$-axis is not an ENDOR shift stationary point for rotation in the nearly $xz$ molecular plane, which means that the PBQ-molecule in its lowest triplet state is no longer planar.

The conclusion from the proton ENDOR study thus is that the PBQ-$h_4$ molecule in its lowest excited triplet state only preserves site inversion symmetry. X-ray examination of the $p$-benzoquinone crystal at room temperature further showed [7] that the molecule in the ground state is planar. The non-planarity of the molecule in the excited state thus seems a purely molecular property similar to the reported non-planarity of the lowest triplet $n\pi^*$ state of formaldehyde [13].

The minor inequivalence of the ortho-ring protons is probably due to hydrogen bonding effects which have shown to be very important in PBQ crystals [6]. The proton ENDOR experiments further show that the $x$-axes of the proton hyperfine structure tensors are counter rotated some 5 degrees and this strongly suggests a chair-form structure of the molecule in the lowest triplet state.

The magnitude of the out-of-plane distortion is not extractable from the present proton ENDOR experiments. The analysis of the phosphorescence spectrum of PBQ-$h_4$ in PBQ-$d_4$ [5] (no progressions in out-of-plane modes!) however indicates the out-of-plane distortion to be minor. We hope to probe the distortion more directly by measuring $^{13}$C-ENDOR on ringsubstituted $^{13}$C-PBQ-$h_4$ isotopes. Preliminary $^{13}$C-ENDOR experiments on one of the $^{13}$C-PBQ-$h_4$ isotopes indeed show that we can certainly complete such a study.

Next to the structural information of the PBQ-$h_4$ molecule in its lowest excited triplet state that is obtained from the proton ENDOR study, we are also able to discuss some qualitative features of the spin-density distribution in this state. From table 2 we calculate the isotropic proton hyperfine interaction constant (h.i.c.) to be +9.6 MHz. Venkataraman et al. [14] have measured the corresponding hyperfine constant of the PBQ-$h_4$ negative ion and found it to be −6.7 MHz. If correlation effects between the unpaired electrons are assumed to be small, which was shown to be the case for the naphthalene lowest excited triplet state [15], we can calculate from the above data the unpaired n-electron density at the protons in the zero-point level of the lowest triplet state in PBQ-$h_4$. Assuming for calculation purposes a planar structure for the PBQ-$h_4$ molecule in its lowest triplet state and its reduced form (negative ion), the isotropic proton h.i.c. for the lowest triplet state can be expressed by the following McConnell type relation:

$$a_H = \tfrac{1}{2}\,(a_H^{(-)} + \rho_H^n\, Q_0), \qquad (6)$$

werein $a_H^{(-)}$ is the isotropic h.i.c. for the negative ion and $\rho_H^n$ is the unpaired n-electron spin density at the proton and $Q_0$ a constant that is 1420.4 MHz [16].

With eq. (6) and the hyperfine data quoted (vide retro) we calculate $\rho_H^n$ is $1.8 \times 10^{-2}$. The proton ENDOR measurements thus provide in this case direct evidence for the suggested delocalization of the unpaired n-electron density throughout the molecular frame [17]. The anisotropic part of the proton hyperfine interaction in the lowest triplet state of PBQ-$h_4$ is determined by the total spin-density distribution in this state. A manifestation hereof is the observed $15 \pm 2^\circ$ rotation of the largest principal value of the hyperfine-interaction tensor versus the C–H ground state bond direction [18]. We are now pursuing $^{13}$C- and $^{17}$O-ENDOR measurements to completely solve the spin-density distribution in the zero-point level of the lowest triplet of PBQ-$h_4$. We are also engaged in a proton ENDOR study of the lowest triplet state in PBQ-$dh_3$, -2,6-$d_2h_2$, -$d_3h$ and -$CH_3$ in the hope of obtaining a better insight in the cause and consequences of the non-Born–Oppenheimer effects that we observe in the lowest $n\pi^*$ triplet state of PBQ.

In a following paper we will report the results of all these ENDOR experiments and compare the results with theoretical calculations of the spin density distribution in the lowest triplet state of PBQ.

## 5. Cross relaxation nuclear double resonance (CRENDOR)

An important advantage of ENDOR experiments

over EPR hyperfine measurements is that, knowing the electron spin state wherein the nuclear transitions occur one can determine directly the absolute sign of the hyperfine coupling constants. In PBQ-$h_4$ we observe stron ENDOR transitions on the EPR low field ($\langle 0| \leftrightarrow |-1\rangle$) line and weak ENDOR transitions on the high field ($\langle +1| \leftrightarrow |0\rangle$) line. However, both set of transitions are found on the same side of the free proton ENDOR signal and thus occur in the same electron spin state. Although one would guess from intensity considerations that the ENDOR transitions observed were due to nuclear spin flips in the $|-1\rangle$ state (strong field approximation), definite proof for this assumption was lacking.

We have however obtained such proof from the observation of r.f. induced changes in the cross relaxation signal, where the electron spin state, in which the nuclear spin flips were induced, was known.

For a magnetic field parallel to the $z$-axis of one of the PBQ-$h_4$ molecules in the unit cell, at a field value that corresponds to $\sim \frac{1}{2} D$ the energy gap between the $|0\rangle$ and $|+1\rangle$ electron spin levels (high field approximation) is identical to the Zeeman splitting in a doublet spin system. At this point cross relaxation [19] (population exchange) between the triplet excited molecule and this doublet spin system can occur which is observed as an increase in the phosphorescence intensity from the PBQ-molecule monitored (see fig. 2). As cross relaxation is a nuclear spin conserving process, the transitions in the triplet and radical spin system thus take place between electron spin states of the same nuclear spin configuration. If for some reason (e.g., temperature) the population of the nuclear spin states is different, r.f. induced nuclear spin flips will change the population of the cross relaxing electron-nuclear spin state and thus modulate the cross relaxation signal intensity. The results of such an experiment are also shown in fig. 3 and as we know now that these nuclear spin flips must occur in the $|+1\rangle$ electron spin state the results are unambiguous. This CRENDOR experiment thus shows that the ENDOR transitions that we observe (see also fig. 3) indeed occur in the $|-1\rangle$ electron spin state as was guessed. An angular dependent CRENDOR study can be made in the case of PBQ-$h_4$ and the results obtained are in very good agreement with those predicted on basis of the results of our ENDOR experiments.

This new CRENDOR technique may thus be helpful in obtaining additional information regarding hyperfine interactions in excited states. We expect such r.f. induced nuclear spin flips also to be observable in the doublet spin system.

## 6. Experimental

The $p$-benzoquinone isotopic mixed crystals were grown from a Bridgeman furnace and cleaved or cut with a sharp razor blade in the desired direction.

Optical detection of EPR and ENDOR was accomplished as follows: The PBQ crystal was mounted against a rotatable quartz light pipe inside a quartz cold finger tip glass dewar of the type used by Hornig et al. [20], and excited with a 1000 watt Xenon lamp through the bottom of the cavity. The excitation light was filtered by the Corning filters 4-72 and 7-54 and the total phosphorescence output was detected through a Corning filter 3-71 by a Philips 150 UVP photomultiplier. Field measurements were made using an AEG proton flux meter, while EPR frequency measurements were made with an HP 340B transfer oscillator, a 30 MHz Dymec transfer oscillator synchronizer and an HP 5245 L electronic counter. Measurements below 750 gauss were not possible due to lack of a probe in this area. The ENDOR set up used, basically consisted out of a Varian-E9 EPR spectrometer and a HP 8601 A (100 kHz–110 MHz) sweep generator. The output of the HP 8601 A was amplified by an IFI M 5000 wide band amplifier (max. output 10 watt) and fed into the ENDOR coil that was in series with a 50 Ω terminating resistor.

The ENDOR coil mounted inside the dewar consisted out of three windings in the center of which was the sample. Optimum ENDOR signals were obtained through 1 kHz FM modulation of the r.f. source while using a microwave power of 2-10 mW. At 4.2 K optical detection of EPR signals of the g-inversion level was just possible, but all the ENDOR experiments on the g-inversion level reported here were performed at $\sim$ 1.8 K.

## 7. Summary and conclusions

This paper contains the results of EPR and proton ENDOR experiments on the lowest inversion levels

of the *p*-benzoquinone-$h_4$ triplet state in an isotopic mixed crystal.

An interesting conclusion of the present study is that the molecule in its lowest excited state is non-planar, much like what would be expected if *p*-benzoquinone would be considered as a formaldehyde dimer.

Our experiments further show that the deuteration effects observed on the fine-structure and *g*-tensor principal values are due to the widely different values that these parameters attain in both inversion levels.

The proton ENDOR experiments have also shown the expected delocalization of the n-electron density throughout the molecular frame to occur.

Finally we expect the reported CRENDOR effects occasionally to be a useful tool in the study of hyperfine interactions in excited states.

We consider the results reported here a first step towards our goal of a better understanding of the pseudo Jahn–Teller effects that occur in the lowest triplet state of *p*-benzoquinone. In a forthcoming paper (part III of this series) we will present additional results of proton, carbon-13 and oxygen-17 ENDOR experiments on isotopic species of *p*-benzoquinone.

## References


[1] R.L. Fulton and M. Gouterman, J. Chem. Phys. 35 (1961) 1059; 41 (1964) 2280;
M. Gouterman, J. Chem. Phys. 42 (1965) 351.

[2] R.M. Hochstrasser and C.A. Marzzacco, in: Molecular Luminescence, ed. E.C. Lim (Benjamin, New York, 1969) p. 631.

[3] R.M. Hochstrasser, L.W. Johnson and H.P. Trommsdorff, Chem. Phys. Letters 21 (1973) 251;
H. Veenvliet and D.A. Wiersma, Chem. Phys. Letters 22 (1973) 87.

[4] H. Veenvliet and D.A. Wiersma, Chem. Phys. Letters 33 (1975) 305.

[5] H. Veenvliet and D.A. Wiersma, J. Chem. Phys. 60 (1974) 704.

[6] H. Veenvliet and D.A. Wiersma, Chem. Phys. 8 (1975) 432.

[7] J. Trotter, Acta Cryst. 13 (1960) 86.

[8] B.N. Taylor, W.H. Parker and D.N. Langenberg, Rev. Modern Phys. 41 (1969) 375.

[9] M. Sharnoff and E.B. Iturbe, J. Chem. Phys. 62 (1975) 145.

[10] M. Batley and R. Bramley, Chem. Phys. Letters 15 (1972) 337.

[11] G. Feher, Phys. Rev. 103 (1956) 500, 834. For a recent review article on ENDOR see:
A.L. Kwiram, Ann. Rev. Phys. Chem. 22 (1971) 133.

[12] C.A. Hutchison and G.A. Pearson, J. Chem. Phys. 43 (1965) 2545; 47 (1967) 520.

[13] G.W. Robinson and V.E.Di Giorgio, Can. J. Chem. 36 (1958) 31;
V.E.Di Giorgio and G.W. Robinson, J. Chem. Phys. 31 (1954) 1678.

[14] B. Venkataraman, B.G. Segal and G.K. Fraenkel, J. Chem. Phys. 30 (1959) 1006.

[15] P. Ehret and H.C. Wolf, Z. Naturforsch. 23A (1968) 1740.

[16] F.M. Pipkin and R.H. Lamberts, Phys. Rev. 127 (1962) 3, 787.

[17] R. Hoffman and J.R. Swenson, J. Phys. Chem. 74 (1970) 415.

[18] P. Diehl and C.L. Khetrapal, Mol. Phys. 14 (1968) 327.

[19] W.S. Veeman and J.H. van der Waals, Chem. Phys. Letters 7 (1970) 65.

[20] A.W. Hornig and J.S. Hyde, Mol. Phys. 6 (1963) 33.

"Discovering a new technique
is the dream of a scientist".

CHAPTER 4

# OPTICAL NUCLEAR POLARIZATION IN THE EXCITED STATE THROUGH CROSS-RELAXATION AND ITS USE IN THE STUDY OF THE CARBON-13 HYPERFINE COUPLING IN THE LOWEST TRIPLET STATE OF 1-$^{13}$C-*p*-BENZOQUINONE

Jan H. LICHTENBELT, Jan G.F.M. FREMEIJER and Douwe A. WIERSMA
*Laboratory for Physical Chemistry, University of Groningen, Zernikelaan, Paddepoel, Groningen, The Netherlands*

In this paper the phenomenon of optical nuclear polarization in the excited state through cross-relaxation is described. It is shown that when the populating and depopulating rates of the triplet spin sublevels are known the absolute nuclear polarizations can be calculated and that optical detection of the nuclear alignment in at least one electron spin state is quite often feasible.

The paper further deals with the magnetic resonance properties of the lowest triplet state in 1-$^{13}$C-*p*-benzoquinone whereof the zero-field splitting parameters and carbon-13 hyperfine data are reported. The carbon-13 hyperfine data, obtained by optical detection of ENDOR and CRENDOR, indicate that in the lowest $n\pi^*$ triplet state of *p*-benzoquinone the $\pi$-electron spin density at the carbonyl carbon and oxygen are about equal while the remaining carbon atoms carry about half this spin density.

## 1. Introduction

The phenomenon of nuclear spin polarization in the ground state through optical pumping has been the subject of several studies in the past decade [1]. The effect originates from the combination of electron spin-selective intersystem crossing and hyperfine interaction.

The presence of nuclear spin alignment in triplet excited states is naturally of great interest as it may enable us to detect nuclear transitions with greatly enhanced sensitivity.

In a previous paper [2] we showed that a very high degree of nuclear spin polarization can be achieved at the cross-relaxation magnetic field of a triplet excited molecule and a doublet spin system. In the present paper we describe and analyze this effect in greater detail.

We further report usage of the effect to obtain the hyperfine coupling tensor of the carbonyl $^{13}$C nucleus in the lowest triplet state of 1-$^{13}$C-*p*-benzoquinone-$h_4$ and discuss the implications of this measurement towards the geometry of and spin density distribution in this state of the molecule.

## 2. Nuclear spin polarization through cross-relaxation

Veeman et al. [3,4] recently described and analyzed in detail the level anticrossing (LAC) and cross-relaxation (CR) effects that occur in phosphorescent organic crystals.

One of the conclusions reached was that these effects might possibly be used to achieve nuclear spin alignment in triplet excited states of molecules.

In the course of our EPR and ENDOR experiments on the lowest triplet state of PBQ [2] we found clear evidence that at least CR produces a high degree of nuclear spin polarization.

This nuclear alignment was optically detected through observation of radio frequency induced changes of the phosphorescence cross-relaxation signal and this new technique was named CRENDOR, an acronym for cross relaxation nuclear double resonance. In this note we will further analyze the cross-relaxation effect at 1.8 K between a triplet excited *p*-benzoquinone-carbonyl-$^{13}$C (1-$^{13}$C-PBQ-$h_4$) molecule and a photochemically produced radical both as guests in a PBQ-$d_4$ host lattice.

For the moment we will only consider the $^{13}$C nuclear spin in the triplet state and a doublet electron-spin sys-

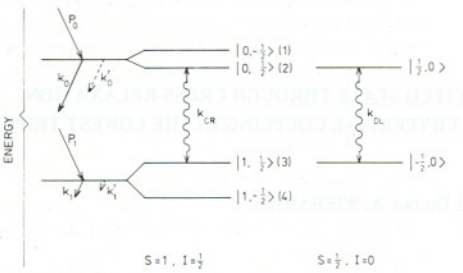


Fig. 1. Energy level scheme at cross-relaxation of a system consisting out of a triplet state spin system with a nuclear spin $\frac{1}{2}$ ($S = 1$, $I = \frac{1}{2}$) and a doublet spin system ($S = \frac{1}{2}$, $I = 0$) for a magnetic field along the fine-structure $z$-axis. Note that $D$ is negative. $P$ stands for populating rate, $k$ for total decay rate, $k^r$ for radiative decay rate, $k_{cr}$ for cross-relaxation rate and $k_{dl}$ for spin–lattice relaxation rate.

tem without nuclear spins. This model is realistic in the sense that in the doublet electron-spin system no nuclear alignment is observed (vide infra).

For a magnetic field parallel to the principal $z$-axis of the fine-structure tensor, which coincides with the long molecular ($z$) axis of 1-$^{13}$C-PBQ-$h_4$, the cross-relaxation situation sketched in fig. 1 is reached at a magnetic field of ~386 gauss.

First consider the situation outside the crossing region, where the two spin systems are uncoupled.

As spin–lattice relaxation at 1.8 K among the triplet spin components is slow compared to all decay constants [2], the steady state populations $N_0$ and $N_1$ of the $|0\rangle$ and $|+1\rangle$ triplet spin sublevels are only determined by the populating ($P$) and decay ($k$) rates as follows:

$$N_0/N_1 = P_0 k_1/P_1 k_0. \qquad (1)$$

In the specific case of PBQ the populating rates are unknown, but as feeding of the triplet spin system occurs via the host exciton band, we imagine that $P_0$ and $P_1$ are almost identical, which implies [5] that

$$N_0/N_1 = k_1/k_0 = \tfrac{1}{2}(k_x + k_y)/k_z = \tfrac{1}{30}.$$

Outside the crossing region the electron spin system thus is strongly polarized. Note however that the ratio $P_0 k_1/P_1 k_0$ is dependent of the magnetic field orientation and this directly determines the maximum attainable electron spin polarization.

The spin system of the stable photochemically produced radical is outside the crossing region most likely in Boltzmann equilibrium with the lattice.

When the two spin systems are brought into contact with each other at the cross-relaxation field then what happens depends on the relative magnitudes of the different rate constants of the coupled systems. Veeman et al. [4] showed that when cross-relaxation is described as a contact between heat reservoirs of different temperatures, a permanent change of the phosphorescence intensity due to CR, as observed in PBQ, only occurs if the following inequality holds:

$$k_1 < k_{cr} < k_{dl}.$$

Herein $k_1$ is the decay rate of the $|+1\rangle$ triplet state level, $k_{cr}$ the CR rate between the triplet and doublet spin system and $k_{dl}$ the spin–lattice relaxation rate of the doublet spin system. In this case CR effectively induces spin-lattice relaxation among the triplet spin sublevels.

This process however is only nuclear spin selective when also the following relation holds: $k_{cr} < 2\pi\Delta\nu_N$; whereby $\Delta\nu_N$ is the energy difference between the nuclear spin states of the same electron spin level. This inequality assures that the nuclear spinstates are not within the uncertainty energy-width of the cross-relaxation process. In only that case, and assuming slow nuclear spin–lattice relaxation, we succeed in converting the electron spin polarization into nuclear polarization. With reference to fig. 1 we calculate (ignoring the Boltzmann factor) for the steady state populations of the different hyperfine levels at low temperature:

$$N_1 = P_0/k_0, \qquad (2a)$$

$$N_2 = [k_1 P_0 + k_{cr}(P_0 + P_1)]/[k_1 k_0 + k_{cr}(k_0 + k_1)], \qquad (2b)$$

$$N_3 = [k_0 P_1 + k_{cr}(P_0 + P_1)]/[k_1 k_0 + k_{cr}(k_0 + k_1)], \qquad (2c)$$

$$N_4 = P_1/k_1. \qquad (2d)$$

When $k_{cr} \gg k_1, k_0$ one calculates for the phosphorescence intensity change induced by CR from eqs. (2):

$$\Delta I = [(P_0 + P_1)/(k_0 + k_1)]\,(k_0^r + k_1^r) - (P_0/k_0)\,k_0^r - (P_1/k_1)k_1^r, \qquad (3)$$

whereby $k_0^r$ and $k_1^r$ are the radiative constants of the $|0\rangle$ and $|+1\rangle$ spin sublevels.

For PBQ it is further known [5] that $k_0 \gg k_1$ which

implies that $\Delta I$ becomes:

$$\Delta I = P_1\left(\frac{k_0^r + k_1^r(1+P_0/P_1)}{k_0} - \frac{k_1^r}{k_1}\right). \quad (4)$$

Under the same condition $k_{cr} \gg k_0, k_1$ we calculate for the absolute nuclear polarization (ANP) defined as $|N_i - N_j|/(N_i + N_j)$, in the $|0\rangle$ and $|+1\rangle$ electron spin level respectively the following:

$$|k_0 P_1 - k_1 P_0| / [k_0(2P_0 + P_1) + k_1 P_0] \quad (5a)$$

and

$$|k_0 P_1 - k_1 P_0| / [k_1(2P_1 + P_0) + k_0 P_1]. \quad (5b)$$

For a magnetic field along the fine-structure $z$-axis of PBQ and assuming $P_0 = P_1$ we find, using the fact that $k_1/k_0 = \frac{1}{30}$:

$\mathrm{ANP}_{|0\rangle} = 29/91$ and $\mathrm{ANP}_{|+1\rangle} = 29/33$.

CR in the case of PBQ thus produces a high degree of nuclear spin polarization especially in the $|+1\rangle$ electron spin level for a magnetic field parallel $z$.

This nuclear spin alignment was previously detected [2] through observation of radio frequency induced changes in the CR effect of PBQ and we will now proceed by calculating the expected change of the CR effect. Consider therefore the effect of a strong rf field that is resonant with a nuclear transition in the $|+1\rangle$ electron spin state. CR than effectively occurs between the levels 2 and 3,4 of fig. 1 and produces a change in the steady state populations. Assuming again $k_{cr}$ to greatly exceed $k_0$ and $k_1$ we calculate in this situation the following steady state populations:

$$N_1 = P_0/k_0, \quad (6a)$$

$$N_2 = N_3 = N_4 = (P_0 + 2P_1)/(k_0 + 2k_1). \quad (6b)$$

The phosphorescence intensity change of the CRENDOR effect is then calculated to be:

$$\Delta I = [(P_0+2P_1)/(k_0+2k_1)]\ (k_0^r+2k_1^r)$$

$$-[(P_0+P_1)/(k_0+k_1)]\ (k_0^r+k_1^r) - (P_1/k_1)k_1^r. \quad (7)$$

Utilizing the fact that $k_0 \gg k_1$ in PBQ $\Delta I$ is found to be:

$$\Delta I = P_1\left(\frac{k_0^r + k_1^r(3+P_0/P_1)}{k_0} - \frac{k_1^r}{k_1}\right). \quad (8)$$

Comparison of this expression with eq. (4) shows that the CRENDOR effect in the $|+1\rangle$ electron spin state even *exceeds* the CR effect. Using the same approximations we calculate for the CRENDOR effect in the $|0\rangle$ electron spin state:

$$\Delta I = -P_1 k_1^r / 2k_0. \quad (9)$$

It is interesting to note here that, despite considerable effort, we have so far only been able to detect these CRENDOR transitions in the $|+1\rangle$ electron spin state of PBQ.

This could be due to either a negligible value of $\Delta I$ in (9) or to the fact that the relation $k_{cr} < 2\pi\Delta\nu_N$ no longer holds. Unfortunately in the case of PBQ the radiative rate constants are unknown so we cannot decide in this matter.

So far in the analysis of the CRENDOR effect we have assumed that the relation $k_{cr} \gg k_0, k_1$ holds. As yet we have not been able to verify this, but an upper estimate of $k_{cr}$ may be obtained from our CRENDOR spectra where the lowest observed transition is found at 6 MHz. This ascertains that $k_{cr} < 2\pi \times 6$ MHz. As $k_{cr}$ is directly related to the intermolecular interaction between the cross-relaxing species one expects of course a whole range of $k_{cr}$ values. As shown in fig. 3, we indeed observe a change in the phosphorescence intensity of PBQ crystals in a magnetic field from zero up to $\sim$ 760 gauss and the "sharp" CR resonance on this broad feature then must be due to CR between a triplet species and specific non-neighbour doublet spin-systems. The quoted upper limit for $k_{cr}$ and the nuclear spin polarizations calculated thus only refer to the "sharp" CR signal at 386 gauss in fig. 3. So far we have not concerned ourselves with the effect of cross-relaxation on possible nuclear spin polarization in the doublet spin system. Veeman et al. (4) showed that in order not to saturate the CR effect one demands $k_{cr} \lesssim k_{dl}$ which results in a negligible nuclear polarization in the doublet species. In conclusion of this section we state that analysis of the CR effect shows that, knowing the populating and depopulation rates of a triplet spin system, one can easily calculate the induced absolute nuclear spin polarizations. The possibility of optical detection of this nuclear alignment however critically depends on the ratio between the radiative and non-radiative decay constants of the system.

### 3. Angular dependence of the cross-relaxation field

In PBQ, and most likely in many other molecules, the nuclear polarization induced by CR can be optically detected and used to obtain excited state hyperfine parameters.

To fully exploit the possibilities of this new CREN-DOR technique the angular dependence of the cross-relaxation field needs to be known and in this section we therefore examine the energy-match between a triplet and doublet spin system in greater detail.

The energy of the triplet electron spin states is in first approximation determined by the spin hamiltonian:

$$\mathcal{H}_t = \beta_e \boldsymbol{H} \cdot \mathbf{g}_t \cdot \hat{\boldsymbol{S}} - (X\hat{S}_x^2 + Y\hat{S}_y^2 + Z\hat{S}_z^2), \qquad (10)$$

whereby $X$, $Y$ and $Z$ are the energies of the three spin sublevels in zero-field and the $\mathbf{g}_t$ tensor in general is anisotropic. For the doublet spin-system the energies are determined by the Zeeman-term only:

$$\mathcal{H}_d = \beta_e \boldsymbol{H} \cdot \mathbf{g}_d \cdot \hat{S}. \qquad (11)$$

To match the energy difference in the doublet spin system with one of the energy gaps in the triplet spin system the following third degree polynom in $H^2$ determines the CR magnetic field:

$$\begin{aligned}&(\beta_e^2 H^2)^3 [(4g_t^2 - g_d^2)(g_t^2 - g_d^2)^2] \\ &- (\beta_e^2 H^2)^2\, 3[A(4g_t^2 - 2g_d^2)(g_t^2 - g_d^2) + 9F'^2] \\ &+ (\beta_e^2 H^2)\, 3[A^2(4g_t^2 - 3g_d^2) + 18BF'] \\ &- (4A^3 + 27B^2) = 0. \qquad (12)\end{aligned}$$

In eq. (12) the following definitions have been used:

$$g_i = (I^T \cdot \mathbf{g}_i \cdot \mathbf{g}_i^T \cdot I)^{1/2}, \quad i = t, d,$$

$$F' = I^T \cdot \mathbf{g}_t \cdot \mathbf{F} \cdot \mathbf{g}_t^T \cdot I,$$

whereby $\mathbf{F}$ is the fine structure tensor, with eigenvalues $X$, $Y$ and $Z$;

$$H = IH,$$

with $I$ the unit magnetic field vector;

$$A = (XY + XZ + YZ), \qquad B = (XYZ).$$

Note that $\mathbf{g}_d$, $\mathbf{g}_t$, $\mathbf{F}$ and $I$ should be defined with respect to the same axis system.

For most organic molecules $g_t \approx g_d$ which ensures that one root of eq. (12) will greatly exceed the other two. Physically this means that CR then occurs between Zeeman states, where the difference in $g$-values compensates for the zero-field splitting in the triplet spin system. However only the real root of eq. (12) at low magnetic fields is the physically interesting one and we now proceed by assuming that $g_t = g_d$. An analytic solution of this simplified equation can only be obtained if in addition we assume $X = Y$. In that case the cross-relaxation field ($H_{cr}$) is calculated to be:

$$H_{cr} = \frac{1}{2g\beta_e}\left|\frac{Z}{3I_z^2 - 1}\right| [3(4I_z^2 - 1)]^{1/2}, \qquad (13)$$

where $I_z$ is the $z$-component of $I$ in the fine-structure axis system.

This expression for $H_{cr}$ shows that $H_{cr} \to \infty$ at the magic angle and that cross-relaxation no longer occurs when the angle between the magnetic field and the $z$-axis of the fine-structure-tensor exceeds 60°. Fig. 2 shows the angular dependence of the cross-relaxation

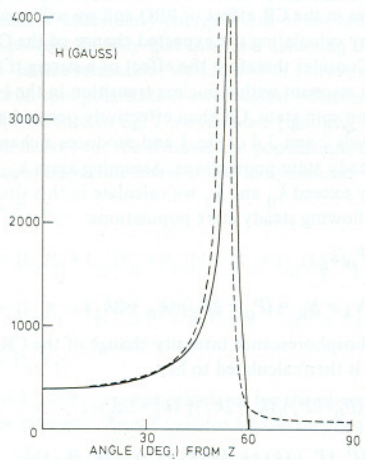


Fig. 2. Cross-relaxation field of a triplet–doublet spin system versus angle of rotation in the $xz$ principal plane of the triplet state spin system. At zero degrees the magnetic field is along the $z$-axis of the fine-structure tensor. For the solid curve $D = -2174$ MHz, $E = 0$ and $g_t = g_d = g_e$ while for the dashed curve $g_d = g_e$ and for the triplet state species the fine structure and $g$-tensor values for 1-$^{13}$C-PBQ-$h_4$ of table 1 were taken.

field in this simple case. In fig. 2 we have further included an example where $X \neq Y \neq Z$ which requires numerical solution of eq. (12).

Finally it should be realized that at the low fields where CR occurs in these organic solids a first order solution of the CRENDOR transition frequency, as is custumory in the treatment of the high field ENDOR data [6], is no longer warranted.

In the case of 1-$^{13}$C-PBQ-$h_4$ we therefore extracted the $^{13}$C hyperfine coupling constants from the CRENDOR data through diagonalization of the 6 by 6 interaction matrix resulting from a spin $S = 1$ and $I = \frac{1}{2}$ system. The hamiltonian describing this system is

$$\mathcal{H} = \beta_e \boldsymbol{H} \cdot \mathbf{g} \cdot \hat{\boldsymbol{S}} - (X\hat{S}_x^2 + Y\hat{S}_y^2 + Z\hat{S}_z^2)$$

$$+ \hat{\boldsymbol{I}} \cdot \mathbf{A} \cdot \hat{\boldsymbol{S}} - g_n \beta_n \boldsymbol{H} \cdot \hat{\boldsymbol{I}}. \qquad (14)$$

Finally we note that the difference in CRENDOR transition frequency calculated from a first order and exact treatment of the spin-hamiltonian of eq. (14) for 1-$^{13}$C-PBQ-$h_4$ amounts to 35 kHz. This is 3.5 times the standard deviation of each measured frequency and therefore exact solution of the energies is preferred.

## 4. Optically detected EPR, ENDOR and CRENDOR of 1-$^{13}$C-PBQ-$h_4$

In a recent paper [2] we reported the results of an optically detected EPR and proton ENDOR study of PBQ-$h_4$ in a PBQ-$d_4$ host crystal at 1.8 K. The results showed that the molecule in the excited state is somewhat distorted, into most likely a chair form, and that the unpaired n-electron density is not completely localized at oxygen. We further reported the unprecedented large effects of mono-deuteration on both the fine-structure parameters and $g_{zz}$ value of PBQ-$h_4$ and explained this as arising from mixing of the lowest inversion levels in the triplet state of PBQ-$h_4$ [5,7].

These unusual features of PBQ motivated us to a detailed study of some isotopic species of PBQ and in this paper we report and discuss the magnetic resonance properties of 1-$^{13}$C-PBQ-$h_4$, where one of the carbonyl carbons is a carbon-13 nucleus, as guest in a PBQ-$d_4$ host crystal at 1.8 K.

In connection with the nuclear spin polarization effects discussed in a previous section, we note here that the hyperfine coupling of the carbon-13 nucleus only could be obtained by performing next to ENDOR also CRENDOR experiments. In order to extract from these experiments the carbon-13 hyperfine coupling parameters the fine-structure parameters and $g$-tensor of 1-$^{13}$C-PBQ-$h_4$ need to be known. These data were obtained from angular dependent EPR measurements performed and analyzed as previously [2] reported. As in case of PBQ-$h_4$ [2] a 5° out-of-plane rotation of the $y$-axis of the fine-structure tensor was observed and table 1 contains the fine-structure parameters where for comparison we have also included the analogous data of PBQ-$h_4$.

Table 1
Fine-structure parameters and $g$-tensor principal values in the lowest triplet state of $p$-benzoquinone-$h_4$ [2] and 1-$^{13}$C-$p$-benzoquinone-$h_4$ as quests (1 mol%) in $p$-benzoquinone-$d_4$ at 1.8 K as obtained from high field optically detected EPR measurements

| | 1-$^{13}$C-PBQ-$h_4$ | PBQ-$h_4$ |
|---|---|---|
| $D$ (MHz) | −2174 ± 1.5 | −2051 ± 1 |
| $E$ (MHz) | 115 ± 1 | 115 ± 1 |
| $g_{xx}$ | 2.0053 ± 0.0010 | 2.0045 ± 0.0005 |
| $g_{yy}$ | 2.0043 ± 0.0010 | 2.0035 ± 0.0005 |
| $g_{zz}$ | 2.01026 ± 0.00010 | 2.00994 ± 0.00008 |

The increase in the $|D|$ and $g_{zz}$ parameter on carbon-13 isotopic substitution only is again surprisingly large and further supports the interpretation of these effects in terms of mixing of molecular [2,5,7] rather than crystal [8] states. The difference in the fine-structure parameter $|D|$ of the two isotopic species in fact is so large that this allows their seperate observation in the CR and LAC effect as is shown in fig. 3.

The carbon-13 hyperfine coupling parameters were obtained by performing ENDOR measurements on the $|\Delta m_s| = 1$ EPR transitions for the magnetic field in the molecular $(yz)$ plane and CRENDOR measurements in a perpendicular $(xz)$ plane. For a magnetic field along the molecular $z$-axis both ENDOR and CRENDOR transitions could be observed. However a 5°! out-of-plane rotation from this axis permitted no longer observation of the ENDOR transitions.

Fig. 4 shows the CRENDOR spectrum obtained for a magnetic field along the molecular $z$-axis. The single line at 17.6 MHz is due to a $^{13}$C-nuclear transition and the quadruplet of lines at 6.9 MHz is due to proton nuclear transitions in the $m_S = 1$ level.

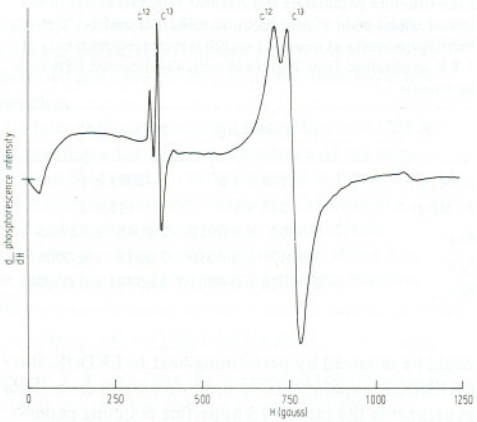


Fig. 3. Cross-relaxation (386 gauss) and level anticross effect (772 gauss) in the phosphorescence of $1^{13}$-C-*p*-benzoquinone-$h_4$ at 1.8 K for a magnetic field parallel to the molecular *z*-axis. Note the broad underlying cross-relaxation effect at low magnetic field.

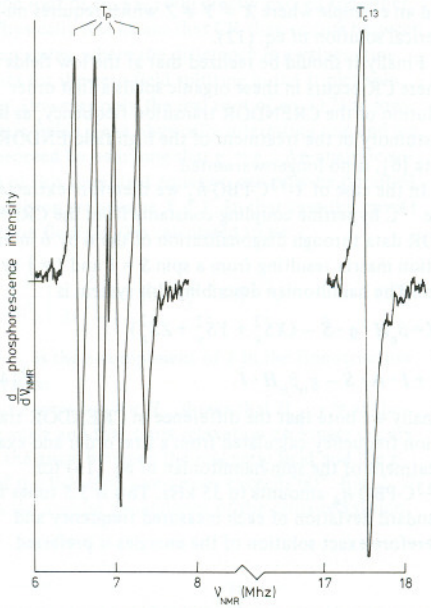


Fig. 4. Optical detection of the nuclear spin alignment at the cross-relaxation field (~ 386 gauss) (CRENDOR) in the lowest triplet state of 1-$^{13}$C-*p*-benzoquinone-$h_4$ as guest in *p*-benzoquinone-$d_4$ at 1.8 K. The magnetic field is oriented along the molecular *z*-axis of one of the PBQ molecules in the unit cell. The single line ($T^{13}_C$) is due to carbon-13 and the quadruplet ($T_p$) arises from the protons.

The observation of four proton CRENDOR lines shows that the introduction of a single $^{13}$C-nucleus in the carbonyl position leads to an observable loss of molecular (not crystal site) inversion symmetry. The coupling between the electronic and nuclear motions indeed must be very strong!

The angular dependence in the *xz* plane of the CR effect and of the carbon-13 CRENDOR difference frequency together with the computer fitted curves is shown in fig. 5.

The angular dependence in the *yz* plane of one of the EPR transitions ($\langle 0| \leftrightarrow |-1\rangle$) and the carbon-13 ENDOR sum frequency is shown in fig. 6.

The computer fittings of figs. 5 and 6 were obtained as follows: The angular dependence of the EPR effect was used to obtain the data of table 1.

The CR effect was calculated from the data in table 1 and eq. (12) whereby an isotropic $g_e$ value for the radical was assumed. The CRENDOR transition frequency was least squares fitted to the exact solution of eq. (14) together with the ENDOR transition frequency which was calculated from a first order expression given previously (eq. (5) of ref. [2]).

The carbon-13 hyperfine data obtained from these results are presented in table 2 and refer to the ground-state molecular axis system [9]. The absolute signs of the hyperfine elements were secured through observation of $^{13}$C ENDOR transitions on both the $|+1\rangle$ and $|-1\rangle$ electron spin states while in case of the $^{13}$C CRENDOR transition the electron spin state in which the nuclear transition occurred was known. We further note here that although coincidence of the *z*-principal axis of the $^{13}$C-hyperfine tensor with the carbonyl direction of PBQ in the groundstate is demanded by our experiments, a small out-of-plane rotation of the *y*-axis would have escaped detection in the present experiment. This is due to the fact that neither ENDOR nor CRENDOR spectra could be obtained for a magnetic field rotation in the *xy* molecular plane.

The implication of the alignment of the *z*-axis of the

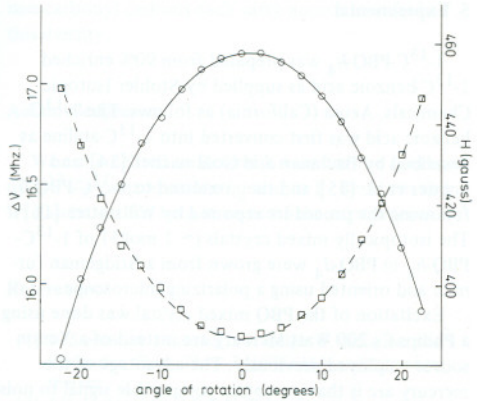


Fig. 5. Angular dependence of the cross-relaxation field (squares) and carbon-13 CRENDOR difference frequency (circles) for the lowest triplet state in 1-$^{13}$C-*p*-benzoquinone-$h_4$ at 1.8 K. The solid lines are computer fittings using the data displayed in tables 1 and 2. $\Delta\nu$ represents the difference between the measured carbon-13 CRENDOR frequency and the free carbon-13 frequency at the cross-relaxation field. The magnetic field is rotated in the (nearly) *xz* molecular plane and at zero degrees is (nearly) parallel to the long molecular *z*-axis.

Table 2
The carbon-13 hyperfine tensor principle values of the lowest triplet state in 1-$^{13}$C-*p*-benzoquinone-$h_4$ as guest in *p*-benzoquinone-$d_4$ at 1.8 K. The principal axis system of the $^{13}$C-hyperfine tensor coincides (within the accuracy of our measurements) with the ground state molecular axis system. The numbers between parentheses were obtained from ab initio calculations on PBQ [12]

| Experimental (MHz) | Isotropic part (MHz) | Anisotropic part (MHz) |
|---|---|---|
| $A_{xx} = -\ 2.7$ | | $A'_{xx} = +9.0\ (\ 7.54)$ |
| $A_{yy} = -15.15$ | $A_{iso} = -11.7$ | $A'_{yy} = -3.5\ (-3.55)$ |
| $A_{zz} = -17.26$ | | $A'_{zz} = -5.5\ (-3.99)$ |

$^{13}$C-hyperfine tensor with the groundstate carbonyl direction is that the excited state chairform [2] of PBQ has been reached through only out of plane displacement of the non-carbonyl carbon atoms. Our recently reported [2] proton-ENDOR measurements did not allow such a conclusion. The $^{13}$C-hyperfine tensor elements themselves contain information about the spin-density distribution in the excited state of the molecule.

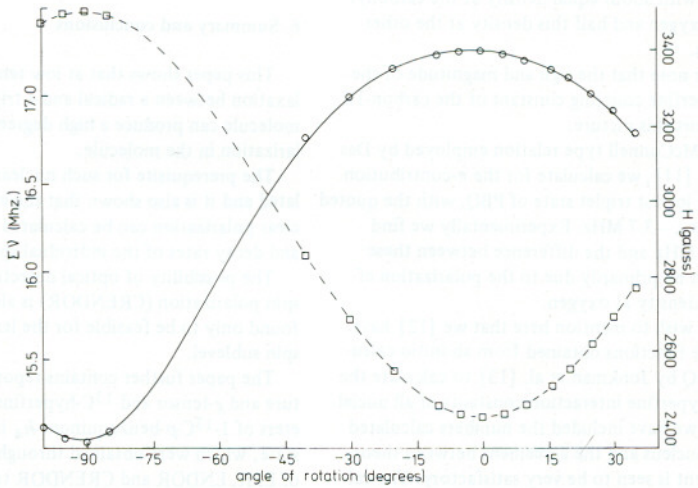


Fig. 6. Angular dependence of the EPR ($\langle 0| \leftrightarrow |-1\rangle$) transition field (squares) and carbon-13 ENDOR sum frequency (circles) for the lowest triplet state in 1-$^{13}$C-*p*-benzoquinone-$h_4$ at 1.8 K. The solid lines are computer fittings using the data displayed in tables 1 and 2. $\Sigma\nu$ represents the sum of the carbon-13 ENDOR frequency and the free carbon-13 frequency at the EPR transition field studied. The magnetic field is rotated in the (nearly) *yz* molecular plane and at zero degrees is (nearly) parallel to the long molecular *z*-axis.

From the fact that the pure anisotropic $^{13}$C-hyperfine elements are not far from a 2:−1:−1 ratio we conclude that the $\pi$-electron spin density residing at the $^{13}$C-nucleus itself is mainly responsible for the anisotropic hyperfine coupling.

For a spin-density of 1 at the $^{13}$C-nucleus the principal hyperfine elements are 128, −64 and −64 MHz [10] and this yields for the $\pi$-spin density at the carbonyl carbon ($\rho_1^\pi$) 0.14★. This is a lower limit for $\rho_1^\pi$ since the effect of n-spin density at oxygen will decrease the (absolute) values of the anisotropic hyperfine elements caused by $\rho_1^\pi$ and therefore $\rho_1^\pi \geqslant 0.14$. Das and Fraenkel [11] determined $\rho_1^\pi$ in the negative ion of PBQ to be between 0.15 and 0.18 depending on the solvent. Our measurements therefore indicate that correlation effects between the n and $\pi$ unpaired electrons indeed are small as assumed previously [2]. The non-carbonyl carbon $\pi$-spin density in the lowest triplet state of PBQ will therefore be quite close to its value (0.09) in the negative ion.

We then calculate for the $\pi$-spin density at oxygen $(\rho_7^\pi) \lesssim 0.18$. This means that in the lowest $n\pi^*$ triplet state of PBQ the electron excited out of the oxygen lone pair orbital into the $\pi^*$ orbital is delocalized over the molecule with about equal density at the carbonyl-carbon and oxygen and half this density at the other carbon atoms.

We further note that the sign and magnitude of the isotropic hyperfine coupling constant of the carbon-13 nucleus support this picture.

Using the McConnell type relation employed by Das and Fraenkel [11], we calculate for the $\pi$-contribution to $A_{iso}^C$ in the lowest triplet state of PBQ, with the quoted $\pi$-spin densities, −3.7 MHz. Experimentally we find $A_{iso}^C = -11.7$ MHz and the difference between these numbers must be primarily due to the polarization effect of the n-density at oxygen.

We finally wish to mention here that we [12] have used the wave functions obtained from ab-initio calculations on PBQ by Jonkman et al. [13] to calculate the anisotropic hyperfine interaction constants of all nuclei.

In table 2 we have included the numbers calculated for the $^{13}$C-nucleus and the agreement between theory and experiment is seen to be very satisfactory. The calculations and detailed discussion thereof will be presented in a future publication.

★ The total $\pi$-spin density is normalized to 1.

## 5. Experimental

1-$^{13}$C-PBQ-$h_4$ was prepared from 90% enriched 1-$^{13}$C-benzoic acid as supplied by Stohler Isotopic Chemicals, Azusa (California) as follows. The 1-$^{13}$C-benzoic acid was first converted into 1-$^{13}$C-aniline as described by Bachman and Goldmacher [14] and Snyder et al. [15] and then oxidized to 1-$^{13}$C-PBQ-$h_4$ following the procedure reported by Willstätter [16]. The isotopically mixed crystals (~ 1 mol%) of 1-$^{13}$C-PBQ-$h_4$ in PBQ-$d_4$ were grown from a Bridgeman furnace and oriented using a polarizing microscope.

Excitation of the PBQ mixed crystal was done using a Philips Cs 200 Watt Mercury arc instead of a Xenon source employed previously. The advantage of the mercury arc is that we obtain comparable signal to noise ratio in our experiments while less heating the sample. The concentration of the photochemically produced radicals was optimized by exciting the crystal at 4.2 K for about 5 minutes with the unfiltered output of the excitation source.

For further details on detection of EPR, ENDOR and CRENDOR ref. [2] should be consulted.

## 6. Summary and conclusions

This paper shows that at low temperature cross-relaxation between a radical and a triplet state excited molecule can produce a high degree of nuclear spin polarization in the molecule.

The prerequisite for such nuclear alignment is formulated and it is also shown that the exact degree of nuclear polarization can be calculated if the populating and decay rates of the individual spin sublevels are known.

The possibility of optical detection of this nuclear spin polarization (CRENDOR) is also examined and found only to be feasible for the least radiative electron spin sublevel.

The paper further contains report of the fine-structure and $g$-tensor and $^{13}$C-hyperfine coupling parameters of 1-$^{13}$C-$p$-benzoquinone-$h_4$ in its lowest triplet state, which were obtained through optical detection of EPR, ENDOR and CRENDOR transitions at 1.8 K.

From the $^{13}$C-hyperfine data it was concluded that in the lowest triplet state of $p$-benzoquinone the $\pi$-electron spin density distribution is such that the carbonyl carbon and oxygen carry about equal density while the

non-carbonyl carbons each carry approximately half this density.


## Acknowledgement

We are indebted to Berend Kwant for the synthesis of 1-$^{13}$C-*p*-benzoquinone-$h_4$ and to L. Benthem and W. Zandvoort for help in some of the experiments.


## References


[1] D. Stehlik, A. Doehring, J.P. Colpa, E. Callaghan and S. Kesmarky, Chem. Phys. 7 (1975) 165, and references therein.

[2] J.H. Lichtenbelt, J.G.F.M. Fremeijer, H. Veenvliet and D.A. Wiersma, Chem. Phys. 10 (1975) 107.

[3] W.S. Veeman and J.H. van der Waals, Chem. Phys. Lett. 7 (1970) 65.

[4] W.S. Veeman, A.L.J. van der Poel and J.H. van der Waals, Mol. Phys. 29 (1975) 225.

[5] H. Veenvliet and D.A. Wiersma, Chem. Phys. 8 (1975) 432.

[6] C.A. Hutchison and G.A. Pearson, J. Chem. Phys. 43 (1965) 2545; 47 (1967) 520.

[7] H. Veenvliet and D.A. Wiersma, Chem. Phys. Lett. 33 (1975) 305.

[8] B.H. Loo and A.H. Francis, J. Chem. Phys. 65 (1976) 5076.

[9] J. Trotter, Acta Cryst. 13 (1960) 86.

[10] W.V. Smith, P.P. Sorokin, I.L. Gelles and G.J. Lascher, Phys. Rev. 115 (1959) 1546.

[11] M.R. Das and G.K. Fraenkel, J. Chem. Phys. 42 (1965) 1350.

[12] J.H. Lichtenbelt, D.A. Wiersma, H.T. Jonkman and G.A. van der Velden, Chem. Phys. 22 (1977) 297.

[13] H.T. Jonkman, G.A. van der Velde and W.C. Nieuwpoort, Quantum Chemistry – The State of the Art, Proceedings of S.R.C. Atlas Symposium, No. 4 (1974) p. 243.

[14] G.B. Bachman and J.E. Goldmacher, J. Org. Chem. 29 (1964) 2576.

[15] H.R. Snijder, C.T. Elstom and D.B. Kellom, J. Am. Chem. Soc. 75 (1953) 2014.

[16] R. Willstätter and S. Dorogi, Ber. 42 (1939) 2147.

"It is wonderful to discover the physical meaning of (computer) numbers."

CHAPTER 5

# STRUCTURE AND DYNAMICS OF THE LOWEST TRIPLET STATE IN *p*-BENZOQUINONE. III. A STUDY OF THE n AND π SPIN-DENSITY DISTRIBUTION

Jan H. LICHTENBELT, Douwe A. WIERSMA
*Laboratory for Physical Chemistry, University of Groningen, Groningen, The Netherlands*

and

Harry T. JONKMAN and Gerrit A. VAN DER VELDE
*Laboratory for Theoretical Chemistry, University of Groningen, Groningen, The Netherlands*

The results of an ab-initio SCF calculation of the hyperfine coupling parameters in the $n\pi^*$ lowest triplet state of *p*-benzoquinone are reported and discussed. New results of a ring carbon-13 and oxygen-17 ENDOR study on the lowest triplet state of *p*-benzoquinone are also reported. Excellent agreement with experiment is obtained for the anisotropic hyperfine interaction constants which implies that the SCF description of the singly occupied orbitals is basically correct. The basic picture of the lowest triplet excited state spin-density distribution that is obtained from theory and experiment is, that the excited π-electron is delocalized over the molecule, while the n-electron is largely (≈75%) confined to the oxygen atoms. The effect of the delocalization of the n-electron however is clearly evident from the experiments.

## 1. Introduction

In the past couple of years there has been significant progress in the understanding of the spectroscopic properties of the lowest $n\pi^*$ states in *p*-benzoquinone (PBQ). Especially from the pioneering work of Trommsdorff [1] it became clear that the quinones are very special in the sense that their lowest optically accessible g and u $n\pi^*$ electronic states are only split by a few hundred wavenumbers. Moreover the lowest $n\pi^*$ states are quite isolated from higher excited states of the molecule. These features then make the *p*-benzoquinones unique candidates for a detailed study of the effect of pseudo Jahn–Teller coupling among near degenerate states.

The qualitative effect of such a near degeneracy is well understood [2] but a quantitative understanding of the details of the optical spectra in the quinones has not been obtained yet.

In our laboratory we have made special study of the lowest $n\pi^*$ triplet state in PBQ and some of its isotopes.

The lowest triplet state of PBQ is attractive for a spectroscopic study as it shows sharp absorption and emission spectra and therefore the effect of electric [3] and magnetic [4] fields on these spectra can be analyzed in great detail. Also EPR and ENDOR spectra of this state of the molecule in mixed [5] and isotopically mixed [6,7] crystals may be obtained. Especially the ENDOR experiments give new information on the wavefunctions of the unpaired electrons which play a dominant role in the vibronic coupling process.

In part I of this series [6] we have reported on the spectroscopy of the lowest $n\pi^*$ triplet state in PBQ. In part II [7] the results of an EPR and proton-ENDOR investigation on this state were reported. In a recent paper [8] we reported the results of an ENDOR study on the carbonyl-carbon-13 hyperfine coupling in the same state. In the present paper (part III) we wish to report some new ENDOR data on the lowest triplet

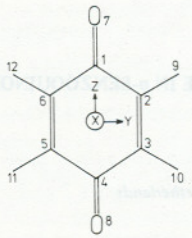


Fig. 1. Choice of axis system and numbering of the atoms in *p*-benzoquinone.

state of *p*-benzoquinone and to confront all the ENDOR data obtained so far [7,8] with the results of an ab-initio SCF calculation on PBQ.

It will be shown that the ab-initio molecular orbitals for the unpaired n and $\pi$-orbitals yield hyperfine interaction constants that compare very favourably with the experimentally observed ones. From this fact it is concluded that the SCF description of the singly occupied orbitals is basically correct.

The ab-initio results are further decomposed into atomic contributions which gives a detailed insight into the various contributions to the hyperfine coupling. From these calculations the limitations of a purely semi-empirical analysis of the ENDOR data also becomes very clear.

## 2. Computational details

The ab-initio SCF calculation of the hyperfine coupling constant in the lowest $n\pi^*$ triplet state of PBQ were carried out with the program SYMOL [9] written by van der Velde. In the calculations the experimental geometry of the ground state of PBQ as reported by Trotter [10] was used and the atoms are numered as shown in fig. 1. The basis set used consisted of six s and three p gaussian type orbitals (GTO's) on the C and O atoms, and three s GTO's on the H atoms.

The basis functions were contracted to a double zeta basis and the orbital exponents and the contraction coefficients used are identical to those previously employed by Jonkman et al. [11] in their calculation of the excitation energies of PBQ.

The main error in the present spin-density calculation probably stems from the neglect of all correlation (spin-polarization) effects. Especially the calculated spin-density of the s-orbitals on the carbonyl carbon and oxygen is zero, because both open shell orbitals have nodes on these atoms. For all other atoms both the isotropic and anisotropic hyperfine parameters are calculated. It should be noted that recently reported proton ENDOR [7] measurements on PBQ have shown that the molecule in the excited state is slightly distorted. A further complication, when comparing theory and experiments, arises from the fact that asymmetric isotopic substitution in PBQ is known to affect slightly the spin-density distribution in the lowest triplet state [6]. In the present calculation we have ignored these effects and assume that the molecule in the excited state preserves the full $D_{2h}$ symmetry.

## 3. Experimental

The isotopically mixed crystals of PBQ were grown in a Bridgeman furnace and cleaved or cut with a sharp razorblade in the desired direction. 7-$^{17}$O-PBQ-$h_4$ was prepared through exchange of the $^{16}$O-isotope with oxygen-17 enriched water (20%) in benzene, a procedure described by Becker et al. [12]. The enrichment of $^{17}$O in PBQ obtained, was found to be ca. 16% and mixed crystals with PBQ-$d_4$ were grown containing ca. 0.6 mol % of the $^{17}$O-PBQ isotope. The oxygen-17 enriched water was purchased from Stohler Isotopic Chemicals. 1, 2, 3, 5, 6-$^{13}C_5$-PBQ-$h_4$ was synethesized through oxidation of the corresponding aniline according to a procedure described by Willstätter and Dorogi [13].

In fact UL-$^{13}$C-analine (90 at%), also obtained from Stohler Isotopic Chemicals, was used in the synthesis. The ENDOR spectra of the oxidation product however clearly showed that the phosphorescing species in a PBQ-$d_4$ mixed crystal was the 1, 2, 3, 5, 6-$^{13}C_5$-PBQ-$h_4$ isotope. The UL-$^{13}$C-PBQ-$h_4$ species is either above or too close to the PBQ-$d_4$ host exciton band to act as a trap.

For further details of the ENDOR set-up we refer to previous reports of this laboratory on this subject [7,8].

Table 1
Fine-structure parameters and $g$-tensor principal values in the lowest triplet state of 1,2,3,5,6-$^{13}C_5$-PBQ-$h_4$ and 7-$^{17}$O-PBQ-$h_4$ as guests (≈ 1 mol %) in PBQ-$d_4$ at 1.8 K as obtained from high field optically detected EPR measurements

| | 1,2,3,5,6-$^{13}C_5$-PBQ-$h_4$ [a] | 7-$^{17}$O-PBQ-$h_4$ |
|---|---|---|
| $D$ (MHz) | −2236 (± 1.5) | ≈ −2051 |
| $E$ (MHz) | 116 (± 1.0) | ≈ 121 |
| $g_{xx}$ | 2.0053 (± 0.0010) | |
| $g_{yy}$ | 2.0043 ((± 0.0010) | |
| $g_{zz}$ | 2.01002 (± 0.00015) | ≈ 2.010 |

[a] Note that also in this PBQ isotope the fine-structure tensor is found to be ca. 5° rotated about the molecular $z$ axes. In the analysis of the EPR data it is further assumed that the $g$- and fine-structure tensor spatially coincide.

## 4. Results

### *4.1. EPR and ENDOR data*

Table 1 contains the fine-structure parameters and $g$-tensor principal values in the lowest triplet state of PBQ of those isotopically substituted species whereof we have obtained new ENDOR data. We will not comment on these parameters in this paper but it is interesting to note that the $D$ fine-structure parameter of 7-$^{17}$O-PBQ is virtually identical [7] to that of normal PBQ, while all other asymmetrically substituted PBQ's have significant different $D$ fine-structure parameters [6–8]. The hyperfine interaction parameters of all isotopes measured so far are displayed in table 2. The proton and carbonyl-carbon-13 ENDOR data have been previously reported but the non-carbonyl-carbon-13 and oxygen-17 data are new. Table 2 shows that for 7-$^{17}$O-PBQ we have only been able to determine the absolute value of the $y$-element of the oxygen hyperfine interaction constant.

The sign ambiguity in this case arises from the fact that this hyperfine element was obtained from high field EPR rather than ENDOR experiments. So far we have not been able to detect any fine structure on the EPR lines along the $x$ and $z$ magnetic field directions and therefore the $x$ and $z$ hyperfine elements are undetermined. We have also failed to detect oxygen ENDOR or CRENDOR transitions in 7-$^{17}$O-PBQ along any magnetic field direction. Further note that in $^{13}C_5$-PBQ the ortho non-carbonyl-carbon atoms ($C_2$, $C_3$) have different isotropic hyperfine interaction constants which shows that the spin-density distribution is sensitive to isotopic substitution.

### *4.2. Ab-initio SCF hyperfine interaction constants*

From the SCF triplet state wavefunction we have

Table 2
Measured and calculated hyperfine interaction parameters of $p$-benzoquinone in its lowest $n\pi^*$ triplet state. Note that all hyperfine interaction constants are given in MHz and that $\varphi_z$ is the angle between the oxygen–oxygen direction and the $z$-axis of the (local) hyperfine tensor in the molecular plane

| | Experimental | | | | | Ab-initio calculated [c] | | | | |
|---|---|---|---|---|---|---|---|---|---|---|
| | $A_{xx}$ | $A_{yy}$ | $A_{zz}$ | $\varphi_z$ | $A_{iso}$ | $A_{xx}$ | $A_{yy}$ | $A_{zz}$ | $\varphi_z$ | $A_{iso}$ |
| C1 | 9.0 | −3.5 | −5.5 | 0.0° | −11.7 | 7.54 | −3.55 | −3.99 | 0.0° | 0.00 |
| C2 [a] | 2.8 | 2.0 | −4.7 | −26° | 17.4 | 2.93 | 1.55 | −4.48 | −25.0° | 25.47 |
| C3 | 2.8 | 2.0 | −4.7 | 28° | 19.3 | 2.93 | 1.55 | −4.48 | 25.0° | 25.47 |
| O7 | | \|54.5\| | | ≈ 0° | | 2.61 | −35.30 | 32.69 | 0.0° | 0.00 |
| H9,11 [b] | −3.1 | 4.7 | −1.6 | 17.9° | 9.6 | −3.09 | 4.47 | −1.38 | 14.5° | 6.38 |
| H10,12 | −3.1 | 4.7 | −1.6 | −12.4° | 9.6 | −3.09 | 4.47 | −1.38 | −14.5° | 6.38 |

[a] The absolute numbering of C-2 or -3 is not known.
[b] The proton-hyperfine interaction parameters of $H_{10,12}$ are slightly different from those previously reported [7]. This is due to the fact that in the previous analysis of the ENDOR data, the sign of one of the off diagonal hyperfine tensor elements was chosen wrongly. Full report on these data will be given in a future publication [31].
[c] In the calculations we have used the following conversion factors for $g_e\beta_e g_n\beta_n$; 79.063 MHz Å$^3$ for hydrogen, 19.890 MHz Å$^3$ for carbon and −10.716 MHz Å$^3$ for oxygen, where the $g$-values are assumed to be isotropic.

Tabel 3

Decomposition of the hyperfine interaction parameters into atomic contributions. Values in parentheses are interference contributions and contributions of symmetry related atoms are taken together. All hyperfine values are in MHz and $\varphi_z$ is the angle between the oxygen–oxygen direction and the $z$ axis of the hyperfine tensor in the molecular plane

| | | $A_{xx}$ | $A_{yy}$ | $A_{zz}$ | $A_{zy}$ | $A_{iso}$ |
|---|---|---|---|---|---|---|
| (a) – C1 hyperfine interactions | | | | | | |
| C 2, 3, 5, 6 | "1s" | – 0.01 ( 0.02) | 0.01 (–0.02) | 0.00 ( 0.00) | 0.00 ( 0.00) | 0.00 ( 0.00) [a] |
| H9,10,11,12 | 1s | – 0.01 ( 0.02) | 0.02 (–0.05) | –0.01 ( 0.03) | 0.00 ( 0.00) | 0.00 ( 0.00) |
| C 2, 3, 5, 6 | "2s" | – 0.30 (–0.14) | 0.45 ( 0.29) | –0.15 (–0.15) | 0.00 ( 0.00) | 0.00 ( 0.00) [a] |
| C 2, 3, 5, 6 | $2p_z$ | – 0.01 ( 0.06) | 0.02 (–0.15) | –0.01 ( 0.09) | 0.00 ( 0.00) | 0.00 ( 0.00) |
| O7, 8 | $2p_y$ | – 1.76 ( 0.38) | – 0.94 (–0.54) | 2.70 ( 0.16) | 0.00 ( 0.00) | 0.00 ( 0.00) |
| C1, 4 | $2p_y$ | – 1.18 (–0.13) | 2.35 ( 0.34) | –1.17 (–0.21) | 0.00 ( 0.00) | 0.00 ( 0.00) |
| C 2, 3, 5, 6 | $2p_y$ | – 0.25 (–0.26) | 0.27 ( 0.43) | –0.01 (–0.17) | 0.00 ( 0.00) | 0.00 ( 0.00) |
| all | n | – 3.58 | 2.48 | 1.11 | 0.00 | 0.00 |
| O7, 8 | $2p_x$ | – 0.46 (–0.77) | – 0.96 ( 0.65) | 1.42 ( 0.13) | 0.00 ( 0.00) | 0.00 ( 0.00) |
| C1, 4 | $2p_x$ | 11.62 ( 0.10) | – 5.88 ( 0.26) | –5.73 (–0.35) | 0.00 ( 0.00) | 0.00 ( 0.00) |
| C 2, 3, 5, 6 | $2p_x$ | – 0.10 ( 0.74) | 0.22 (–0.30) | –0.12 (–0.44) | 0.00 ( 0.00) | 0.00 ( 0.00) |
| all | $\pi$ | 11.12 | – 6.02 | –5.09 | 0.00 | 0.00 |
| | $n + \pi$ | 7.54 | – 3.54 | –3.98 | 0.00 | 0.00 |
| diagonalised | n | – 3.58 | 2.48 | 1.11 | 0.0° | 0.00 |
| | $\pi$ | 11.12 | – 6.02 | –5.09 | 0.0° ($\varphi_z$) | 0.00 |
| | $n + \pi$ | 7.54 | – 3.54 | –3.98 | 0.0° | 0.00 |
| (b) – O7 hyperfine interactions | | | | | | |
| C 2, 3, 5, 6 | "1s" | 0.00 ( 0.00) | 0.00 ( 0.00) | 0.00 ( 0.00) | 0.00 ( 0.00) | 0.00 ( 0.00) [a] |
| H9,10,11,12 | 1s | 0.00 ( 0.01) | 0.00 (–0.03) | 0.00 ( 0.02) | 0.00 ( 0.00) | 0.00 ( 0.00) |
| C 2, 3, 5, 6 | "2s" | 0.05 (–0.11) | 0.00 ( 0.21) | –0.05 (–0.10) | 0.00 ( 0.00) | 0.00 ( 0.00) [a] |
| C 2, 3, 5, 6 | $2p_z$ | 0.00 ( 0.04) | 0.00 (–0.10) | 0.00 ( 0.06) | 0.00 ( 0.00) | 0.00 ( 0.00) |
| O7, 8 | $2p_y$ | 23.12 (–0.17) | –46.19 ( 0.19) | 23.07 (–0.02) | 0.00 ( 0.00) | 0.00 ( 0.00) |
| C1, 4 | $2p_y$ | 0.03 (–0.05) | 0.02 ( 0.06) | –0.05 (–0.01) | 0.00 ( 0.00) | 0.00 ( 0.00) |
| C 2, 3, 5, 6 | $2p_y$ | 0.03 (–0.04) | 0.00 ( 0.11) | –0.04 (–0.07) | 0.00 ( 0.00) | 0.00 ( 0.00) |
| all | n | 22.92 | –45.74 | 22.82 | 0.00 | 0.00 |
| O7, 8 | $2p_x$ | –22.05 ( 0.79) | 11.04 (–0.51) | 11.01 (–0.28) | 0.00 ( 0.00) | 0.00 ( 0.00) |
| C1, 4 | $2p_x$ | 0.07 ( 0.74) | 0.31 (–0.42) | –0.38 (–0.32) | 0.00 ( 0.00) | 0.00 ( 0.00) |
| C 2, 3, 5, 6 | $2p_x$ | 0.05 ( 0.09) | 0.02 ( 0.01) | –0.07 (–0.10) | 0.00 ( 0.00) | 0.00 ( 0.00) |
| all | $\pi$ | –20.31 | 10.45 | 9.87 | 0.00 | 0.00 |
| | $n + \pi$ | 2.61 | –35.29 | 32.69 | 0.00 | 0.00 |
| | | | | | $\varphi_z$ | |
| diagonalised | n | 22.92 | –45.74 | 22.82 | 0.0° | 0.00 |
| | $\pi$ | –20.31 | 10.45 | 9.87 | 0.0° ($\varphi_z$) | 0.00 |
| | $n + \pi$ | 2.61 | –35.29 | 32.69 | 0.0° | 0.00 |

Table 3 (continued)

| | | $A_{xx}$ | $A_{yy}$ | $A_{zz}$ | $A_{zy}$ | $A_{iso}$ |
|---|---|---|---|---|---|---|
| (c) – C2 hyperfine interactions | | | | | | |
| C 2, 3, 5, 6 | "1s" | −0.01 ( 0.00) | 0.00 ( 0.00) | 0.02 ( 0.00) | 0.00 ( 0.03) | 37.87 (−6.81) [a] |
| H 9,10,11,12 | 1s | −0.04 (−0.04) | 0.04 ( 0.11) | 0.00 (−0.07) | 0.03 ( 0.03) | 0.01 ( 0.53) |
| C 2, 3, 5, 6 | "2s" | −0.04 ( 0.05) | 0.00 (−0.09) | 0.04 ( 0.04) | 0.03 (−0.45) | 2.01 (−9.16) [a] |
| C 2, 3, 5, 6 | $2p_z$ | −0.09 (−0.05) | −0.09 (−0.03) | 0.18 ( 0.07) | 0.00 (−0.52) | 0.03 ( 0.85) |
| O 7, 8 | $2p_y$ | −0.40 ( 0.07) | −0.14 ( 0.00) | 0.54 (−0.07) | −0.29 ( 0.08) | 0.00 ( 0.03) |
| C 1, 4 | $2p_y$ | −0.05 (−0.08) | 0.04 ( 0.09) | 0.01 (−0.02) | −0.06 (−0.09) | 0.00 (−0.05) |
| C 2, 3, 5, 6 | $2p_y$ | −1.57 (−0.10) | 2.98 ( 0.16) | −1.41 (−0.06) | 0.05 (−0.77) | 0.00 ( 0.16) |
| all | n | −2.40 | 3.06 | −0.66 | 1.89 | 25.47 |
| O 7, 8 | $2p_x$ | −0.18 ( 0.07) | −0.06 ( 0.00) | 0.24 (−0.07) | −0.16 ( 0.08) | 0.00 ( 0.00) |
| C 1, 4 | $2p_x$ | −0.22 ( 0.31) | 0.24 (−0.10) | −0.02 (−0.21) | −0.27 ( 0.00) | 0.00 ( 0.00) |
| C 2, 3, 5, 6 | $2p_x$ | 5.04 ( 0.26) | −2.58 (−0.09) | −2.46 (−0.17) | 0.02 (−0.05) | 0.00 ( 0.00) |
| all | $\pi$ | 5.29 | −2.60 | −2.69 | − 0.38 | 0.00 |
| | n + $\pi$ | 2.88 | 0.46 | −3.35 | 1.51 | 25.47 |
| | | | | | $\varphi_z$ | |
| diagonalised | n | −2.36 | 3.88 | −1.52 | −22.8° | 25.47 |
| | $\pi$ | 5.29 | −2.26 | −3.03 | −41.5° ($\varphi_z$) | 0.00 |
| | n + $\pi$ | 2.93 | 1.55 | −4.48 | −25.0° | 25.47 |
| (d) – H9 hyperfine interactions | | | | | | |
| C 2, 3, 5, 6 | "1s" | −0.07 ( 0.05) | 0.08 (−0.08) | −0.01 ( 0.02) | 0.09 (−0.05) | 0.00 ( 0.00) [a] |
| H 9,10,11,12 | 1s | −0.01 (−0.02) | 0.00 (−0.17) | 0.01 ( 0.19) | 0.00 ( 0.10) | 3.82 ( 1.12) |
| C 2, 3, 5, 6 | "2s" | −0.86 ( 0.70) | 1.38 (−0.59) | −0.52 (−0.11) | 0.89 (−1.03) | 1.45 (−4.48) [a] |
| C 2, 3, 5, 6 | $2p_z$ | −0.02 ( 0.04) | 0.00 (−0.14) | 0.02 ( 0.11) | 0.00 (−0.04) | 0.07 ( 0.59) |
| O 7, 8 | $2p_y$ | −1.12 ( 0.11) | 0.84 (−0.17) | 0.29 ( 0.06) | −1.11 ( 0.06) | 0.00 ( 0.01) |
| C 1, 4 | $2p_y$ | −0.06 (−0.04) | 0.10 ( 0.08) | −0.04 (−0.04) | 0.00 ( 0.04) | 0.00 ( 0.00) |
| C 2, 3, 5, 6 | $2p_y$ | −0.97 ( 0.24) | 0.60 (−0.24) | 0.37 ( 0.00) | 1.59 (−0.50) | 2.28 ( 1.54) |
| all | n | −2.04 | 1.69 | 0.35 | 0.07 | 6.38 |
| O 7, 8 | $2p_x$ | −0.50 ( 0.17) | 0.43 (−0.23) | 0.07 ( 0.06) | −0.47 ( 0.12) | 0.00 ( 0.00) |
| C 1, 4 | $2p_x$ | −0.48 ( 0.01) | 0.87 ( 0.17) | −0.38 (−0.19) | 0.05 ( 0.23) | 0.00 ( 0.00) |
| C 2, 3, 5, 6 | $2p_x$ | −0.15 (−0.10) | 0.85 ( 0.32) | −0.70 (−0.22) | 1.26 ( 0.16) | 0.00 ( 0.00) |
| all | $\pi$ | −1.05 | 2.41 | −1.36 | 1.35 | 0.00 |
| | n + $\pi$ | −3.09 | 4.10 | −1.01 | 1.42 | 6.38 |
| | | | | | $\varphi_z$ | |
| diagonalised | n | −2.04 | 1.70 | 0.35 | 2.8° | 6.38 |
| | $\pi$ | −1.05 | 2.85 | − 1.80 | 17.8° ($\varphi_z$) | 0.00 |
| | n + $\pi$ | −3.09 | 4.47 | − 1.38 | 14.5° | 6.38 |

[a] In the SCF wavefunction the carbon "2s" orbital contains only the "outer" part of the atomic carbon 2s orbital. For computational convenience the "inner" part is joined to the atomic 1s orbital to form the "1s" carbon SCF orbital.

calculated the isotropic and anisotropic hyperfine interaction constants and the results are also given in table 2. The table shows that the overall agreement, especially in the case of the anisotropic hyperfine interaction constants ($A_{aniso}$), between theory and experiment is very good. The calculation of the orientation of the principal axes of the hyperfine tensors is also in good agreement with experiment.

In order to be able to give more physical insight into the "meaning" of the results of the theoretical calculation we have unravelled the anisotropic hyperfine elements into atomic contributions. The results of this decomposition are gathered in table 3, which will form the basis for the following discussion.

A first conclusion we draw, from a look at table 3 is, that interference contributions (the sum of all atomic non-diagonal hyperfine interaction terms) to $A_{aniso}$, which in table 3 are within parentheses, are not negligible. In a McConnel–Strathdee [14] and point-dipole [15] calculation of the anisotropic hyperfine interaction constants these terms are not fully taken into account.

A second interesting conclusion is, that in a molecule of the size of PBQ for a calculation of the anisotropic hyperfine interaction constants, the *complete* unpaired electron density distribution has to be taken into account. This, of course, makes a purely semi-empirical determination of the excited state spin-density distribution extremely difficult.

We now proceed by discussing in greater detail, per atom, the highlights of table 3.

## 5. Discussion of the results

### *5.1. The carbonyl-carbon atom*

Table 3a shows that the main contribution to $A_{aniso}$, as exptected [8], is due to $2p_x(\pi)$ density at carbon itself. From a net population analysis (vide infra) it follows that the net $\pi$-"spin-density" residing at this carbon atom is 0.156. We then calculate † a value of 150 MHz for the carbon-13 hyperfine interaction constant per unit $\pi$ spin-density. This number is in good agreement with the value of 156 MHz reported by Adam and Weissman [16] and some 15% higher than the value reported by Smith et al. [17]. This latter value was recently used by us in a preliminary analysis of the carbon-13 ENDOR data [8].

Table 3a further shows that the contribution of the $2p_y(n)$ spin-density is far from negligible. Especially the contribution of the n spin-density residing at oxygen and carbon itself is shown to be important. Table 3a also shows that the contributions of the n and $\pi$ spin-density to $A_{aniso}$ are indeed of opposite sign. This confirms one of our previous assumptions made in the semi-empirical analysis of the carbon-13 ENDOR data [8].

The isotropic hyperfine interaction constant is calculated to be zero. Its finite values (–11.7 MHz) therefore must be due to mixing with excited configurations in which open $a_g$ and $b_{1u}$ orbitals are occupied. Semi-empirically we can calculate $A^{\pi}_{iso}$ using the relation derived by Broze and Luz [18,19] for the carbon-13 isotropic hyperfine coupling. They obtain the following relation:

$$A^{\pi}_{iso}(C_1) = 145.9\,\rho^{\pi}_{C_1} - 38.9\,(\rho^{\pi}_{C_2} + \rho^{\pi}_{C_6}) - 68.0\,\rho^{\pi}_{O_7}\ \text{MHz}.$$

For the n-contribution the following relation then seems plausible:

$$A^{n}_{iso}(C_1) = -68.0\,\rho^{n}_{O_7}\ \text{MHz}.$$

For the lowest triplet state in PBQ we then calculate, using the gross atomic population (GAP) spin-density of table 4 (vide infra)

$$A^{n+\pi}_{iso}(C_1) = -9.5\ \text{MHz},$$

which is in reasonable agreement with the experimental value. The carbon-13 isotropic hyperfine coupling thus is dominated by polarization effects mainly of the n spin-density at oxygen.

### *5.2. The oxygen atom*

Table 3b clearly shows that the oxygen hyperfine interaction parameters are almost exclusively due to n and $\pi$ spin-density residing at the oxygen atom itself. The implication of this result is that measurement of these hyperfine parameters combined with knowledge of the oxygen atomic hyperfine interaction constant gives a precise determination of the $2p_x(\pi)$ and $2p_y(n)$ density at oxygen.

† In *all* calculations the normalization condition $\Sigma_i \rho^{n}_i + \Sigma_j \rho^{\pi}_j = 1$ is used, note however that in table 4 the n and $\pi$ "spin-densities" individually are normalized ($\Sigma_i \rho^{n}_i = \Sigma_j \rho^{\pi}_j = 1$).

Our measurements of the total (isotropic plus anisotropic) hyperfine interaction constant $|A_{yy} + A_{iso}|$ suggests that $A_{iso} \approx -19.2$ MHz. The alternative choice of $A_{iso} \approx 89.8$ MHz is rejected as this would have certainly led to an observable hyperfine pattern for the magnetic field along the $x$ and $z$ molecular axes. The SCF calculation thus predicts hyperfine splittings of $-16.6$ and 13.5 MHz of the EPR transitions along the $x$ and $z$ molecular directions. Using the calculated n net atomic population of 0.394 at oxygen (vide infra) we calculate for the oxygen atomic interaction constant $-235$ MHz.

Morton [20] has calculated a value of $-288$ MHz for this constant but from the EPR measurements by Wong and Lunsford [21] on the $^{17}O^-$ ion this constant is found to be $-231$ MHz, in good agreement with our calculation. We further note that from the $\pi$ net atomic population density this constant is calculated to be $-200$ MHz. This result shows that one cannot expect atomic hyperfine interaction constants to be identical for $\pi$ and n electrons. This fact introduces an extra uncertainty in a semi-empirical analysis of hyperfine interaction constants.

*5.3. The non-carbonyl-carbon atom*

The dominant contribution to $A_{aniso}$ in this case arises from the $2p_x$ and $2p_y$ spin-density residing at the ring-carbon itself. The interference contributions however, especially from the unpaired n-density distribution, are not negligible. Table 3d further shows that the $zz$ element of the hydrogen atom hyperfine tensor is almost exclusively determined by the $\pi$ density at the neighbouring carbon atom. Using the experimentally obtained value $A_{zz} = -1.6$ MHz we then calculate [19,22] for the $\pi$ density at $C_2$, $\rho^{\pi}_{C_2} = 0.09$ which is in good agreement with the GAP spin-density of table 4. We have also analyzed the contributions of the different atomic orbitals to the isotropic hyperfine interaction constant of the ring-carbon atom. Table 3c shows that this constant is mainly determined by the unpaired spin-density in the s-orbitals of carbon. Interference effects in this case are also found to be very important. In a semi-empirical treatment of the isotropic hyperfine coupling we would have assumed that only the carbon 2s spin-density is responsible for $A^{n}_{iso}$.

The *$\pi$-contribution* to the isotropic hyperfine interaction can be calculated using the semi-empirical relation derived by Karplus and Fraenkel [23]:

$$A^{\pi}_{iso}(C_2) = 99.7\,\rho^{\pi}_{C_2} - 38.9\,(\rho^{\pi}_{C_1} + \rho^{\pi}_{C_3})\text{MHz}.$$

Using the GAP spin-density of table 4 we calculate $A^{\pi}_{iso}(C_2) = -0.4$ MHz. We then "find", using the mean experimental value of $A_{iso}(C_2,C_3)$ of 18.3 MHz, for $A^{n}_{iso}$: 18.3 + 0.4 = 18.7 MHz. For unit spin-density in a 2s carbon orbital the isotropic hyperfine splitting is known to be 3342 MHz [23]. We then calculate for the 2s spin-density of carbon (2) $\rho^{n}_{C_2} = 0.011$ which compares very nicely with the GAP spin-density displayed in table 4.

*5.4. The hydrogen atom*

Table 3d shows that there are numerous contributions to the anisotropic hyperfine coupling tensor of hydrogen. It therefore seems virtually impossible to calculate these tensor elements semi-empirically with any accuracy. The excellent agreement between the measured and calculated anisotropic hyperfine parameters of this atom further supports the idea that the SCF description of the singly occupied $\pi$ and n-orbitals is basically correct.

We have also decomposed the hydrogen isotropic hyperfine coupling into atomic contributions and the results are also given in table 3d. Note that the interference contribution from the carbon 2s orbital gives the largest contribution to the isotropic hyperfine coupling. In a previous semi-empirical treatment of the proton ENDOR [7], we assumed only the 1s spin-density at hydrogen itself to be responsible for the observed isotropic hyperfine coupling constant. In that calculation we ignored the contributions from other atoms and table 3d shows that this is clearly not warranted. The previous calculated 1s density at hydrogen thus must be considered an upper limit.

Further note that the experimentally measured value of the proton hyperfine coupling parameter also contains a contribution of polarization due to the unpaired $\pi$ density. Taking this into account we calculate for $A^{n}_{iso} = 12.7$ MHz which is twice as large as the value of 6.39 MHz, obtained from an ab-initio calculation. This large discrepancy is mainly due to the fact that the wavefunction we use is known [24] to give a poor description near the nucleus.

Table 4
Gross (GAP) and net (NAP) atomic population densities as calculated from the ab-initio SCF wavefunction of the lowest $n\pi^*$ triplet state in *p*-benzoquinone

| | | GAP | NAP |
|---|---|---|---|
| C2, 3, 5, 6 | "1s" | < 0.001 | 0.004 |
| H9,10,11,12 | 1s | 0.007 | 0.006 |
| C2, 3, 5, 6 | "2s" | 0.012 | 0.046 |
| C2, 3, 5, 6 | $2p_z$ | 0.001 | 0.002 |
| O7, 8 | $2p_y$ | 0.370 | 0.394 |
| C1, 4 | $2p_y$ | 0.016 | 0.012 |
| C2, 3, 5, 6 | $2p_y$ | 0.036 | 0.033 |
| | Σ | 1.000 | 1.176 |
| O7, 8 | $2p_x$ | 0.153 | 0.220 |
| C1, 4 | $2p_x$ | 0.163 | 0.156 |
| C2, 3, 5, 6 | $2p_x$ | 0.092 | 0.066 |
| | Σ | 1.000 | 1.016 |

## 6. The excited state spin-density distribution

In a semi-empirical analysis of hyperfine interaction constants one calculates a spin-density distribution rather than a wavefunction. Of course in the MO picture the wavefunction is spread out over the entire of the molecule (atoms and bonds) and the usage of atomic spin-densities can only be considered a first approximation. It is still very useful, especially when discussing chemical reactivity, to construct a picture of the spin-density distribution in a state.

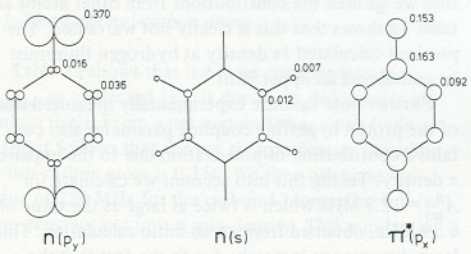


Fig. 2. The calculated gross atomic population (GAP) in the n and $\pi^*$ orbitals of the lowest triplet state of *p*-benzoquinone. Note that the size of the orbital is chosen to be proportional to the square root of the GAP.

From the SCF wavefunction we can calculate what is known as the net atomic population (NAP) and the gross atomic population (GAP) [25] distribution. The NAP of an orbital at an atom is found by taking the square of the coefficient of this AO in the SCFMO. In the GAP the overlap contributions among different atoms are also taken into account. They are divided equally among the corresponding atoms and then added to the NAP. The GAP "spin-density distribution" should thus come closest to the spin-density distribution derived empirically. The semi-empirical calculations of the $2p_x$ and 2s spin-density at the non-carbonyl-carbon atom support this idea. Table 4 contains the net and gross atomic populations as calculated from the SCF triplet state wavefunction.

Note that the overlap corrections introduce appreciable shifts in the "spin-density distribution", which illustrates that an atomic spin-density distribution only gives a rough picture of the wavefunction. The GAP spin-density distribution in both the singly occupied n and $\pi^*$ orbital is pictured in fig. 2. These pictures show that the unpaired $\pi$-electron is almost equally divided among the carbonyl groups and the central ringsystem. The unpaired n-electron density in contrast is largely confined (75%) to the oxygen atoms.

We further note that the $\pi$-electron spin-density distribution in the lowest triplet state of PBQ is very similar to the one determined for the *p*-benzo-semiquinone radical [26]. This confirms a previous assumption made [7] that the correlation effects between the n and $\pi$-electron are small. As this was also shown to be the case for the $\pi$ and $\pi^*$-electron in the lowest triplet state of naphthalene [27] it does not seem to be farfetched to suggest that presumably in general for large molecules correlation effects between the unpaired electrons are small. This than seems a very useful *rule of thumb* in a semi-empirical analysis of the spin-density distribution in the lowest photo-excited triplet state of (hetero-) aromatics.

## 7. Summary and conclusions

This paper contains the results of an ab-initio calculation of the hyperfine coupling parameters in the lowest triplet state of *p*-benzoquinone.

A general conclusion is that interference effect contributions to the hyperfine splittings cannot always be

ignored. Analysis of the calculations further shows that only the oxygen hyperfine coupling parameters are completely determined by the $\pi$ and n spin-density residing at oxygen and full determination of these parameters still remains desirable. The excellent agreement between the experiments and calculations leads us to the conclusion that the SCF description of the singly occupied orbitals is basically correct.

The conclusion then is that the unpaired $\pi$-electron is delocalized over the molecule, while the n-electron is largely confined to the oxygen atoms. The effect of the delocalization of the n-electron however is clearly recognizable and cannot be ignored in the analysis of the ENDOR data. In this regard we find it very surprising that Hutchison and Kohler [28] and Anderson and Kohler [29], in an analysis of the proton-ENDOR data of diphenylmethylene were able to consistently interpret their results by assuming that the $\sigma$ spin-density in this molecule is completely localized at the methylene carbon atom. This paper shows that in the case of PBQ such an assumption would have completely failed. The excited state electron spin-density distribution obtained for PBQ also justifies one of our previous assumptions [6], namely that the contribution of the second-order spin–orbit coupling at oxygen completely dominates the fine-structure parameter of PBQ.

Finally the ab initio SCF wavefunctions used in this study should provide an excellent basis for vibronic coupling calculations [30] on the lowest triplet state of PBQ.

## Acknowledgement

We are most indebted to Berend Kwant for the synthesis of the isotopic species of PBQ. We also gratefully acknowledge the help and support of Jan G.F.M. Fremeijer during the measurements. One of us (G.A. van der Velde) gratefully acknowledges financial support from the Netherlands Foundation for Chemical Research (S.O.N.).

## References

[1] H.P. Trommsdorff, J. Chem. Phys. 56 (1972) 5358.
[2] R.L. Fulton and M. Gouterman, J. Chem. Phys. 41 (1964) 2280;
R.M. Hochstrasser and C.A. Marzzacco, in: Molecular luminescence, ed. E.C. Lim (Benjamin, New York, 1969) p.631;
A.R. Gregory, W.H. Henneker, W. Siebrand and M.Z. Zgierski, J. Chem. Phys. 65 (1976) 2071.
[3] H. Veenvliet and D.A. Wiersma, Chem. Phys. 2 (1973) 69; Chem. Phys. Letters 22 (1973) 87.
[4] H.P. Trommsdorff, Chem. Phys. Letters 1 (1967) 214; H. Veenvliet and D.A. Wiersma, Chem. Phys. Letters 33 (1975) 305.
[5] A.I. Attia, B.H. Loo and A.H. Francis, Chem. Phys. Letters 22 (1973) 537.
[6] H. Veenvliet and D.A. Wiersma, Chem. Phys. 8 (1975) 432.
[7] J.H. Lichtenbelt, J.G.F.M. Fremeijer, H. Veenvliet and D.A. Wiersma, Chem. Phys. 10 (1975) 107.
[8] J.H. Lichtenbelt, J.G.F.M. Fremeijer and D.A. Wiersma, Chem. Phys. 18 (1976) 93.
[9] G.A. van der Velde, Thesis, University of Groningen (1974).
[10] J. Trotter, Acta Cryst. 13 (1960) 86.
[11] H.T. Jonkman, Thesis, University of Groningen (1975); H.T. Jonkman, G.A. van der Velde and W.C. Nieuwpoort, Quantum Chemistry The State of the Art, Proceedings of S.C.R. Atlas Symposium, Vol. 4 (1974) p. 245.
[12] E.D. Becker, H. Ziffer and E. Charney, Spectrochim. Acta 19 (1963) 1871.
[13] R. Willstätter and S. Dorogi, Ber. 42 (1939) 2147.
[14] H.M. McConnell and J. Strathdee, Mol. Phys. 2 (1959) 129.
[15] C.A. Hutchison Jr. and G.A. Pearson, J. Chem. Phys. 47 (1967) 520.
[16] F.C. Adam and S.I. Weissman, J. Am. Chem. Soc. 80 (1958) 2057.
[17] W.V. Smith, P.P. Sorokin, I.L. Gelles and G.J. Lasher, Phys. Rev. 115 (1959) 1546.
[18] M. Broze and Z. Luz, J. Chem. Phys. 51 (1969) 749.
[19] K. Scheffler and H.B. Stegmann, Elektronenspin Resonanz (Springer, Berlin, 1970) chs. C and D.
[20] J.R. Morton, Chem. Rev. 64 (1964) 453.
[21] N.B. Wong and J.H. Lunsford, J. Chem. Phys. 55 (1971) 3007.
[22] T. Cole, C. Helles and H.M. McConnell, Proc. Natl. Acad. Sci. US 45 (1959) 525.
[23] M. Karplus and G.K. Fraenkel, J. Chem. Phys. 35 (1961) 1312.
[24] S. Fraga and G. Malli, Many electron systems. Properties and interactions (Saunders, Philadelphia, 1968) pp. 8, 70.
[25] R.S. Mulliken, J. Chem. Phys. 23 (1955) 1833.
[26] J. Gendell, J.H. Freed and G.K. Fraenkel, J. Chem. Phys. 37 (1962) 2832;
M.R. Das and G.K. Fraenkel, J. Chem. Phys. 42 (1965) 1350.
[27] H. Hirota, C.A. Hutchison Jr. and P. Palmer, J. Chem. Phys. 40 (1964) 3717;
A.D. McLachan, Mol. Phys. 5 (1962) 51.
[28] C.A. Hutchison Jr. and B.E. Kohler, J. Chem. Phys. 51 (1969) 3327.
[29] J.M. Anderson and B.E. Kohler, J. Chem. Phys. 65 (1976) 2451.
[30] M.F. Merienne-Lafore and H.P. Trommsdorff, J. Chem. Phys. 64 (1976) 3791.
[31] J.H. Lichtenbelt and D.A. Wiersma, Chem. Phys. 34 (1978) 47.

"Does the model fit the experiments?"

# STRUCTURE AND DYNAMICS OF THE LOWEST TRIPLET STATE IN *p*-BENZOQUINONE. IV. THE EFFECT OF MILD SUBSTITUTION ON THE PROTON ENDOR SPECTRA

Jan H. LICHTENBELT and Douwe A. WIERSMA
*Laboratory for Physical Chemistry, University of Groningen, Groningen, The Netherlands*

The effect of mild (deuterium and methyl) substitution on the proton ENDOR spectra in the lowest $n\pi^*$ triplet state of *p*-benzoquinone is reported and analyzed. The conclusion is that, as recently suggested by Merienne-Lafore and Trommsdorff, *p*-benzoquinone in its lowest triplet state is best described as a dimer.

## 1. Introduction

In the past couple of years several papers on the optical [1–3] and magnetic resonance spectroscopy [4] of the lowest triplet state in *p*-benzoquinone (PBQ) have appeared. Well established now is the fact that the lowest $n\pi^*$ triplet state ($B_{1g}$) in PBQ is strongly vibronically coupled to a nearby (340 $cm^{-1}$) $A_u$ $n\pi^*$ triplet state. The effect of this coupling manifests itself most dramatically in the extreme sensitivity of the optical and magnetic resonance spectra towards isotopic substitution [5–7]. Our understanding of this isotope effect, even on a qualitative level, however, is still marginal. This motivated us to a further study of the effect of mild (deuterium and methyl) substitution on the proton ENDOR spectra of PBQ.

In this final report on proton ENDOR spectra of PBQ we are specifically concerned with PBQ-$h_4$, PBQ-$dh_3$ and PBQ-$CH_3$ (toluquinone, TOL). Additional (incomplete) data of 2,6 PBQ-$d_2h_2$, PBQ-$d_3h$ and mono deutero (ring) toluquinone are also reported and used to support assignments made. Analysis of the data shows that mono deutero- and methyl-substitution in PBQ leaves the $C_{2v}$ symmetry (approximately) of the unsubstituted half of the molecule virtually intact. This finding lends support to the hypothesis, recently forwarded by Merienne-Lafore and Trommsdorff [8] that PBQ may be considered as a dimer for its lowest $n\pi^*$ (singlet and triplet) states.

## 2. Experimental details

All isotopically mixed crystals used were grown from the Bridgman furnace with a guest concentration of about 1 mole %. Ringdeuterated toluquinone-$d_3$ was obtained by an (acid) exchange of the corresponding hydroquinone followed by an oxidation with chromic acid as described by Charney and Becker [9]. PBQ-$d_3h$ was found as an "impurity" in pure PBQ-$d_4$ and TOL-$dh_2$ as a by-product in the formation of TOL-$d_3$. The other materials were obtained as described previously [5].

The setup used to detect the excited state magnetic resonance signals (EPR and ENDOR) has also been described [5,6] and we emphasize that all results reported here were obtained at about 2 K. The **g** and **D** tensors of the species studied and given in table 1 were determined through angular dependent measurements of the magnetic field value at which the optically detected $\Delta M_s = \pm 1$ EPR transitions occurred. "Half field" ($\Delta M_s = \pm 2$), LAC and CR magnetic field values were also used to improve the accuracy of the tensor elements. In all cases we found that the **g** and **D** tensors coincide. In addition, for toluquinone we find that the **g** and **D** tensors coincide with a molecular axes system whereby the $z$ axis is the oxygen–oxygen axis, the $y$ "in plane" axis parallel to the cleavage plane [10] and the $x$ axis perpendicular to both. For *p*-benzoquinone we find instead, that while the $z$ axis of the **g** and **D** tensors coincides with the oxygen–oxygen direction

Table 1
g- and fine structure tensors in the lowest $n\pi^*$ triplet state of *p*-benzoquinone and toluquinone

| | PBQ-$h_4$ [a] | PBQ-$dh_3$ [a] | PBQ-2,6$d_2h_2$ | PBQ-$d_3h$ | TOL-$h_3$ | TOL-6$dh_2$ [c] |
|---|---|---|---|---|---|---|
| $X$(MHz) | −798.2 | −915.5 | | | −1317(5) | −1392 |
| $Y$(MHz) | −569.1 | −705.5 | b) | b) | − 912(5) | −1023 |
| $Z$(MHz) | 1376.3 | 1621.0 | 2282 | 2065 | 2229(1) | 2415 |
| $g_{xx}$ | 2.0045 | 2.0045 | | | 2.0042(13) | 2.0047 |
| $g_{yy}$ | 2.0035 | 2.0038 | | | 2.0038(12) | 2.0040 |
| $g_{zz}$ | 2.00994 | 2.01038 | 2.0108 | 2.0107 | 2.01084(14) | 2.01131 |
| host | | PBQ-$d_4$ | | | TOL-$d_3$ | |

a) From ref. [5].
b) From the position of the $\Delta M_S = 2$ transition of PBQ-2,6$d_2h_2$ and PBQ-$d_3h$ measured in the same crystal it is concluded that $E_{d_2h_2} < E_{d_3h}$.
c) Values given are obtained from one measurement whereby the magnetic field is parallel to each principal axis.

the $y$ axis is rotated some −5 degrees from the molecular plane. A recent low-temperature crystal structure determination of *p*-benzoquinone shows [11] that the molecular plane is tilted 3.2° away from the cleavage $(20\bar{1})$ plane. The proton ENDOR data taken at the $\Delta M_S = -1$ transition were used to determine the hyperfine tensors **A**. CRENDOR [6] data were also obtained and used for additional (sign) information.

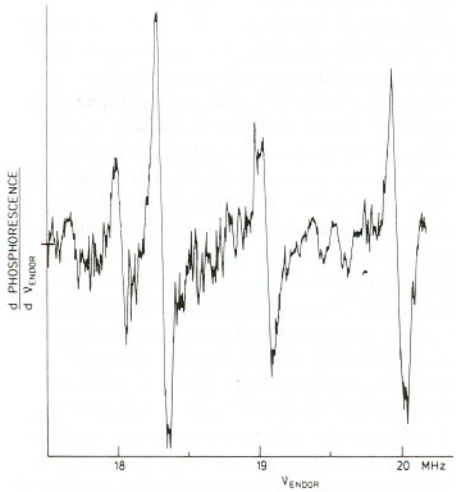


Fig. 1. Optically detected ENDOR spectrum of PBQ-$dh_3$ as guest in PBQ-$d_4$ at 1.8 K with the permanent magnetic field at an angle of −15° from the $z$ axis in a (nearly) molecular plane. Note that the approximate 1:2:1:2 intensity ratio of the four ENDOR lines derives from six possible inequivalent protons. The ENDOR spectrum is from the $M_S = -1$ electron spin state with a free proton frequency $\nu_p$ = 10.377 MHz and an EPR frequency $\nu_{EPR} \approx 9.04$ GHz.

In a primary fitting procedure only three hyperfine elements were least-square fitted. For ENDOR the first order frequency equation [5] was used and for CRENDOR the full 6 x 6 hamiltonian matrix ($S = 1, I = ½$) was diagonalised [6]. At least three (nearly) perpendicular rotation planes were used in the total fit of all six hyperfine elements. The signs of the rotation angles, which determine the sign of the nondiagonal hyperfine elements, were obtained from the ENDOR data of the two translational inequivalent molecules (for the $A_{xy}$ and $A_{xz}$ elements) or by the angular dependence of the EPR for both these two molecules. As in toluquinone the $x$-axes of the two translational inequivalent molecules coincide, our ENDOR data were not accurate enough to discriminate between two (very similar) solutions of the hyperfine tensors. In all calculations we have further assumed the hyperfine tensor to be symmetric and ignored the nuclear dipole–dipole interactions.

## 3. Results

Fig. 1 shows an example of an ENDOR spectrum obtained for PBQ-$dh_3$ in PBQ-$d_4$ at 2 K. Note that the spectrum contains only four lines of alternating intensity (approximately 1 : 2 : 1 : 2). The same was

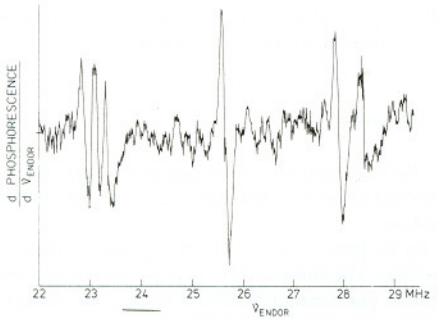


Fig. 2. ENDOR spectrum of toluquinone-$h_3$ in toluquinone-$d_3$ of the $M_S = -1$ electron spin state and with the magnetic field parallel to the $y$ axis. Three of the methyl proton ENDOR lines at about 23 MHz and the aromatic protons are found at higher frequencies for this orientation. $\nu_p$ = 15.670 MHz and $\nu_{EPR}$ = 9.095 GHz.

observed for all orientations of the mixed crystal.

For PBQ-$CH_3$ in ring deuterated PBQ-$CH_3$ six proton ENDOR lines were observed for all crystal orientations. A typical example of an ENDOR

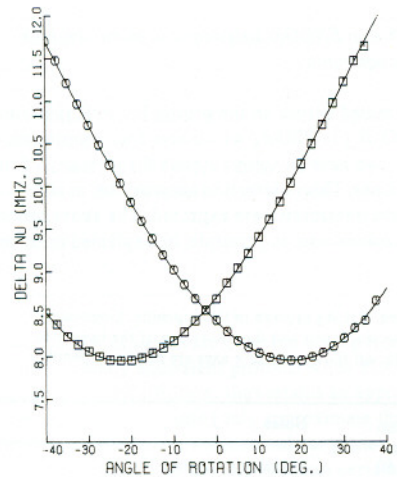


Fig. 3. Computer fitted (solid lines) and experimental proton ENDOR frequencies versus angle of rotation in the (nearly) molecular plane of PBQ-$h_4$ in the lowest $n\pi^*$ triplet state, as guest in PBQ-$d_4$ crystal at 1.8 K. Note that zero degrees is close to the $z$ axis. Protons 9 and 11 are marked by a circle and protons 10 and 12 by a square. See fig. 6 for numbering of protons.

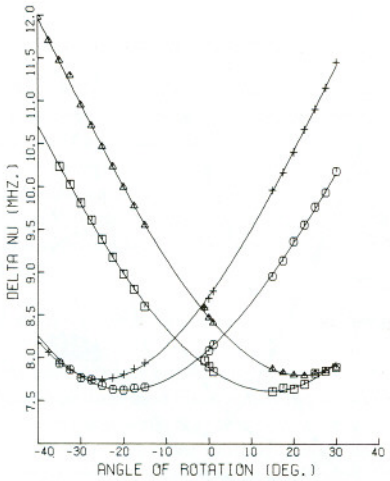


Fig. 4. Computer fits of PBQ-$dh_3$ proton ENDOR frequencies. See also text to fig. 3. Experimental intensities for the protons numbered 9 (□):10(+):11(△):12(○) is approximately 1:2:2:1.

spectrum is shown in fig. 2. The triplet of lines (near 23 MHz) is assigned to the methyl-protons, while the other lines must be due to ring-protons.

Figs. 3, 4 and 5 give an impression of the fit obtained between the experimental points and the curves calculated by the computer from the spin-hamiltonian (eq. 4 of ref [5]) with the hyperfine interactions included.

The final hyperfine tensors obtained for all ring protons in perproto, mono-deutero and methyl *p*-benzoquinone are gathered in the appendix. First note that the final results given here for PBQ-$h_4$ are somewhat different from the ones reported previously [5]. This is due to the fact that in the original fit a wrong choice was made in the sign of one of the off-diagonal hyperfine tensor elements.

Note also that for PBQ-$CH_3$ we are left with two solutions for the hyperfine coupling tensors. Fortunately, the difference between the two solutions is small and of no importance in the context of the present paper. The hyperfine coupling tensors of the methyl protons have also been determined but they will be reported and discussed in a forthcoming paper

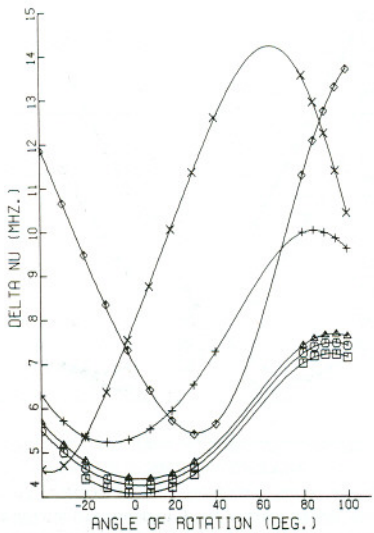


Fig. 5. Computer fits of the proton ENDOR frequencies of TOL-$h_3$ as guest in TOL-$d_3$ crystal. See also text to fig. 3. The three lowest lines show the angle dependences of the methyl protons. Note that the two aromatic protons of TOL-$dh_2$ give about the same angle dependences as the protons of TOL-$h_3$ marked with ◇ and x (numbers 11 and 10, respectively) measured from $-10°$ until $+25°$. The proton with number 12 (+) is lacking in TOL-$dh_2$.

[14]. Finally, we have summarized in table 2 the round off principal values of the hyperfine coupling constants in a form more suitable for discussion. Note that in the case of PBQ-$h_4$ and PBQ-$dh_3$ the average is given of the nearly equivalent proton hyperfine coupling constants.

## 4. Discussion

The main problem of this paper is to assign the different hyperfine interaction tensors to specific protons.

In the parent compound, PBQ-$h_4$ this is a trivial problem. The molecule is at a center of inversion and protons positioned para with respect to one another are equivalent. The protons ortho to one another are not related by a space group symmetry element and may therefore be different. The slightly different proton hyperfine coupling tensors observed are therefore ascribed to protons being ortho to another and the difference is caused by the crystal field.

The assignment in the case of PBQ-$dh_3$ and PBQ-$CH_3$ is less trivial and will be given in the following sections. In fig. 6 the axes and atom numbering in *p*-benzoquinone is given whereby the substituent is attached to, unless stated otherwise, carbon atom 2.

### *4.1. Proton ENDOR assignment in mono deutero p-benzoquinone*

As stated before, in the proton ENDOR spectrum of PBQ-$dh_3$ in PBQ-$d_4$ we observe four transitions, of which two have (roughly) double the intensity of the other ones. This observation surprised us, as six separate transitions were expected. The above observation however can, in principle, be explained in three

Table 2
Short review of the experimental hyperfine tensors of PBQ-$h_4$, PBQ-$dh_3$ and TOL-$h_3$ as given in the appendix. Given are the diagonalized tensor elements, the angle of rotation $\varphi_z$ between the molecular $z$ axis and the projection of the hyperfine $z$ axis in the molecular plane and the isotropic hyperfine interaction in MHz. All the hyperfine $x$ axes are nearly perpendicular to the molecular plane

| | $A_{xx}$ | $A_{yy}$ | $A_{zz}$ | $\varphi_z$ | $A_{iso}$ | Notes |
|---|---|---|---|---|---|---|
| PBQ-$h_4$ | −3.06 | 4.66 | −1.60 | ±15° | 9.60 | inversion symmetry |
| PBQ-$dh_3$ | −3.34 | 4.63 | −1.29 | ±13° | 8.92 | protons 9 and 12 (int. ≈ 1) |
| | −2.91 | 4.85 | −1.94 | ±19° | 9.76 | protons 10 and 11 (int. ≈ 2) |
| TOL-$h_3$ | −1.70 | 2.51 | −0.81 | 5° | 5.10 | methyl protons $A^A = \frac{1}{3}(A_1 + A_2 + A_3)$ |
| | −2.10 | 5.95 | −3.85 | −28° | 8.65 | aromatic proton 10 |
| | −1.95 | 5.24 | −3.29 | 25° | 8.80 | aromatic proton 11 |
| | −3.85 | 4.42 | −0.59 | − 4° | 5.85 | aromatic proton 12 |

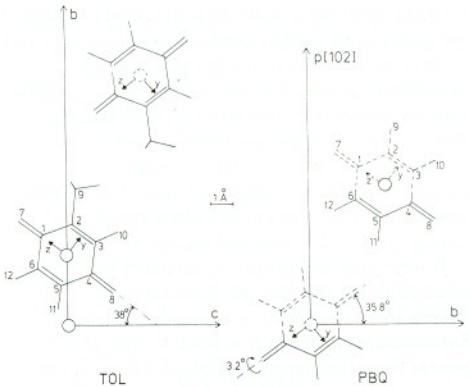


Fig. 6. The crystal structure of toluquinone (TOL) from Trommsdorff et al. [10,15] and of *p*-benzoquinone (PBQ) as determined by van Bolhuis and Kiers [11]. Drawn are the projections in the cleavage planes. In both crystals there is a $2_1$ screw axis parallel to the horizontal axis of the figure. The TOL molecules are parallel to the (100) crystal plane, while the PBQ molecules are 3.2° rotated around the O–O direction, from the $(20\bar{1})$ plane.

different ways. The first possible explanation rests on the assumption that protons 10 and 12 are equivalent. The PBQ-$dh_3$ molecule would thus still have, interaction wise, a "center of symmetry". This however is incompatible with the optical spectra of the molecule [3].

A second possible explanation relies on the assumption that substitution of the deuterium atom on either the 2 or 3 position would result in identical free molecule hyperfine interaction parameters for protons 11 and 12. This assumption however, seems in direct conflict with the proton ENDOR spectra of 1-$^{13}$C-*p*-benzoquinone [6]. In this molecule four proton ENDOR signals are observed arising from two groups of nearly equivalent protons. While PBQ on carbonyl-$^{13}$C substitution, thus retains an approximate $\sigma_v(z)$ mirror plane (only approximate through the crystal field) the orthogonal mirror plane $\sigma_v(y)$ is lost. This last mirror plane $\sigma_v(y)$ is thus certainly not expected to be present in PBQ-$dh_3$.

The only explanation then consistent with all other data (e.g. optical Stark effect) is that deuterium substitution on either position 2 or 6 results in identical free molecule hyperfine interaction parameters for protons in positions 10 and 11. The small absolute difference in hyperfine coupling of protons 10 and 11 is presumably only caused by the crystal field.

The assignments of the different hyperfine coupling tensors to the different protons can now be made, using only the predicted angle of rotation [7] of the in-plane hyperfine tensor axes. The assignment made is also included in table 2.

Note that the molecule on isotopic substitution retains approximate $C_{2v}$ symmetry at the unsubstituted half.

### *4.2. Proton ENDOR assignments in toluquinone*

As table 2 shows in toluquinone, two of the aromatic protons have quite similar hyperfine interaction constants while the third proton exhibits a rather different hyperfine splitting. Again, in principle, there are three possible assignments for the third (exceptional) proton. However in view of the assignment made in mono-deutero *p*-benzoquinone we assign the third proton to position 12. The other assignments are then easily made and included in table 2.

The following additional measurements on a ring-deuterated isotope of toluquinone support our assignment. In isotopically mixed crystals of toluquinone we have also measured proton ENDOR spectra of a mono ring substituted deutero isotope of toluquinone. In this isotope, as given in fig. 5, the exceptional proton evidently was replaced by deuterium. Moreover, measurement of the fine-structure constants of this isotopic impurity revealed this isotope to have a significantly larger fine structure parameter $D$ (see table 1) than toluquinone itself. As we have found that the fine-structure parameter $D$ of PBQ-2,6$d_2h_2$ exceeds that of PBQ-$dh_3$ (as shown in table 1), this finding is only consistent with the assumed deuterium substitution in position 12. Additional support for the assignments made may be derived from the resulting relationship between the fine-structure parameter $D$ and the angle of rotation (in the molecular plane) $\alpha$ of the proton hyperfine tensor. In fig. 7 we have displayed all data available on isotopes of *p*-benzoquinone and note that there is a very consistent relationship between $\alpha$ and $D$. Also note that the methyl perturbation nicely fits into this picture.

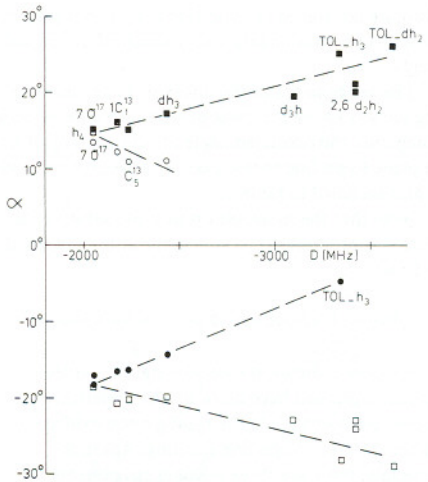


Fig. 7. The rotation angle $\alpha$ of the y-z proton hyperfine submatrices (of the lowest $n\pi^*$ triplet state) versus the fine structure parameter $D$. The proton numbering is: 9(○), 10(□), 11(■), 12(●). All molecules are PBQ as guest in PBQ-$d_4$ except the toluquinones (TOL) which are guests in TOL-$d_3$. $C_5^{1\,3}$ means 1,2,3,5,6 $C_5^{1\,3}$-PBQ [6]. Note that $|d\alpha/dD|$ for protons 9 and 12 is about twice as large as for protons 10 and 11.

We remark here that the assignment made seems in direct conflict with the one previously made in the tolusemiquinone ion by Venkataraman et al. [12]. These authors, assuming "sum addition rules" to hold for the isotropic hyperfine constant, concluded that in the tolusemiquinone ion the isotropic hyperfine constant of proton 11 and 12 are almost identical. From our experiments we must conclude however, that in the lowest $n\pi^*$ triplet state of toluquinone the hyperfine tensors of protons 10 and 11 are very similar. It is hard to imagine [7, 12] that the $\pi$ spin density distribution in the lowest triplet state is so dissimilar from that found in the tolusemiquinone and we therefore conclude that the previous assignments made for the hyperfine couplings in tolusemiquinone are erroneous.

## 5. Conclusions

The main conclusion of this paper is that the hypothesis, put forward by Merienne-Lafore and Trommsdorff [8], that *p*-benzoquinone in its lowest $n\pi^*$ singlet and triplet states may be considered as a dimer, is correct.

The isotope effect on the fine structure and hyperfine structure constants in *p*-benzoquinone then basically derives from two effects. The first one is that "isotopic" (deuterium, methyl) substitution changes the zero-order excitation energy of the substituted fragment. The second one is that isotopic substitution in general will also effect the vibronic mixing between the monomer excited $n\pi^*$ states.

It seems worthwhile then to comment here on our observation [7] that isotopic substitution of oxygen-16 by oxygen-17 or -18 hardly affects the fine-structure parameter $D$ in PBQ. In view of our present understanding of the isotopic effect we can only interpret this as evidence for the fact that the oxygen atom is at rest in the modes that vibronically mix the near degenerate $n\pi^*$ triplet states.

Finally our EPR and proton ENDOR measurements show that there is a very distinct correlation between the increase in $D$, $g_{zz}$ (table 1) and the change of the hyperfine tensor elements (table 2) on isotopic substitution. In mono deutero *p*-benzoquinone we see from the hyperfine data in table 2 that the absolute value of $A_{xx}$ becomes larger at the substituted site of the molecule. Results of previously reported [7] calculations of the proton anisotropic hyperfine elements show that the increase of $|A_{xx}|$, in a substituted "dimer", can be explained by assuming a slight "localization" of the $n\pi^*$ excitation, on the oxygen of the substituted fragment. This idea is also confirmed by semi-empirical calculations of the Derbyshire type [13]. The importance of charge transfer in the $n\pi^*$ excitation is not assessed by the experiments presented.


## Acknowledgement

We are very grateful to Berend Kwant for the synthesis of the deuterated quinones. The help of Jan G.F.M. Fremeijer in the experiments is also gratefully acknowledged.


## Appendix

Experimental proton hyperfine tensor elements (in MHz) of the lowest $n\pi^*$ triplet state of

*p*-benzoquinone and toluquinone, given in the molecular axes system. The relation between the molecular and crystal axes system is given in fig. 6. In parentheses are given the errors by the ENDOR experiments.

PBQ-$h_4$:
proton 10 and 12:
6.664(20)
−0.757(42) 13.732(34)
0.165(12) −1.797(7) 8.536(5)
proton 9 and 11:
6.814(17)
1.389(33) 13.477(28)
0.108(11) 1.555(5) 8.416(4)

PBQ-$dh_3$ (with the excitation "localized" on the 9–12 side)
proton 9:
5.705(41)
−0.885(80) 13.211(65)
−0.258(18) 1.194(11) 7.894(5)
proton 10:
6.884(24)
−0.396(67) 14.045(46)
0.059(10) −2.126(8) 8.515(4)
proton 11:
6.956(32)
−0.783(96) 13.724(72)
−0.338(24) 1.924(13) 8.461(6)
proton 12:
5.601(30)
−0.381(115) 13.181(63)
−0.023(20) −1.384(9) 7.981(5)

TOL-$h_3$
Given are two indistinguishable (by experimental errors) solutions.
*Solution one*:
aromatic proton 10:
6.594(86)
0.221(54) 12.470(40)
−0.051(45) −4.027(48) 6.906(25)
aromatic proton 11:
6.831(95)
−0.091(59) 12.497(39)
0.061(47) 3.295(49) 7.080(25)
aromatic proton 12:
2.022(23)
0.098(10) 10.288(8)
0.005(11) −0.391(11) 5.288(6)
*Solution two*:
aromatic proton 10:
6.515(77)
−0.296(46) 12.527(35)
−0.002(38) −4.005(40) 6.910(21)
aromatic proton 11:
6.865(88)
0.172(45) 12.474(36)
−0.030(42) 3.303(44) 7.080(23)
aromatic proton 12:
2.019(30)
−0.084(12) 10.242(9)
−0.002(14) −0.379(14) 5.290(7)

TOL-6$dh_2$:
One measurement in the molecular plane gave us the following elements:
proton 10:
–
– 12.24(26)
– −4.15(2) 6.89(1)
proton 11:
–
– 12.09(39)
– 3.40(7) 6.90(2)

## References


[1] R.M. Hochstrasser, L.W. Johnson and H.P. Trommsdorff, Chem. Phys. Letters 21 (1973) 251; H.P. Trommsdorff, J. Chem. Phys. 56 (1972) 5358.
[2] A.H. Francis, Ph.D. Thesis, University of Michigan, USA (1969);
T.M. Dunn and A.H. Francis, J. Mol. Spectry. 50 (1974) 14.
[3] H. Veenvliet and D.A. Wiersma, Chem. Phys. Letters 22 (1973) 87; J. Chem. Phys. 60 (1974) 704; Chem. Phys. Letters 33 (1975) 305; Chem. Phys. 8 (1975) 432.
[4] A.I. Attia, B.H. Loo and A.H. Francis, Chem. Phys. Letters 22 (1973) 537.
[5] J.H. Lichtenbelt, J.G.F.M. Fremeijer, H. Veenvliet and D.A. Wiersma, Chem. Phys. 10 (1975) 107.
[6] J.H. Lichtenbelt, J.G.F.M. Fremeijer and D.A. Wiersma, Chem. Phys. 18 (1976) 93.
[7] J.H. Lichtenbelt, D.A. Wiersma, H.T. Jonkman and G.A. van der Velde, Chem. Phys. 22 (1977) 297.

[8] M.F. Merienne-Lafore and H.P. Trommsdorff, J. Chem. Phys. 64 (1976) 3791.
[9] E. Charney and E.D. Becker, J. Chem. Phys. 42 (1965) 910
[10] H.P. Trommsdorff, Mol. Phys. 24 (1972) 519.
[11] F. van Bolhuis and C.T. Kiers, Acta Cryst. 34b (1978) 1015.
[12] B. Venkataraman, B.G. Segal and G.K. Fraenkel, J. Chem, Phys. 30 (1959) 1006.
[13] W. Derbyshire, Mol. Phys, 5 (1961) 225.
[14] J.H. Lichtenbelt and D.A. Wiersma, Chem. Phys. 39 (1979)
[15] H.P. Trommsdorff, D. Bordeaux and D. Mentzafos, C.R. Acad. Sci. Paris C 271 (1970) 45.

CHAPTER 7

# STUDY OF THE RESIDUAL LINEWIDTH OF THE LEVEL-ANTI-CROSSING SIGNAL IN *p*-BENZOQUINONE

Lambertus BENTHEM, Jan H. LICHTENBELT and Douwe A. WIERSMA
*Laboratory for Physical Chemistry, University of Groningen, Groningen, The Netherlands*

The linewidth of the level-anti-crossing (LAC) signal in *p*-benzoquinone has been examined using optical detection of magnetic resonance between states in the avoided crossing region. The results are used to separate the homogeneous (due to hyperfine coupling) from the inhomogeneous (due to disorder) contribution to the LAC linewidth.

## 1. Introduction

In recent years the phenomenon of level-anti-crossing (LAC) in excited triplet states of organic molecules has received considerable attention. This is not so surprising as the effect not only causes a high degree of nuclear spin polarisation in the groundstate [1] but also gives rise to intensity changes in the phosphorescence which can be exploited to determine molecular zero-field splitting parameters [2]. Especially since the pioneering work of Veeman and co-workers [2,3], the nature and consequences of the LAC effect in phosphorescent organic crystals is well understood.

One aspect of the LAC effect in excited triplet states, namely the observed linewidth, however has not been dealt with in detail †. This motivated us to a profound study of the LAC linewidth in the lowest $n\pi^*$ triplet state of *p*-benzoquinone (PBQ) in an isotopically mixed crystal. This system was chosen as intense LAC signals are observable [4] and as important, the fine structure and hyperfine structure constants of the excited triplet state are known [4,5]. An additional advantage is that the crystal structure of PBQ is ideally suitable for obtaining perfect alignment of the molecular *z* axis (oxygen–oxygen direction) with the external magnetic field.

The width of the LAC signal was examined by analyzing optically detected radio-frequency induced EPR transitions among the spin sublevels in the anti-crossing region. Such signals were previously detected by Veeman in benzophenone [3] but no detailed analysis was reported.

The conclusion of the paper presented here is that the residual line-width of the LAC effect is determined by hyperfine coupling and molecular disorder in the mixed crystal as suggested by Veeman [3]. Finally we want to emphasize the quantitative aspect of the work presented in this paper. Using the previously reported fine-structure and proton hyperfine-structure constants of PBQ [4] we employ exact calculations of the LAC phenomenon to separate the homogeneous (due to hyperfine coupling) from the inhomogeneous (molecular disorder) contribution to the LAC linewidth.

† See note added.

## 2. Experimental

The experimental setup for the observation of low-frequency EPR signals is basically identical to the one described earlier [4]. The same coil as previously used in the ENDOR experiments was now employed in the optical detection of the low frequency EPR transitions. The only difference with the ENDOR experiments was that instead of 3 W for the ENDOR in the present experiments only 30 mW power was needed. We further resorted to 30% amplitude modulation at 1 kHz to phase sensitive detect the EPR transitions in the anti-crossing region. The oscillating $H_1$ field could be

oriented either parallel or perpendicular to the permanent magnetic field.

The 1% mixed crystal of *p*-benzoquinone-$h_4$ in *p*-benzoquinone-$d_4$ was grown using a Bridgman furnace and oriented such that the long molecular axis was parallel to the external magnetic field direction.

### 3. Computational procedures

In order to calculate the energies of and the transition probabilities in a system consisting of electron spins interacting with a set nuclei a computer program was written that diagonalized the complete spin-hamiltonian of the system. The hamiltonian that describes the triplet spin system of a molecule is of the following well-known form:

$$\hat{\mathcal{H}} = \beta H \cdot \mathbf{g} \cdot \hat{S} + \hat{S} \cdot \mathbf{D} \cdot \hat{S} + \sum_{i=1}^{n} \hat{S} \cdot \mathbf{A}^i \cdot \hat{I}^i - \sum_{i=1}^{n} \beta_N H \cdot \mathbf{g}_N^i \cdot \hat{I}^i , \quad (1)$$

where the symbols have the usual meaning [6].

The hermitian matrix $\mathbf{H}$, for basis functions of the "strong field" type $|\varphi\rangle = |M_S, M_{I_1}, \ldots M_{I_n}\rangle$, is then calculated in the computer program by direct product multiplication of the unit- and spin submatrices as described by Poole and Farach [7]. The spin submatrices itself are calculated using a general expression as e.g. given by Rose [8]. The only input parameters that the program needs are the magnetic field vector, the *g*- and (hyper)fine matrices and the spin multiplicities. In the actual calculations the non-collinearity of the principal axes system of the *g*, *D* and *A* tensors in PBQ [4] is taken into account and the only assumption made is that the *A* tensor is symmetric. As the matrix $\mathbf{H}$ is of order $(2S + 1)\ \Pi_{i=1}^{n}\ (2I_i + 1)$ we can only calculate, with the available computer space, the eigenvectors and energies of a triplet spin system containing no more than five hydrogen atoms. The transition probability ($P_{kl}$) for an induced transition between the states $\psi_k$ and $\psi_l$ is calculated using the following expression:

$$P_{kl} = \frac{2\pi}{\hbar^2} \left| \langle \psi_k | \beta H_1 \cdot \mathbf{g} \cdot \hat{S} - \sum_{i=1}^{n} \beta_N H_1 \cdot \mathbf{g}_N^i \cdot \hat{I}^i | \psi_l \rangle \right|^2 \cdot \delta(\omega_{kl} - \omega) . \quad (2)$$

Hereby $H_1$ is the oscillating r.f. field.

Using the decomposition of $|\psi_k\rangle$ in terms of the high-field functions $|\varphi_i\rangle$; $|\psi_k\rangle = \Sigma_{i=1}^{n}\ c_{ik}|\varphi_i\rangle$ eq. (2) is transformed to:

$$P_{kl} = \frac{2\pi}{\hbar^2} \left| \sum_{i=1}^{n} \sum_{j=1}^{n} c_{ik}\, H_{ij}^{\text{Zeeman}}\, c_{jl} \right|^2 \delta(\omega_{kl} - \omega) , \quad (3)$$

whereby $\mathbf{H}^{\text{Zeeman}}$ is the hamiltonian matrix for the r.f. perturbation $H_1$, which is calculated analogous to the total hamiltonian ($\hat{\mathcal{H}}$).

The resolution in this calculation was varied between steps of 0.1 G near the avoided crossing region and up to 5 G far off resonance. Care was taken that further refinement of the calculation did not change the outcome. Between the calculated energies other ones, which matched the driving frequency of the $H_1$ field, were interpolated. The corresponding eigenvectors obtained were used for the calculation of the transition moment at the driving frequency. The computer program further sums all the transition probabilities for a fixed energy separation and plots a spectrum as a function of the applied magnetic field.

### 4. Level-anti-crossing in a two-level system

Fig. 1 shows in a simple picture the ideas of the experiments we have performed on PBQ. For a magnetic field along the *z* axis of one of the molecules in the unit cell, anti-crossing occurs between the $|0\rangle$ and $|1\rangle$ electron spin sublevels at a field of ca. 731 G. Note that in PBQ the molecular *z* axis coincides with the *z* principal axis of the fine-structure tensor [4]. The lower part of the figure shows that this effect is observed as a modulation of the phosphorescence. With a radio-frequency field, transitions may be induced between the anti-crossing levels as indicated by the heavy arrows. These transitions may be optically detected as is shown here. The real situation in PBQ of course is far more complex than shown in fig. 1, but from the two-level model we may also calculate the lineshape of the LAC signal. In the following we denote the populating rate constants by $P_i$, the radiative rate constants by $k_i^r$ and the total decay rate constants by $k_i$.

In a two-level system the hamiltonian matrix is

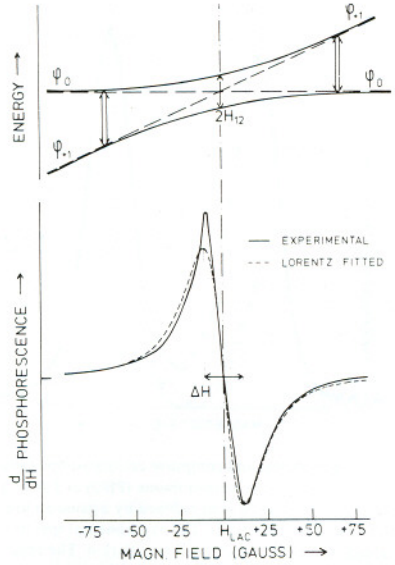


Fig. 1. Two-level picture for level-anti-crossing in *p*-benzoquinone. The lower part of the figure shows the experimental observed signal and the computer fitted curve. Note that this fitting is only made for illustrative purpose. The results of this fitting is not used in the analysis.

$$\mathbf{H} = \begin{pmatrix} H_{11} & H_{12} \\ H_{21} & H_{22} \end{pmatrix}.$$

The eigenvalues are:

$$E^{\pm} = \tfrac{1}{2}(H_{11} + H_{22}) \pm \tfrac{1}{2}[(H_{11} - H_{22})^2 + 4H_{12}^2)]^{1/2}, \tag{4}$$

and for the eigenvectors the following relation holds:

$$c_1^+/c_2^+ = -c_2^-/c_1^- \tag{5}$$
$$= \{H_{22} - H_{11} + [(H_{11} - H_{22})^2 + 4H_{12}^2]^{1/2}\}/2H_{12}.$$

The phosphorescence intensity of the anti-crossing system then becomes:

$$I \propto \Big[\sum_{\pm} [P_1 c_1^{\pm}(c_1^{\pm})^* + P_2 c_2^{\pm}(c_2^{\pm})^*] \times [k_1^{\mathrm{r}} c_1^{\pm}(c_1^{\pm})^* + k_2^{\mathrm{r}} c_2^{\pm}(c_2^{\pm})^*] \Big/ [k_1 c_1^{\pm}(c_1^{\pm})^* + k_2 c_2^{\pm}(c_2^{\pm})^*]\Big]. \tag{6}$$

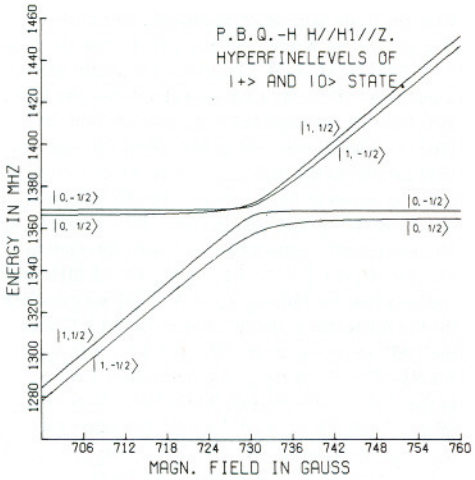


Fig. 2. Calculation of the energies of the spin-levels in the level-anti-crossing region of *p*-benzoquinone. Only one of the four (almost equivalent) protons is included in the calculation. Note that there are only anti-crossings in the LAC region.

This expression can be re-arranged to become of the following form:

$$I \propto P_1 k_1^{\mathrm{r}}/k_1 + P_2 k_2^{\mathrm{r}}/k_2 - \frac{k_1 k_2}{k_1 + k_2}\left[\frac{P_1}{k_1} - \frac{P_2}{k_2}\right]\left[\frac{k_1^{\mathrm{r}}}{k_1} - \frac{k_2^{\mathrm{r}}}{k_2}\right] L \tag{7}$$

where $L$ is Lorentz line shape function:

$$L = \tfrac{3}{4}\sigma^2/(\tfrac{3}{4}\sigma^2 + \Delta H^2),$$

with $\Delta H = H - H_{\mathrm{LAC}}$ and

$$\sigma = \tfrac{2}{3}\sqrt{3}|2H_{12}|\tfrac{1}{2}(k_1 + k_2)(k_1 k_2)^{-1/2}. \tag{8}$$

The first two terms in eq. (7) we recognize as arising from the unperturbed two-level system and the LAC signal thus only results from the last term. The LAC signal is expected to show a lorentzian line shape with a width determined by the interaction strength and the total molecular decay constants. In a system where numerous anti-crossings occur at different field values the observed linewidth of course is determined by a convolution of all the LAC signals occurring.

We note here that the above kinetic derivation of the lineshape of the LAC signal can also be obtained

from the more general quantum-mechanical derivation as given by Wieder and Eck [9]. In case the relation $|2H_{12}| \gg (k_1 k_2)^{1/2}$ holds the linewidths expressions are identical. As a simple example we give here the results of the expected lineshape function for PBQ considering only one proton. With the magnetic field parallel to the molecular $z$ axis anti-crossings occur as shown in fig. 2 between the $|M_S M_I\rangle$ states $|0, \frac{1}{2}\rangle$ and $|1, -\frac{1}{2}\rangle$ and also between $|0, -\frac{1}{2}\rangle$ and $|1, \frac{1}{2}\rangle$. The former anti-crossing has the largest interaction element $|H_{12}| = \frac{1}{2}\, 2^{-1/2}\, (A_{xx} + A_{yy}) = 7.2$ MHz and realizing that for PBQ $k_0/k_{+1} = 30$ [10] we calculate for the full width at half maximum ($\sigma$) 16.8 G with the LAC occurring, at $H = H_{\mathrm{LAC}} + \frac{1}{2}A_{zz} = H_{\mathrm{LAC}} + 1.5$ G. Thereby is $H_{\mathrm{LAC}}$ the field where LAC occurs in the absence of hyperfine interactions. Note that the relation $|2H_{12}| \gg (k_1 k_2)^{1/2}$ holds! The other LAC signal is calculated at $H = H_{\mathrm{LAC}} - \frac{1}{2}A_{zz} = H_{\mathrm{LAC}} - 1.5$ G and for this case $\sigma$ is calculated to be 5.8 G.

Experimentally we observe for PBQ a lineshape for the LAC signal close to lorentzian with a linewidth of 22 G as shown in fig. 1. The simple two-level model thus gives already a very satisfactory picture of the LAC phenomenon in PBQ. In the following section we will show that a closer look at the LAC region reveals that for a quantitative description of the LAC effect in PBQ all four protons should be included.

## 5. Results and discussion

Fig. 3 shows an example of the EPR signals obtained when the magnetic field is scanned through the anti-crossing region while the sample is irradiated at 60 MHz.

The isotopically mixed crystal of PBQ is at 1.8 K and the magnetic field is parallel to the molecular $z$ axis. The smooth curve is calculated by the computer taking into account the hyperfine interaction terms of all four protons. The calculation procedure is explained in section 3. In order to obtain agreement between experiment and theory the calculated stick spectrum need be broadened with a gaussian line shape function with a linewidth of 8.5 G. The interpretation of this gaussian broadening will be given later (vide infra).

In fig. 4 we have plotted the observed magnetic field values for the peak positions of the signals, as

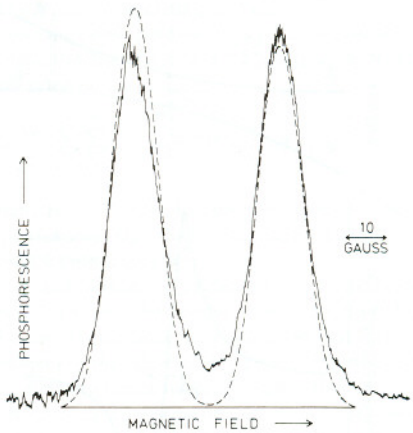


Fig. 3. Experimental and computer calculated optically detected EPR signal of *p*-benzoquinone (PBQ) at 1.8 K. The obtained stick spectrum was broadened by a gaussian line profile with halfwidth of 8.5 gauss. The experimental spectrum was obtained for parallel polarized RF radiation. The result obtained using perpendicular polarized radiation was very similar.

shown in fig. 3, versus the fixed frequency of the oscillator. The smooth curve is the computer calculated one whereby the hyperfine interactions with all four protons are included, the dotted curve is the computer prediction if only one proton interacts with the triplet spin system. The figure clearly shows that inclusion of all protons in the calculation gives superior agreement between theory and experiment which in essence confirms the complexity of the level structure. The important conclusion that we may draw now is that the *homogeneous* component of the residual linewidth of the LAC signal can be completely explained by the excited state hyperfine interactions. The observed linewidth of the LAC signal however cannot be exclusively determined by these interactions as the EPR signals were shown to be gaussian broadened. We suggest this to be due to statistical disorder in the mixed crystal. In order to calculate the amount of disorder needed to explain the observed linewidth we calculated the sensitivity of the peak position of the EPR transitions to small rotations of the molecule around the $y$ axis. Rotation around the $x$ axis should give similar results.

Fig. 5 shows the results of such a calculation and

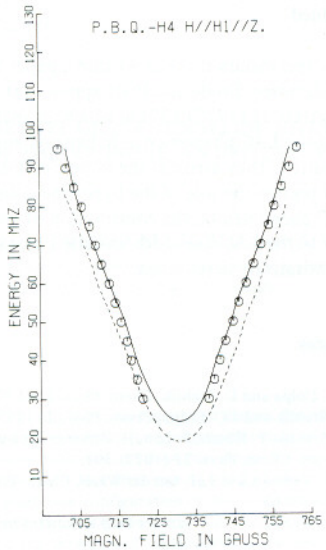


Fig. 4. Plot of the observed peak position ⊙ of the optically detected EPR signals for a fixed frequency versus magnetic field. Perfect alignment of the molecular $z$ axis along the external magnetic field is assumed. The solid line is the computer *calculated* relationship whereby the full spin-hamiltonian of the molecule is used. The dotted curve represents the result of a calculation if only one proton is taken into account.

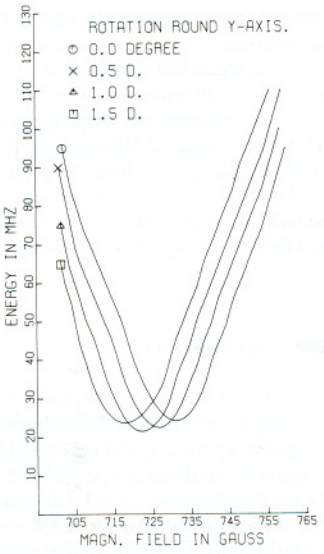


Fig. 5. Calculated curves of the peak positions of the optically detected EPR signals for a fixed frequency versus magnetic field for imperfect alignment of the molecular $z$ axis with the external magnetic field.

we see that rotation of only 0.5° gives a shift in the calculated curve of 4.5 G. Our conclusion therefore is that molecular disorder, amounting to at most rotations of 0.9° either around the $x$ or $y$ axis or both explains the gaussian component of the EPR linewidth. The residual linewidth of the LAC signal thus is not only determined by hyperfine coupling effects but also contains a sizeable component from molecular disorder. The lineshape of the observed LAC signals in general thus should be described neither as a simple lorentzian or gaussian but rather as a sum of Voigt [11] lineshape profiles.

Finally it seems interesting to define the parameters that would describe the LAC effect in PBQ in terms of a pseudo two-level system. From the results displayed in fig. 4 we calculate an effective interaction constant ($V_{\text{eff}}$) of 12 MHz ($|H_{12}|$). A two-level description for the case of PBQ however is far from realistic and shown in fig. 6 where the exact level structure in

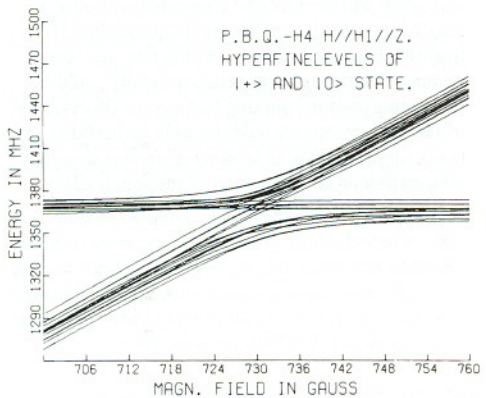


Fig. 6. Calculated level structure of the electron–nuclear spin levels in the level-anti-crossing region of $p$-benzoquinone. Perfect alignment of the molecular $z$ axis along the external magnetic field is assumed.

the anti-crossing region is given. The figure shows that there are numerous crossings and anti-crossings in the avoided crossing region and the effective interaction strength constant is difficult to interpret. In PBQ the constant may be determined by the largest off-diagonal hyperfine element, being 7.2 MHz as calculated in section 4. Such an assignment however is not unambiguous and we therefore conclude that a pseudo two-level approach of the LAC effect, as was done by Mucha and Pratt [12] for $^{13}$C-benzophenone, is not justified.

## 6. Conclusion and suggestion

Detailed study of the level-anti-crossing effect in *p*-benzoquinone shows that the residual linewidth of the LAC signal in a perfectly oriented crystal (with regard to alignment of the magnetic field and a principal axis of the fine-structure tensor) is determined by the excited state hyperfine interaction and molecular disorder. The disorder in *p*-benzoquinone amounts to at most a tilt of 0.9° of the molecular plane. We further suggest the possibility of observing quantum beats from molecules undergoing level-anti-crossing. In the avoided crossing region the electron–nuclear spin states of different parentage are heavily mixed by the hyperfine coupling as fig. 6 shows. Ground state nuclear spin-levels will therefore be connected with several excited state levels introducing the possibility of quantum beat spectroscopy. With a nitrogen laser pumped dye laser such experiments easily could be done using photon counting techniques. Observation of the beat-structure would not only be useful as a check on the calculated level-structure but also yield information on the relaxation of the spin-levels in the avoided crossing region.

## Note added

After this manuscript was written a paper by Kothandaraman, Brode and Pratt appeared (Chem. Phys. Letters 51 (1977) 137) in which an analogous study of the LAC phenomenon in benzophenone was reported. They arrive at the same conclusion as we with regards the role of the hyperfine coupling in the LAC phenomenon; the contribution of molecular disorder to the LAC linewidth was also considered but not quantitatively determined.

## References


[1] J.C. Colpa and D. Stehlik, Chem. Phys. 21 (1977) 273;
D. Stehlik and J.C. Colpa, Chem. Phys. 21 (1977) 289;
D. Stehlik, P. Rösch, P. Lau, H. Zimmermann and K.H. Hauser, Chem. Phys. 21 (1977) 301.

[2] W.S. Veeman and J.H. van der Waals, Chem. Phys. Letters 7 (1970) 65;
W.S. Veeman, A.L.J. van der Poel and J.H. van der Waals, Mol. Phys. 29 (1975) 225.

[3] W.S. Veeman, Ph. D. Thesis, Leiden (1972).

[4] J.H. Lichtenbelt, J.G.F.M. Fremeijer, H. Veenvliet and D.A. Wiersma, Chem. Phys. 10 (1975) 107.

[5] J.H. Lichtenbelt and D.A. Wiersma, Chem. Phys. 34 (1978)

[6] C.A. Hutchison Jr. and B.W. Mangum, J. Chem. Phys. 34 (1961) 908.

[7] C.P. Poole and H.A. Farach, The theory of magnetic resonance (Wiley–Interscience, New York, 1972).

[8] M.E. Rose, Elementary theory of angular momentum, 3th Ed. (Wiley, New York, 1963).

[9] H. Wieder and T.G. Eck, Phys. Rev. 153 (1967) 103.

[10] H. Veenvliet and D.A. Wiersma, Chem. Phys. 8 (1975) 432.

[11] D.W. Posener, Austr. J. Phys. 12 (1959) 184.

[12] J.A. Mucha and D.W. Pratt, Chem. Phys. Letters 30 (1975) 181;
J.A. Mucha and D.W. Pratt, J. Chem. Phys. 66 (1977) 5356.

# METHYL GROUP TUNNELING ROTATION IN THE LOWEST nπ* TRIPLET STATE OF TOLUQUINONE. AN OPTICALLY DETECTED ENDOR, LAC AND CR STUDY

Jan H. LICHTENBELT and Douwe A. WIERSMA
*Laboratory for Physical Chemistry, University of Groningen, 9747 AG Groningen, The Netherlands*

In this paper we report and discuss the effects of methyl group tunneling rotation on the methyl proton ENDOR, LAC and CR spectra in the lowest triplet state of toluquinone at 1.8 K. From a detailed analysis of the ENDOR spectra in the lowest rotational state (A) we obtain for the methyl protons the following isotropic hyperfine interaction constants: $A_1 = A_2 = 34.4$ MHz and $A_3 = -53.7$ MHz. The tunneling frequency ($3J$) is calculated to be 2.9 GHz. The most likely equilibrium configuration of the torsional oscillator is found to be the one whereby the molecular plane is a mirror plane and the out-of-plane methyl protons point towards the closest oxygen atom. We also show that cross-relaxation between $|A\rangle$ and $|E\rangle$ states of *translational equivalent* toluquinone molecules is responsible for the observed sidebands in the level-anti-crossing spectra of toluquinone.

## 1. Introduction

In a recent series of papers [1–5] we have reported on the EPR, ENDOR, level-anti-cross (LAC) and cross-relaxation (CR) spectra of the lowest nπ* triplet state in *p*-benzoquinone (PBQ) and toluquinone (TQ) at 1.8 K. While analyzing the recorded spectra we encountered some puzzling features in the proton-ENDOR and LAC spectra of TQ. First, the proton ENDOR spectrum of the methyl protons in the $m_s = -1$ state showed a triplet of lines with very similar angular dependence [5]. Second, the LAC signal consisted of a triplet of lines instead of one as observed for PBQ. These features intrigued us and in this paper we will show that the observed "anomalies" are due to tunneling rotation of the methyl group in TQ. Methyl group tunneling rotation has been previously observed in molecular radicals and its effect on the methyl proton spin levels, as observed in the EPR and ENDOR spectra, has been studied in great detail by Clough et al. [6–8]. Also detailed NMR studies of methyl group tunneling rotation have been performed [9,10].

Briefly, the methyl group tunneling rotation creates a triple well potential wherein the lowest rotational state has A spatial symmetry. The lowest excited rotational state in this well has spatial symmetry E and is $3J$ in energy above the ground state. Pauli's exclusion principle further requires that the total wavefunction (space ⊗ spin) is anti-symmetric with respect to the exchange of spin and space coordinates of any pair of protons. This prerequisite can only be fulfilled by combining the lowest rotational A state with a quartet A nuclear spin state and the lowest excited rotational E state with a doublet E nuclear spin state.

At temperatures where $3J \approx kT$, ENDOR transitions in both A and E rotational states have been observed in molecular radicals [6]. In the lowest triplet state of toluquinone we have only observed ENDOR transitions in the A rotational ground state. The presence of the nearby E states however is clearly exposed in the methyl proton ENDOR spectra of this state.

The tripling of the LAC spectrum can be understood by assuming that the outer lines are caused by cross-relaxation between the $|A\rangle$ and $|E\rangle$ rotational state of translational equivalent molecules.

The final conclusion is that all experimental results

are consistent with predictions made, on basis of tunneling rotation of the methylgroup in TQ.

## 2. Theory

### *2.1. First order treatment*

The hamiltonian for a hindered rotating methyl group in a triplet state may, using the local $C_3$ symmetry of the methyl group, be written in the following form [6]:

$$\mathcal{H}/h = \nu_e S_z + \boldsymbol{S}\cdot\mathbf{D}\cdot\boldsymbol{S} - \nu_N I_z^A + \tfrac{1}{3}\boldsymbol{S}\cdot(\mathbf{A}^A\cdot\boldsymbol{I}^A + \mathbf{A}^{E_a}\cdot\boldsymbol{I}^{E_b} + \mathbf{A}^{E_b}\cdot\boldsymbol{I}^{E_a}) - J(\boldsymbol{I}^A\cdot\boldsymbol{I}^A - \tfrac{9}{4}) + \tfrac{1}{3}(Q^A\cdot P^A + Q^{E_a}\cdot P^{E_b} + Q^{E_b}\cdot P^{E_a}). \quad (1)$$

The superscripts A, $E_a$, $E_b$ refer to symmetry adapted combinations of operators or tensors according to the following prescription:

$$R^A \equiv R_1 + R_2 + R_3,$$

$$R^{E_a} \equiv R_1 + \epsilon R_2 + \epsilon^* R_3,$$

$$R^{E_b} \equiv R_1 + \epsilon^* R_2 + \epsilon R_3, \quad (2)$$

where $\epsilon = \exp(2\pi i/3)$.

Nuclear spin states of A and E symmetry are also formed using this prescription and expression (1) shows that the quartet ($I = \frac{3}{2}$) A state is lower in energy, by the tunneling frequency $3J$, than the doublet ($I = \frac{1}{2}$) E state. The other symbols in expression (1) have the usual meaning, whereby we note that **D** stands for the fine-structure tensor in the lowest triplet state, $Q$ for the nuclear dipole–dipole interaction and $P$ is a product of nuclear spin operators.

It turns out that, with the basis set chosen, the $|E^a_{m_I}\rangle$ and $|E^b_{m_I}\rangle$ states remain, in first order, degenerate. This unsatisfactory situation, with regards to a perturbational treatment of the problem, can be overcome by exploiting the fact that, most likely, the lowest triplet in TQ retains a mirror plane. In fact our proton ENDOR measurements show (section 3.1) that this supposition is probably correct. In this case $A^1_{zz} = A^2_{zz} \neq A^3_{zz}$, where 1, 2 and 3 are methyl proton indices. New E states of the following form can then be formed:

$$|E'_{m_I}\rangle = \tfrac{1}{2}\sqrt{2}(\epsilon|E^a_{m_I}\rangle + \epsilon^*|E^b_{m_I}\rangle),$$

$$|E''_{m_I}\rangle = \tfrac{1}{2}\sqrt{2}(\epsilon|E^a_{m_I}\rangle - \epsilon^*|E^b_{m_I}\rangle). \quad (3)$$

Using this A, E′ and E″ basis set, the first order energies, for the magnetic field parallel to the fine-structure $z$-axis, are found to be:

$$E(m_s, m_I) = m_s\nu_e - m_I\nu_N - (\tfrac{3}{2}m_s^2 - 1)Z \pm \tfrac{3}{2}J + \tfrac{1}{3}m_s m_I A^A_{zz} + \tfrac{2}{3}\mu m_s m_I A^\Delta_{zz}. \quad (4)$$

Where the plus sign applies for the E states and the minus sign for the A state. Also $\mu = 0$ for $|A\rangle$, +1 for $|E''\rangle$ and −1 for $|E'\rangle$, while $A^\Delta_{zz} = A^3_{zz} - \frac{1}{2}(A^1_{zz} + A^2_{zz})$. The principal fine-structure value is: $Z = -D_{zz}$. Note that for the $m_s = 0$ state the degeneracy among the E states persists. Even in second order perturbation theory this degeneracy remains. From eq. (4) we now easily calculate the first order ENDOR frequencies:

$$\nu^{(1)}_{ENDOR} = \nu_N - \tfrac{1}{3}m_s A^A_{zz} + \tfrac{2}{3}\mu m_s A^\Delta_{zz}. \quad (5)$$

In first order one therefore expects to observe in e.g. the lower A state, for every electron spin level, only one ENDOR transition. Experimentally we observe in the lowest triplet state of TQ a close lying triplet of lines, for every electron spin level, which shows that a first order treatment of the methyl group tunneling rotation is not sufficient.

As we have failed to observe ENDOR transitions which could be assigned to the doublet E state, we will concentrate on the ENDOR frequencies on the $|\pm1,A\rangle$ and $|0,A\rangle$ states in the following sections. At this point we note that the results of the analysis show that for methyl group tunneling in the lowest triplet state of TQ the following conditions hold:

$$3J, \nu_e > |Z| \gg |A^\Delta_{iso}/3| \gg |(A^\Delta_{ij})_{an}|, |A^A_{ij}|, |A^\eta_{ij}|, \nu_N, \quad (6)$$

with $A^\eta \equiv A_1 - A_2$ and $A^\eta_{iso} = 0$. The index "an" is given to the anisotropic elements by themselves, and $i = x, y$, or $z$. We further assume that the second order correction of the pure "high field" $|m_s\rangle$ states is small compared to the tunneling and electronic Zeeman

frequencies. In this case the second order ENDOR frequencies are easily calculated for the magnetic field along principal directions of the fine-structure tensor.

*2.2. Second order ENDOR frequencies in the $|\pm 1, A\rangle$ state*

For a magnetic field parallel to the $z$-axis of the fine-structure tensor ($H \parallel z$) the second order mean ($\bar{\nu}$) and difference ($\Delta\nu$) ENDOR frequencies are found to be:

$$\bar{\nu} = \nu_N - \tfrac{1}{3} m_s A_{zz}^A + m_s (A_{iso}^\Delta)^2 / 9(m_s \nu_e - \tfrac{3}{2} Z - 3J), \tag{7a}$$

$$\Delta\nu = 2(A_{iso}^\Delta)^2 (3J \pm m_s A_{iso}^\Delta)/[81J^2 - (A_{iso}^\Delta)^2] + (A_{iso}^\Delta)^2/9(m_s \nu_e - \tfrac{3}{2} Z - 3J) + \nu_{NN}, \tag{7b}$$

where the plus sign applies for $\Delta\nu \equiv \nu_2 - \nu_1$ and the minus sign for $\Delta\nu \equiv \nu_3 - \nu_2$ with

$$h\nu_1 = |E_{|\pm 1, A_{3/2}\rangle} - E_{|\pm 1, A_{1/2}\rangle}|,$$

$$h\nu_2 = |E_{|1, A_{1/2}\rangle} - E_{|1, A_{-1/2}\rangle}|,$$

$$h\nu_3 = |E_{|\pm 1, A_{-1/2}\rangle} - E_{|\pm 1, A_{-3/2}\rangle}|,$$

and

$$\nu_{NN} = \tfrac{3}{2} (g_N^2 \beta_N^2 / h r^3)(1 - \tfrac{3}{2} \sin^2 \psi), \tag{8}$$

with $\psi$ the angle between the magnetic field vector and the $C_3$ methyl rotation axis. Note that $\nu_{NN}$ is the most important nuclear point dipole–dipole term as derived by Allen [10].

From eq. (7b) we derive the following useful relation:

$$(\nu_3 - \nu_2) - (\nu_2 - \nu_1) = -4 m_s (A_{iso}^\Delta)^3 / [81J - (A_{iso}^\Delta)^2]. \tag{9}$$

This expression shows that measurement of the asymmetry pattern of the ENDOR frequencies yields directly the sign of $A_{iso}^\Delta$!

*2.3. Second order ENDOR frequencies in the $|0, A\rangle$ state*

For the $|0, A\rangle$ state the second order methyl proton energies are also easily calculated for $H \parallel z$ from which the following ENDOR frequencies are obtained:

$$\nu_1 = \nu_N + 2(A_{iso}^\Delta)^2/9(\nu_e + \tfrac{3}{2} Z - 3J) + \nu_{NN} = (E_{|0, A_{-3/2}\rangle} - E_{|0, A_{-1/2}\rangle})/h, \tag{10a}$$

$$\nu_3 = \nu_N + 2(A_{iso}^\Delta)^2/9(\nu_e - \tfrac{3}{2} Z + 3J) - \nu_{NN} = (E_{|0, A_{1/2}\rangle} - E_{|0, A_{3/2}\rangle})/h, \tag{10b}$$

and $\nu_2 = \frac{1}{2}(\nu_1 + \nu_3)$.

By measuring the frequency difference $\Delta\nu_i \equiv \nu_i - \nu_N$ for $H \parallel z$ and by calculating the term $\nu_{NN}$ [see eq. (8)], the tunneling frequency ($3J$) and $A_{iso}^\Delta$ can be calculated as follows:

$$3J = [(\Delta\nu_1' - \Delta\nu_3')/(\Delta\nu_1 + \Delta\nu_3)]\, \nu_e + \tfrac{3}{2} Z, \tag{11a}$$

$$|A_{iso}^\Delta| = 3\{[\Delta\nu_1' \Delta\nu_3'/(\Delta\nu_1 + \Delta\nu_3)]\, \nu_e\}^{1/2}, \tag{11b}$$

where $\Delta\nu_1' \equiv \Delta\nu_1 - \nu_{NN}$ and $\Delta\nu_3' \equiv \Delta\nu_3 + \nu_{NN}$. It is interesting to note here that $\Delta\nu_3$ will always be positive but $\Delta\nu_1$ may be either negative or positive depending on the magnitude of the tunneling frequency compared to $\nu_e + \frac{3}{2} Z$.

## 3. Results

*3.1. The $|-1, A\rangle$ state*

All ENDOR experiments on the methyl proton transitions in the $|-1, A\rangle$ state were performed on the $\langle -1, A| \leftrightarrow |0, A\rangle$ EPR transition in the lowest triplet state to TQ at 1.8 K. From angular dependent ENDOR measurements on the $|-1, A\rangle$ state [5], hyperfine data were collected which are given in table 1. Note that these constants were obtained by averaging over the constants derived for the three separate transitions.

We first remark that the measured orientation of the hyperfine tensor with respect to the molecular plane is in agreement with our earlier (section 2.1) assumption of the molecular mirror plane. The measurements however, do not discriminate between the two possible equilibrium positions of the methyl torsional oscillator which are shown in fig. 1.

We have tried to discriminate between these two possibilities by calculating the anisotropic hyperfine interaction of the methyl protons by using the calculated gross atomic spin densities of PBQ [3] and

Table 1
Hyperfine data from ENDOR transitions in the $|-1, A\rangle$ state. The isotropic hyperfine interaction is: $\frac{1}{3}A^{A}_{iso} = 5.08$ (0.27) MHz. $\phi$ is the angle between the molecular $z$-axis and the projection of the hyperfine principal axis in the molecular plane. $\theta$ is the angle between the molecular $x$-axis and the hyperfine principal axis

| | Principal hyperfine axis | | |
|---|---|---|---|
| | $x'$ | $y'$ | $z'$ |
| $\frac{1}{3}(A^{A}_{ii})_{an}$ (MHz) | −1.70 (0.03) | 2.51 (0.02) | −0.82 (0.05) |
| $\phi$ | – | 94.9° (0.7°) | 4.9° (0.8°) |
| $\theta$ | −1.2° (1.0°) | 90.0° (0.4°) | 90.0° (1.2°) |

using further a Slater orbital model as given by Derbyshire [11]. We find considerable better agreement between our calculation of the anisotropic tensor $\mathbf{A}^{A}$ and experiment for configuration A than B. We note that this "preferred" A configuration was also suggested by Trommsdorff et al. [12] for TQ in the ground-state.

We have also tried to calculate [eqs. (7a) and (7b)] from the measured ENDOR frequencies in the $|-1, A\rangle$ state the tunneling constants $3J$ and $A^{\Delta}_{iso}$. This however failed for reasons presently not known. It is indeed true that in the $|-1, A\rangle$ state the second order shifts are small, which makes determination of the constants $3J$ and $A^{\Delta}_{iso}$ difficult. In retrospect it is quite clear that the ENDOR measurements should have been done on the $|+1, A\rangle$ state where the second order corrections [eqs. (7)] are much larger. However, the analysis of the experiments was performed years after the measurements and it did not seem worthwhile to rebuild the experimental setup.

The only definite information obtainable from the

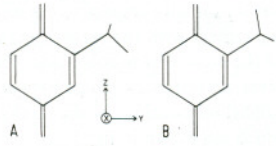


Fig. 1. Two possible equilibrium positions of the methyl group in toluquinone. Note that the short methyl C–H bond is the projection in the molecular plane of the two out-of-plane C–H bondings.

observed asymmetry in the ENDOR transitions of the $|-1, A\rangle$ state is that $A^{\Delta}_{iso}$ is *negative*.

### 3.2. *The* $|0, A\rangle$ *state*

Eq. (10) shows that ENDOR transitions in the $m_s = 0$ state are expected close to the free proton frequency. Fig. 2 shows that there are numerous ENDOR transitions which occur near the free proton energy and our first task is to decide which ones are due to other protons than the guest methyl ones. First we note that there are three ENDOR transitions due to the three aromatic ring protons. They are easily assigned as, for $H \parallel y$ the ENDOR frequencies should equal zero, while rapidly varying for off-axis fields. The dotted lines numbered 1, 2 and 3 are assigned to these obtained on basis of computer calculations [1] using the known hyperfine tensors of these protons [5].

Second we have to realize that the host toluquinone molecules are only ring-deuterated and therefore the methyl protons of the host molecules may couple, mainly through magnetic dipole–dipole coupling with the guest triplet state. We therefore calculated [11], using the gross atomic distribution of spin density in PBQ, the anisotropic hyperfine interaction of all neighbouring methyl protons due to coupling with the guest triplet state. Using these data we subsequently calculated [1] the first order ENDOR frequencies of the $|+1, A\rangle$ state. The results of these calculations, insofar the calculated ENDOR frequencies differed from the free proton frequency, are given by broken lines in fig. 2.

The remaining ENDOR transition ($\nu_N$ +570 kHz for $H \parallel y$) therefore must be due to a transition in the $|0, A\rangle$ state of the guest hindered rotating methyl group. It is gratifying to note that three transitions [obeying eq. (10)] may be identified whereby indeed $\nu_2 = \frac{1}{2}(\nu_1 + \nu_3)$.

From the ENDOR frequencies at $H \parallel y$ and using eqs. (11) we calculated $|A^{\Delta}_{iso}| = 88 \pm 5$ MHz and $3J = 2.9 \pm 0.4$ GHz. Using the fact that $A^{A}_{iso} = 15.3$ MHz (table 1) and $A^{\Delta}_{iso} < 0$ (section 3.1) the methyl proton isotropic hyperfine interactions are calculated to be $A_1 = A_2 = 34.4$ MHz and $A_3 = -53.7$ MHz. With this set of data and including all nuclear–nuclear interactions, we have exactly calculated [using eq. (1)] [4], the angular dependence of these transitions which in fig. 2 are marked by the solid lines.

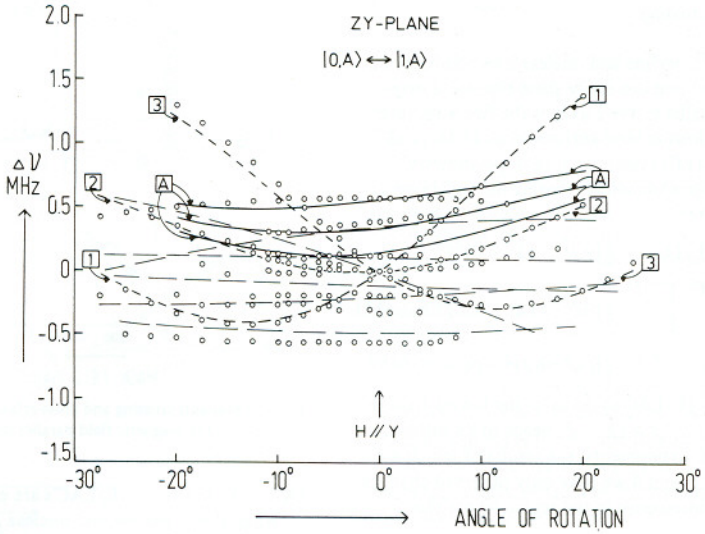


Fig. 2. ENDOR frequencies in the neighbourhood of the free proton frequency $\nu_p$, are given as $\nu_{ENDOR} - \nu_p$ for an EPR transition between the |0, A⟩ and |1, A⟩ levels and for a rotation of the magnetic field in a nearly molecular *zy*-plane. The experimental points are shown by circles and the theoretical frequency angular dependences are given by solid or dashed lines. The aromatic proton ENDOR lines of the guest molecules are numbered by 1, 2 and 3 and are given by short dashed lines. The ENDOR lines of the $m_S = 1$ state of the host methyl protons are given by long dashed lines. The three solid ENDOR lines, numbered with A, are due to the |0, A⟩ transitions of the guest methyl protons.

We finally note that when the calculated values of $A^{\Delta}_{iso}$ and $3J$ are used to predict $\bar{\nu}$ and $\Delta\nu$ for ENDOR transitions in the |−1, A⟩ state, the experimentally observed asymmetry is too large. A reason for this discrepancy, as mentioned earlier, may be that the equilibrium position of the methyl torsional oscillator is not coincident with the molecular plane. The results displayed in table 1 would be consistent with a small out-of-plane rotation.

We conclude however that the overall picture is clearly consistent with the assumption that, in the lowest triplet state of TQ, the methyl group undergoes a tunneling rotation.

In conclusion of this section it seems appropriate to briefly comment on the hyperfine interaction parameters found for the methyl group in the lowest $n\pi^*$ triplet state of TQ as compared with those obtained in the doublet state of molecular radicals [6–8]. In the case of molecular radicals the most important hyperfine interaction is that between the methyl proton and the $\pi$-orbital on the adjacent carbon atom which leads for the isotropic hyperfine interaction to an expression of the well-known form $A_{iso} \approx B_0 + B_2 \cos^2\theta$ [6–8]. This relationship in effect enables one to explicitly formulate functions of the type used in eq. (3).

For the hyperfine interaction of the methyl group protons with unpaired electron spin density in TQ no such a simple relationship exists. This is due to the fact that in this case a methyl proton interacts with the unpaired spin-density of the n-type (mainly localized at oxygen [3]) and also with the unpaired spin-density of the $\pi$-type which is delocalized [3]. Note that in the case of TQ this leads to a significant contribution of the isotropic and *anisotropic* hyperfine interaction to $\mathbf{A}^A$, in contradistinction with the case of a molecular radical, where the isotropic hyperfine interaction contribution to $\mathbf{A}^A$ is dominant.

In the next section we will show that a tunneling rotation also explains the observed sidebands in the LAC spectrum of TQ.

## 4. Level-anti-crossing

When the hyperfine and nuclear interaction terms are disregarded one can easily show that for a magnetic field parallel to the $z$-axis of the fine-structure tensor the following level-anti-crossings (LAC) and level-crossing (LC) (assuming local $C_3$-symmetry [13]) occur for a tunneling rotating methyl group in the triplet state:

$$\begin{aligned} &|1,A\rangle - |-1,E\rangle \text{LC} \;:\; \tfrac{1}{2}[9J^2 - (X-Y)^2]^{1/2}, \\ &\left.\begin{aligned} &|A\rangle - |A\rangle \text{LAC} \\ &|E\rangle - |E\rangle \text{LAC} \end{aligned}\right\} \;:\; \tfrac{1}{2}[9Z^2 - (X-Y)^2]^{1/2}, \quad (12) \\ &|A\rangle - |E\rangle \text{LAC} \;:\; \tfrac{1}{2}[(3Z \pm 6J)^2 - (X-Y)^2]^{1/2}. \end{aligned}$$

For the $|A\rangle - |E\rangle$LAC to occur at the lowest field the extra condition: $3J > |X - Z|$ needs to be fulfilled.

In our LAC experiments, the results of which are shown in figs. 3 and 4 we have only observed changes of the phosphorescence in the region where the


Fig. 3. Level-anti-crossing and cross-relaxation signals of toluquinone for the magnetic field parallel to the fine structure tensor $z$-axis.

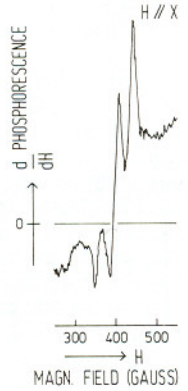


Fig. 4. Level-anti-crossing and cross-relaxation signals of toluquinone for the magnetic field parallel to the fine structure tensor $x$-axis.

$|A\rangle - |A\rangle$ and $|E\rangle - |E\rangle$LAC's are expected.

When the hyperfine and nuclear Zeeman terms are incorporated in a calculation of the expected LAC's we obtain the following for $H \parallel z$:

For the $|A\rangle - |A\rangle$LAC:

$$\nu_e = -\tfrac{1}{2} m_I A^A_{zz} + [(\tfrac{3}{2}Z + \lambda\nu_N)^2 - \tfrac{1}{4}(X-Y)^2]^{1/2}, \quad (13a)$$

where $\lambda = \pm 1$ depending on whether the anticrossing is of the flop-flop ($\Delta m_s = \pm 1$, $\Delta m_I = \pm 1$) or of the flip-flop type ($\Delta m_s = \pm 1$, $\Delta m_I = \mp 1$). The $m_I$ values in eq. (13a) are those of the $|+1\rangle$ state.

For $|E\rangle - |E\rangle$LAC the result is for $H \parallel z$:

$$\nu_e = \mu(\tfrac{1}{3}\xi A^\Delta_{iso} - \tfrac{1}{6}A^A_{zz}) + [(\tfrac{3}{2}Z + \mu\nu_N)^2 - \tfrac{1}{4}(X-Y)^2]^{1/2}, \quad (13b)$$

where for the $m_s = +1$ (or $-1$) state and a flip-flop LAC $\mu = -1$ (or $+1$), while for a flop-flop LAC $\mu = +1$ (or $-1$). $\xi = +1$ for the $|E'\rangle$ state and $-1$ for the $|E''\rangle$ state.

In fig. 5 we have drawn the corresponding energy levels and one can observe that on this energy scale the hyperfine splitting in the A states is negligible. The $\langle 0, A_{m_I}| \leftrightarrow |1, A_{m'_I}\rangle$ LAC's are therefore all expected to occur within the inhomogeneously broadened center line of figs. 3 and 4 which is assigned to these LAC's. The observed sidebands may then be caused by $|E\rangle - |E\rangle$ type LAC's. This possibility how-

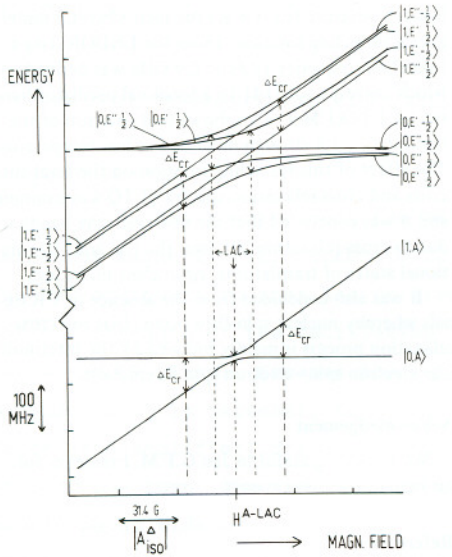


Fig. 5. Energy level scheme with $3J = 2940$ MHz for the $|A\rangle$ and $|E\rangle$ rotational states of the methyl torsional oscillator in the lowest triplet state of toluquinone. On this scale the hyperfine interaction hardly effects the $|A\rangle$ levels, but the $|E\rangle$ electronspin states are split. Note that next to the observed level-anti-crossing only the outermost cross-relaxations are given. Also note that the level-assignment only pertain to the magnetic field region outside the crossing region. For further details consult the text.

ever must be rejected when a quantitative calculation is made.

Experimentally we extract, by computer simulation of the observed lineshape for $H \| z$, that the splitting between the sidebands (where the derivative is zero) is ≈150 MHz. From eq. (13b) we calculate for $H \| z$ the splitting between the $\langle 1, E'_{-1/2}| \leftrightarrow |0, E'_{1/2}\rangle$ and $\langle 1, E''_{-1/2}| \leftrightarrow |0, E''_{1/2}\rangle$ LAC's to be $\frac{2}{3}|A^{\Delta}_{iso}|$. We then find $|A^{\Delta}_{iso}| = 225 \pm 15$ MHz. From the LAC lineshape obtained for $H \| x$ (fig. 4) we extract along similar lines for $|A^{\Delta}_{iso}|$ a value of $290 \pm 20$ MHz.

As both values of $|A^{\Delta}_{iso}|$ obtained are far too large in comparison with the one $(88 \pm 5)$ MHz obtained from ENDOR data we conclude that LAC is not responsible for the sidebands in the "LAC"-signal.

In the following section we will investigate the possibility of CR as the cause of these extra lines.

## 5. Cross-relaxation

When two energy splittings in different spin systems match, efficient exchange of population may occur which in triplet excited states of organics quite often may be detected as a change in the phosphorescence of the sample [13].

In TQ, CR may occur between molecules where one is in an A-rotational and the other in the E-rotational state. A quick calculation shows that CR between translational *in*equivalent TQ molecules for $H \| z$ occur near 650 G, while experimentally a signal is observed near 1200 G.

In the following we therefore only deal with CR between translational equivalent TQ molecules. We further note that, in principle, there are several possible $|A\rangle - |E\rangle$ CR's depending on whether the nuclear spins are flipped (flip-flop and flop-flop) or not.

All possibilities were investigated and for $H \| z$ the following results, obtainable from analytical expressions, were derived:

$$\Delta\nu_{CR}^{\text{flip-flop}} = 3|A^{\Delta}_{iso}|,$$

$$\Delta\nu_{CR}^{\text{flop-flop}} = \tfrac{1}{3}|A^{\Delta}_{iso}|,$$

$$\Delta\nu^{0}_{CR} = \tfrac{1}{6}(\sqrt{17} - 1)|A^{\Delta}_{iso}|;\ \tfrac{1}{6}(\sqrt{17} + 1)|A^{\Delta}_{iso}|;$$

$$\tfrac{4}{3}|A^{\Delta}_{iso}| \text{ and } \tfrac{5}{3}|A^{\Delta}_{iso}|. \qquad (14)$$

$\Delta\nu^{0}_{CR}$ symbolizes the CR processes whereby the nuclear spins are not flipped. The outermost cross-relaxations are shown in fig. 5 at $H^{0}_{CR} = H^{A}_{LAC} \pm \frac{5}{6}|A^{\Delta}_{iso}|$ between $|1, E'_{1/2}\rangle \leftrightarrow |\psi'\rangle$ at one side and between $|1, E''_{1/2}\rangle \leftrightarrow |\psi''\rangle$ at the other side. At the CR magnetic field strengths the $\psi$'s may be written as follows:

$$|\psi'\rangle = \tfrac{2}{3}\sqrt{2}|1, E'_{-1/2}\rangle + \tfrac{1}{3}|0, E'_{1/2}\rangle,$$

$$|\psi''\rangle = \tfrac{2}{3}\sqrt{2}|1, E''_{-1/2}\rangle + \tfrac{1}{3}|0, E''_{1/2}\rangle.$$

The CR induced phosphorescence intensity change will be proportional to the square of the coefficients of the states with identical nuclear parentage.

Our experiments exclude CR processes whereby the nuclear spins are flipped, as otherwise $|A^{\Delta}_{iso}|$ must be 50 MHz (flip-flop) or 450 MHz (flop-flop). Both values of $A^{\Delta}_{iso}$ are again in disagreement with the magnitude of $A^{\Delta}_{iso}$ (88 MHz) derived from the ENDOR data.

The results however are not inconsistent with the assumption that the observed signals are due to cross-relaxation without nuclear spin-flips. Indeed, for such CR processes, the outermost signals are predicted to be split by $\frac{5}{3}|A^{\Delta}_{iso}| = 147$ MHz. Experimentally a splitting between the lines (at zero-derivative points) of 150 ± 15 MHz is observed.

For $H \| x$ the agreement between theory and experiment is less satisfactory. The calculations [4] for this orientation are also more complex and only numerical solutions may be derived.

The following results were obtained:

$$\Delta\nu_{CR}^{\text{flip-flop}} \approx 5.2|A^{\Delta}_{iso}|,$$

$$\Delta\nu_{CR}^{\text{flop-flop}} \approx 1.8|A^{\Delta}_{iso}|.$$

For the CR process whereby no nuclear spin-flips occur ($\Delta\nu^0_{CR}$) no definite relationship was found between $\Delta\nu^0_{CR}$ and $|A^{\Delta}_{iso}|$. For several values of $|A^{\Delta}_{iso}|$, the possible CR fields and relative intensities were exactly calculated [4] after which the "stick" spectra were gaussian broadened and added. The values of $\Delta\nu^0_{CR}$ were then determined from the derivative zero points.

From these computer simulated spectra [4] however it was clear that in all cases the "high" field CR signal should be more intense than the "low" field signal. Fig. 4 shows that this prediction is in agreement with the experiment.

A second important finding was that a slight misorientation (≈1°!) is enough to obtain quantitative agreement between theory and experiment. A misalignment of this order cannot be excluded in our experiments [4] and we therefore conclude that the interpretation of the spectra, as due to CR between translational equivalent TQ molecules, is basically correct.

The absence of CR processes whereby nuclear spin-flips occur must be interpreted as a consequence of the fact that intermolecular electron spin–electron spin interaction instead of the electron spin–nuclear spin interaction, is responsible for the observed CR effects.

## 6. Conclusion

ENDOR experiments on the methyl protons in the lowest $n\pi^*$ triplet state of toluquinone show that at low temperature (ca. 1.8 K) the methyl group undergoes a tunneling rotation. From the ENDOR data a tunneling frequency ($3J$) of 2.9 GHz was derived, which corresponds [14] to a torsional oscillator barrier of 2.77 kJ/Mol. This shows that rotation of the methyl group is strongly hindered at low temperature. The effect of this tunneling rotation on the level-anticross and cross-relaxation spectra of TQ was examined and it was concluded that the observed side-bands are due to cross-relaxation between the $|A\rangle$ and $|E\rangle$ rotational states of translational *equivalent* molecules.

It was also concluded from the absence of CR signals whereby nuclear spin-flips occur, that the cross-relaxation process is mainly induced by the intermolecular electron spin–electron spin interaction.


## Acknowledgement

We are very grateful to Jan G.F.M. Fremeijer for his help in the experiments.


## References


[1] J.H. Lichtenbelt, J.G.F.M. Fremeijer, H. Veenvliet and D.A. Wiersma, Chem. Phys. 10 (1975) 107.

[2] J.H. Lichtenbelt, J.G.F.M. Fremeijer and D.A. Wiersma, Chem. Phys. 18 (1976) 93.

[3] J.H. Lichtenbelt, D.A. Wiersma, H.T. Jonkman and G.A. van der Velde, Chem. Phys. 22 (1977) 297.

[4] L. Benthem, J.H. Lichtenbelt and D.A. Wiersma, Chem. Phys. 29 (1978) 367.

[5] J.H. Lichtenbelt and D.A. Wiersma, Chem. Phys. 34 (1978) 47.

[6] S. Clough and F. Poldy, J. Chem. Phys. 51 (1969) 2076.

[7] S. Clough, J. Hill and F. Poldy, J. Phys. C: Solid State Phys. 5 (1972) 518.

[8] S. Clough and F. Poldy, J. Phys. C: Solid State Phys. 6 (1973) 1953.

[9] F. Apaydin and S. Clough, J. Phys. C: Solid State Phys. 1 (1968) 932;
C. Mottley and C.S. Johnson Jr., J. Chem. Phys. 61 (1974) 1078;
S. Clough and J.R. Hill, J. Phys. C: Solid State Phys. 9 (1976) L645.

[10] P.S. Allen, J. Chem. Phys. 48 (1968) 3031.

[11] W. Derbyshire, Mol. Phys. 5 (1961) 225.

[12] H.P. Trommsdorff, D. Bordeaux and D. Mentzafos, Compt. Rend. Acad. Sci. Paris C271 (1970) 45;
H.P. Trommsdorff, Mol. Phys. 24 (1972) 519.

[13] W.S. Veeman and J.H. van der Waals, Chem. Phys. Letters 7 (1970) 65;
W.S. Veeman, A.L.J. van der Poel and J.H. van der Waals, Mol. Phys. 29 (1975) 225;
W.S. Veeman, Ph.D. Thesis, Leiden (1972).

[14] J.H. Freed, J. Chem. Phys. 43 (1965) 1710.

CHAPTER 9

# THE NMR COIL IMPEDANCE MATCHING CONDITIONS IN ENDOR EXPERIMENTS.

## 1. INTRODUCTION

In an Endor experiment the NMR frequency must be varied while the permanent magnetic field strength is kept constant to fulfil the EPR condition. The NMR equipment further has to give, over a *wide* frequency range, an *optimum* strength of the oscillating NMR field $H_2$, which will be necessary to get an ENDOR signal. Because the impedance of the NMR coil is frequency dependent, it is necessary to change the matching of the coil to the oscillator (and amplifier) during a frequency change, *even* if the NMR coil consists of only one turn. The frequency range available without rematching the NMR coil, should be as wide as possible.

Because it is not possible to combine an optimum NMR field strength with a wide frequency range (vide infra) there are two practical solutions to the matching conditions, depending on whether or not the optimum $H_2$-field should be equal to the maximum available $H_2$-field (delivered by the NMR oscillator and amplifier).

The easiest way is to reduce the reflection of the NMR coil by an external load resistance to the desired level (determined by the amplifier requirements and/or the minimum $H_2$-field for an ENDOR experiment). This is described in detail in section 4. The result is that a wide NMR frequency range is obtained for a chosen coil, resistance and coaxial line length for all NMR oscillator frequencies.

The optimum $H_2$-field is reached when the NMR coil forms a resonant loop with a variable capacitor which is connected to it by a coaxial line. This is necessary because the coil is placed inside and the capacitor outside the liquid helium dewar. The frequency range will be small (1-2 MHz) and this solution is only acceptable for NMR frequencies between 8-30 MHz as described in section 5.

In section 2 the dissipationless coaxial line theory and the Smith chart are briefly discussed. The Smith chart will be shown to be very useful for graphical solutions of the problems. In section 3 some experimental details are given.

## 2. THE IMPEDANCE THEORY AND THE SMITH CHART

To understand the matching conditions of the NMR coil in more detail, we will give in this chapter the impedance theory of coaxial lines [1] and the graphical solutions with the aid of the Smith chart [2].

In calculations on transmission lines it is very useful to work with the reflection coefficient $\rho_r = |\rho_r| e^{j\phi}$

which is defined as: $\rho_r = +V_r/V_i = -I_r/I_i$ (r=reflected and i=incident)

$\rho_r$ will depend in magnitude and phase on the load impedance $Z_r$ as:

$$\rho_r = \frac{Z_r - Z_0}{Z_r + Z_0} = \frac{z_r - 1}{z_r + 1} = -\frac{y_r - 1}{y_r + 1}$$

where $Z_0$ is the characteristic impedance of the coaxial line, $z_r = Z_r/Z_0$ the normalized impedance and $y_r = Y_r/Y_0$ the normalized admittance.

Assuming that the transmission line, which we use, is *dissipationless* (see table 1, section 3) for ENDOR frequencies between $0 \leq \nu \leq 30$ MHz, $|\rho|$ will be a constant over the coaxial line while only $\phi$ changes with $-2\beta d$ (with d the length from the load impedance towards the generator and the phase factor $\beta$ the rotation angle per unit length). A repetition of $\phi$ occurs after a distance of $\frac{1}{2}\lambda$ (half the wave length in the coaxial line).

The reciprocal values of the normalized impedance (=admittance) is found by a $180^\circ$ rotation, because $z(d+\frac{2n+1}{4}\lambda) = y(d) = 1/z(d)$.

To determine an unknown load impedance, one only has to measure the voltage maximum $V_{max}$ and the voltage minimum $V_{min}$ along the line and also the distance from the load impedance to the (first) voltage minimum $d_{V_{min}1}$. The ratio $V_{max}/V_{min}$ is called the Voltage-Standing-Wave-Ratio VSWR and is related to $|\rho|$ as:

$$S = \text{VSWR} = \frac{V_{max}}{V_{min}} = \frac{1 + |\rho_r|}{1 - |\rho_r|} \qquad \text{or} \quad |\rho_r| = \frac{S - 1}{S + 1}$$

The VSWR = $z_r$ for $z_r$ real and $\geq 1$. The reflection angle $\phi_r$ is found from the equation:

$$\phi_r = -\pi + 2\beta d_{V_{min}1} = (1-2n)\pi + 2\beta d_{V_{min}n}$$

The phase factor $\beta$ is the phase rotation angle per unit length:

$$\beta = \omega\sqrt{L'C'} = \omega Z_0 C' = 2\pi/\lambda = \omega/u_p \quad \text{with C' and L' per unit length.}$$

$u_p$ is the phase velocity: $u_p = \omega/\beta = 1/(Z_o C')$.

The *graphical* display of the reflection coefficient $\rho_r$ with $\phi_r$ for different $|\rho_r|$ values is given in the *Smith chart* in figure 1. Because the distance towards the generator is proportional to $-\phi/4\pi$ (outer circle in figure 1b) the circles in figure 1a give the reflection coefficient along a dissipation-less coaxial line.

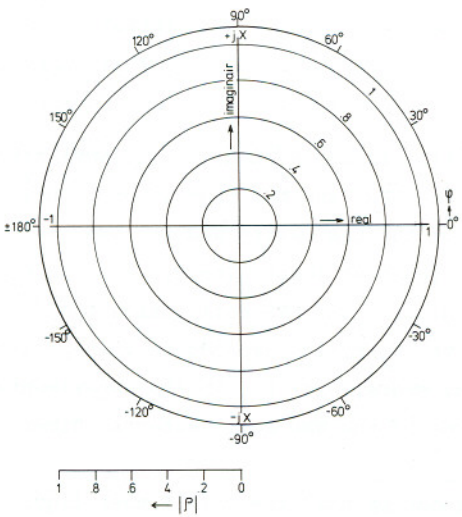


Fig. 1a.

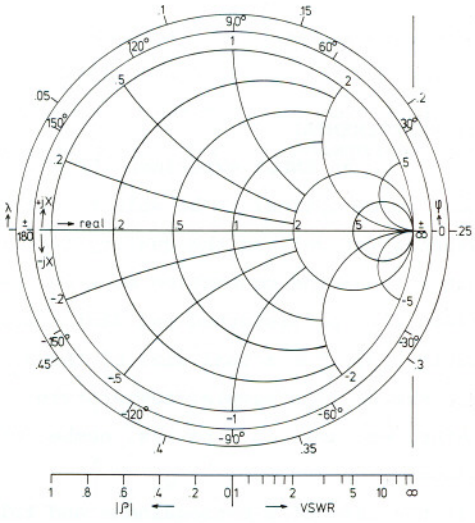


Fig 1b.

Fig. 1a and 1b. *The Smith chart* of the reflection coeffiecient $\rho = |\rho|e^{j\phi}$. With the amplitude $|\rho|$, which is given in figure 1a as equi-distant circles and in figure 1b below the chart just as the corresponding VSWR values. The reflection angle $\phi$ is given in an extra circle around the figures and the proportional distant values (in $\lambda$-units), towards the generator, are given in the outer circle around figure 1b. In this last figure only the equi-real and equi-imaginairy lines of the corresponding normalized impedances and admittances of the reflection coefficient $\rho$ are drawn. Figure 1b is the normal Smith chart.

The corresponding normalized impedance and admittance are given in figure 1b, where the equi-real circles and the equi-imaginary (part of) circles are drawn. The horizontal axis is the real axis and the outer circle with $|\rho|=1$ is valid for purely imaginary impedances (admittances) with the upper half for positive- and the lower half for negative imaginary values. For simplicity the $|\rho|$-circles are not drawn in the Smith chart but its scale is given below the chart together with the corresponding VSWR-values. A reciprocal (normalized) value is found by an inversion.

In the next sections the question arises when the optimum and/or maximum power is reached. When an external impedance $Z_u$ is connected to a constant voltage power supply with internal impedance $Z_0$, the power dissipated is maximal when $Z_u$ matches $Z_0$ *as closely as possible*. This means that the imaginary part of $Z_u$ should be zero and the real part of $Z_u$ should be equal to $Z_0$.

## 3. EXPERIMENTAL

In an ENDOR experiment both oscillating fields $H_1$(EPR) and $H_2$(NMR) often need to be optimal to be able to saturate the EPR- and NMR transitions. This depends not only on the quality factors Q of the EPR cavity and the NMR coil, but also on the connection between the two resonant loops. The $H_1$- and the $H_2$-field will be disturbed and diminished by placing the NMR coil inside the cavity [3]. The actual size of the $H_1$ and the $H_2$-fields depends on the specific experiment (eg. sample, temperature, steady state, etc) and on the experimental setup, eg. available powers, number of turns of the NMR coil, external dimensions, etc.

In the case of p-benzoquinone and toluquinone we used the cold finger liquid helium dewar of Hyde [4] to obtain the low temperature of 1.8 K. The NMR coil of three turns [5] is placed inside the dewar and thus inside the cavity (with the $TE_{102}$ mode). The wires *inside* the cavity are placed perpendicular to the oscillating EPR-$E_1$-field in order to affect the high Q-factor of the cavity as little as possible. The oscillating NMR field $H_2$ can be adjusted in direction from outside and can be oriented either parallel or perpendicualar to the permanent magnetic field H, but always perpendicualar to $H_1$.

To obtain the best values for the real and imaginary parts of the impedance of the coil and of a variable capacitor (which will be used to produce a resonant loop, see section 5) it is best to measure these impedances in the range of the NMR frequencies used. This is in the range of 0-30 MHz. As seen from section 2 the impedances can be calculated from the VSWR and the distance from the load impedance to the voltage minimum on the connected coaxial line. This was done with a resolution of 0.25 meter at 16 MHz. The coil impedance (three turns) was found to be:

$$Z_L = 9 + 2.375\nu j\ \Omega \quad (\nu \text{ in MHz})$$

where the real part of $Z_L$ is *assumed* to be in series with the coil and independent of the frequency over the given range. From the imaginary part the inductance is calculated to be 0.38μH.

The (variable) capacitor impedance was found to be:

$$Z_C = 1102\ //\ 1/j\omega C\ \Omega$$

Here the resistance of 1102Ω is *assumed* to be independent of the frequency and parallel to the variable capacitor C. The capacitance was set on a mean value of 175 pF during this measurement and it is assumed that the real part will be independent of the capacitance value.For the validity of these assumptions see section 6.

Table 1.

The data of the two coaxial lines used.

| | "miniature" coaxial line | "regular" coaxial line |
|---|---|---|
| number | RG/U 174 | RG/U 58A |
| capacitance C' | 96.785 pF/m | 98.425 pF/m |
| inductance L' | 0.2420 μH/m | 0.2461 μH/m |
| phase velocity $u_p$ | $2.0662 \times 10^8$ m/s | $2.0320 \times 10^8$ m/s |
| phase constant β at 1 MHz | 0.03041 rad/m | 0.03092 rad/m |
| dissipation | 0.128 db/m at 10 MHz<br>0.217 db/m at 50 MHz | 0.197 db/m at 100 MHz |
| outer diameter | 2.5 mm | 5.0 mm |

In table 1 the data of the two coaxial lines used are given. In the liquid helium dewar the coaxial line with the smallest diameter was used.

## 4. THE MAXIMUM NMR FREQUENCY RANGE

When the load impedance (of which the NMR coil will be a part) will be matched at one frequency $\nu_0$ to a coaxial line with the oscillator/amplifier, all power will be dissipated in the load impedance and there will be no reflections. However, when the NMR frequency varies during an ENDOR experiment the load impedance is no longer matched to the line and power starts to be reflected. The broad band power amplifier IFI M5000 used, functions without hazard for damage as long as the reflection coefficient $|\rho| \leq 0.6$ or the VSWR $\leq 4$. Thus the transformed impedance at the amplifier must be within the area of the circle S=4 in the Smith chart of the figures 2.

The NMR coil impedance for all the generator (HP 8601A) frequencies are given in figure 2a on the equi-real circle $Z_L = (0.18 + 0.0475x\nu\ j)xZ_0\ \Omega$ from A ($\nu$=0 MHz) with marks at every 10 MHz until B ($\nu$=110 MHz). It is seen directly that for all frequencies the VSWR caused by the load impedance $Z_L$ itself will be > 4. The easiest way to reduce this reflection is to introduce a resistance $R_u$, just outside the dewar for dissipation reasons, in series with this coil and connected to a coaxial line as shown in figure 3.

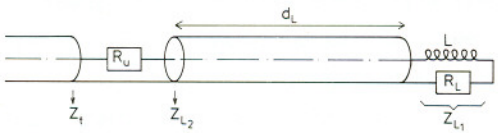


Fig. 3. The experimental setup of the NMR-coil in series with a load resistance $R_u$ connected by coaxial line with length $d_L$ and the corresponding impedances.

The total impedance $Z_t$ can then be changed to such a value as to obey the relation VSWR $\leq 4$. This is accomplished by the addition of the resistance $R_u$ to the real part of the impedance $Z_{L_2}$, so that the imaginary part will not change. Here $Z_{L_2}$ is the impedance of $Z_{L_1}$ transformed by the coaxial line between the coil and the resistance. However the impedance $Z_{L_2}$ is not allowed to have a value in the hatched area* in figure 2, because in this area an

* note: The hatched area is formed by the line HGDC in figure 2 which is part of the VSWR=4 circle and two equi-imaginary circles which touche the VSWR=4 circle. The absolute imaginary value of these last two circles will be: $(S^2-1)/2SxZ_0\ j\ \Omega$ and for S=4 this will be: $1.875xZ_0\ j\ \Omega$.

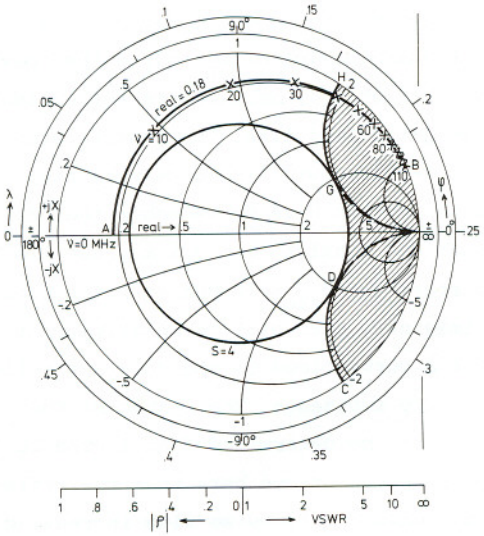


Fig. 2a. The impedance of the NMR-coil is given on the equi-real line from A (ν=0 MHz) with marks at every 10 MHz until B (ν=110 MHz). The load impedance of the NMR-amplifier should be in the area inside the circle S=4, where the VSWR is less than four. A (transformed) impedance in the hatched area can never be changed to the VSWR≤4 area by a load resistance in series with it.

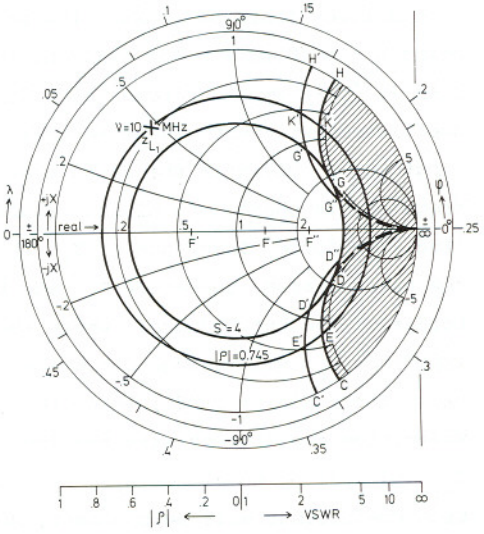


Fig. 2b. The same as figure 2a except for the circle $|\rho|=0.745$, which gives the transformation of the NMR-coil impedance at 10 MHz along a dissipationless coaxial line. The load impedance is given by F. The total impedance of the coil and the load resistance is given by D and G, when the (transformed) coil impedance is respectivily in point E and K, depending on the frequency. For a coil impedance E' a load impedance F' or F" is necessary to give a total impedance D' or respectivily D".

extra resistance will never make the VSWR less than four (the equi-imaginary lines in this area do not cross the VSWR ≤ 4 area). However by a proper choice of the length of the coaxial line $d_L$, the impedance $Z_{L_2}$ can always be placed somewhere outside the hatched area and it is possible by introducing a series resistance $R_u$, to reduce the VSWR below the value of four. This may be done for *each* frequency.

We have to choose the resistance $R_u$ and the coaxial line length $d_L$ such, that the VSWR stays less then four for a maximum range of frequencies *without* changing these two parameters. We give an example for a frequency range extending

from a lower limit of 10 MHz. The coil impedance is given in figure 2b at point $Z_{L_1} = (0.18 + 0.475\ j) \times Z_0\ \Omega$. The transformation of $Z_{L_1}$ along the coaxial line is given by the circle $|\rho| = 0.745$ through $Z_{L_1}$, because the reflection coefficient will not change in this dissipationless line. The coaxial line length $d_L$, given in the Smith chart in λ-units, will increase when the frequency is changed to higher values. We further have to remember that $Z_{L_2}$ (the transformed impedance of $Z_{L_1}$ through the coaxial line $d_L$) may not lie in the hatched area. Therefore $Z_{L_2}$ has to start for $\nu_{min} = 10$ MHz at point E on the border of the hatched area, where the imaginary part will be negative. This impedance $Z_{L_2}$ will change clockwise over a curve close to the constant reflection circle $|\rho| = 0.745$, when the frequency increases. The change of the reflection coefficient with the frequency can be determined from figure 2a for $Z_{L_1}$ and will be equal for $Z_{L_2}$. For simplicity we assume here that the reflection coefficient will be constant, so $Z_{L_2}$ changes clockwise with increasing frequencies until point K is reached at the other side of the forbidden area. This point determines the maximum frequency $\nu_{max}$ of the range.

By connecting the resistance $R_u$ with the impedance of point F (at $\nu_{min} = 10$ MHz the impedance of $Z_{L_2}$ (point E) is changed to $Z_t$ at point D, where the VSWR is just four. By increasing the frequency, the VSWR becomes less then four and the total impedance ends for $\nu_{max}$ just at point G, when $Z_{L_2}$ arrives at point K. For frequencies outside this range the VSWR will become greater than four. The increase of the reflection coefficient of $Z_{L_2}$ with the frequency makes the total impedance $Z_t$ to lie outside the VSWR=4 area at a frequency $\nu'_{max} < \nu_{max}$.

This combination of series resistance, NMR coil and coaxial line will give the maximum possible frequency range within the limitations of a permissible power reflection. This will be the best solution when the power in the coil will be sufficient to give ENDOR intensity. In this case that the power amplifier can dissipate more reflected power, the NMR frequency range will not be much larger, because for higher VSWR values than four, the power in the NMR coil will decrease rapidly and will soon be to small to observe an ENDOR transition.

By taking the coaxial line length $d_L$ such that at the minimum frequency the impedance of $Z_{L_2}$ will be on the CD'D" equi-imaginary line, the resistance $R_u$ can be chosen in a range from point F' to F". The total impedance $Z_t$ will then

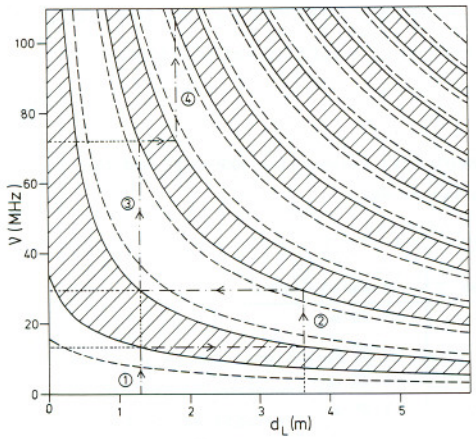


Fig. 4a. The coaxial line length of the coil with serial resistance of 50Ω *versus* the NMR frequency for different VSWR values. This plot is for a coaxial line with phase velocity $u_p$ of $2.0662 \times 10^8$ m/s. The minimum coaxial length is the hight of the liquid helium dewar and is 1.3 meter. The line ---- is the equi-VSWR=2 line and the hatched areas have VSWR values ≥4. The 1,2,3 and 4 lines give the frequency dependences of four coaxial lines which are necessary to satisfy the condition VSWR≤4 for frequencies up to 100 MHz.

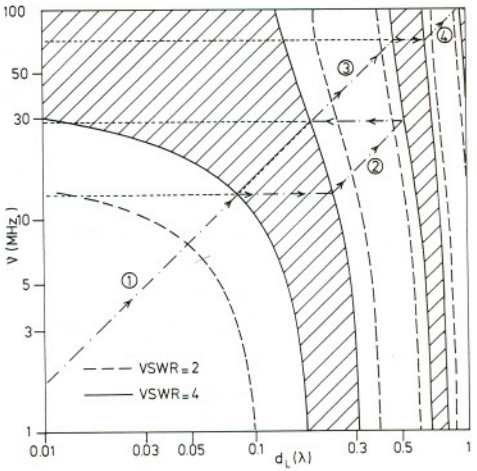


Fig. 4b. A *general* plot of figure 4a, except that this is a double logarithmic plot and that the coaxial line length is now in λ-units, which will be independent of the phase velocity. The equi-coaxial-length lines (in meters) are parallel to the hatching of the area with a VSWR greater than four.

be between point D' and D". The advantage is that, although the frequency range is only slightly smaller for this coaxial line length, the power in the NMR coil will be larger for smaller values of the resistance. The choice of $R_u = Z_0 = 50\ \Omega$ will give satisfactory results and in figure 4a and 4b the coaxial line length as function of the frequency for VSWR values of two and four are drawn. In figure 4a the specific solution is given for the coaxial line RG/U 174 with phase velocity $u_p$ of $2.0662 \times 10^8$ m/sec. With a minimum coaxial line length (inside the dewar) of 1.3 meter possible combinations of frequency ranges and coaxial line lengths are given in table 2 and by the dashed lines in figure 4a. A general solution, independent of the line used, is given in figure 4b. Because the length is here in λ-units*, the equi-

* note: $d_L(\text{in } \lambda) = \nu/u_p . d_L(\text{in meters})$.

coaxial-length-lines (in meters) will in a double logarithmic plot versus the frequencie have a direction coefficient of one. Therefore the hatching in the figure 4b is drawn with the same direction coefficient of one.

Table 2.

The frequency range of the coaxial lines (RG/U 174) between the NMR-coil and the series resistance for a VSWR≤4 as shown in figure 4a.

| numbers in figure 4a | frequency range | coaxial length |
|---|---|---|
| 1 | < 13.0 MHz | 1.30 m |
| 2 | 13.0 - 29.5 MHz | 3.60 m |
| 3 | 29.5 - 72.0 MHz | 1.30 m |
| 4 | 72.0 -106.5 MHz | 1.85 m |

## 5. THE OPTIMUM NMR MAGNETIC FIELD

The optimum NMR $H_2$-field is reached when the coil L forms with a capacitor C a resonant circuit with low losses (high Q-factor). Therefore, for an optimal field, the value of the capacitor must change when the NMR frequency varies. This must be done outside the dewar and the problem then is that the impedance change of the coil by the coaxial line between this coil and the capacitor changes the resonance condition completely. In the case that the coil impedance is transformed to an impedance with a capacitive character by this line, no resonance condition can be created at all.

The solution is, for a given frequency $\nu_0$, to make the coaxial line length $d_{t_0}$ equal to $nx\frac{1}{2}\lambda$, so the coil impedance $Z_{L_1}$ has the same value at the capacitor-end $Z_{L_3} = Z_{L_1}$ of the dissipationless coaxial line ( see figure 5a) and the same resonance condition of $C \approx 1/\omega^2 L$ can be maintained.

A small deviation of the length $d_{t_0}$ will change the impedance $Z_{L_3}$ by a small amount and therefore the capacitance has to change a little to the new resonance condition $C' \approx 1/\omega^2 L'$, with $\omega L' = \mathrm{Img}(Z_{L_3})$.

If there is a real part in the coil impedance and/or in the capacitor impedance it is possible, by varying the total coaxial line length $d_t$, to find *two* places somewhere on this line where $Z_t = Z_{L_2} // Z_{C_2} = Z_0$ as shown in figure 5b. Each solution has a different value of $d_t$. For these values of $d_t$ the resonant

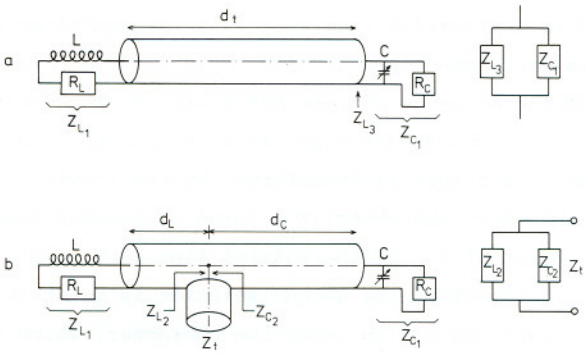


Fig. 5. The resonant loop formed by a coil L and a capacitor C connected by a coaxial line. Given are the different impedances at the end and somewhere on the line. The equivalent circuits are drawn beside these figures.

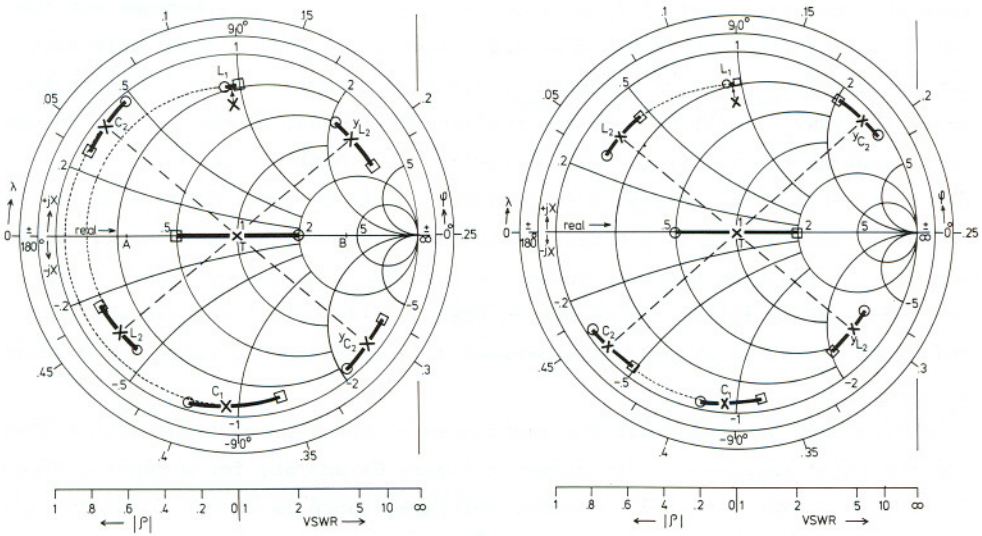


Fig. 6a. Fig. 6b.

Fig. 6a and 6b. The two *resonant* loop solutions for a NMR frequency $\nu_0$ of 20 MHz. Drawn are the impedances with the condition that the total impedance $Z_t$ will give a VSWR less than two. The impedance numbering is the same as in figure 5 except the symbol T for $z_t$. The reciprocal values of $z_{L_2}$ and $z_{C_2}$ are found by a 180° rotation and have the values of $y_{L_2}$ and $y_{C_2}$ respectivily. The crosses are the impedances for VSWR=1. The circles give the impedances for the lowest frequency at which the VSWR=2 and the squares for the highest frequency with the same condition. The values of these frequencies and the corresponding capacitor values are respectivily given in figure 7a and 7b.

loop is matched to the coaxial line and the power amplifier such that the maximum power is dissipated in this loop. This gives an *optimum* current through the NMR coil and therefore an optimum NMR $H_2$-field, for the given frequency $\nu_0$. One of the two solutions is given in figure 6b for $\nu_0$ = 20 MHz. The coil impedance $Z_{L_1}$ (given by a cross) is transformed by the coaxial line (with length $d_L$) to $Z_{L_2}$ with an inductive character. $Z_{L_2}$ forms a resonant loop with $Z_{C_2}$ (the transformed impedance of $Z_{C_1}$ by the coaxial line with length $d_C$), which must have a capacitive character. The second solution is given in figure 6a. Here $Z_{L_2}$ has a capacitive- and $Z_{C_2}$ an inductive character, which together form a resonant loop with total impedance $Z_0$.

If the NMR frequency is varied around $\nu_0$ and the coaxial line lengths are not changed, the condition of the maximum power dissipated $Z_t = Z_0$ cannot be maintained. The optimum power will now be reached, by varying the capacitance, when the imaginary part of $Z_t$ will be zero (see section 2). Because not too much power may reflect to the amplifier, the real part of $Z_t$ may only vary between $Z_0/VSWR_{max} < Z_t < Z_0 x VSWR_{max}$, given by points A and B in figure 6a, where the $VSWR_{max}$ will be four for the amplifier used. At the extreme values of $Z_t$ however the $H_2$- field will be far from the optimum value and it is better to change the coaxial line lengths to make $Z_t$ equal to $Z_0$ again for the new NMR frequency $\nu_0'$. In practice it is found that, with a set coaxial lines and without too much $H_2$-field losses, a reasonable frequency range can be obtained when we fulfil the condition VSWR $\leq$ 2 (see too figure 7a and 7b). This will always be a compromise between a large frequency range and a large $H_2$-field.

The frequency dependence of the impedances of the two solutions with a VSWR$\leq$2 for the total impedance $Z_t$ is given in figure 6a and 6b, for a central frequency of $\nu_0$ = 20 MHz. At this frequency the capacitance is chosen to be $C = 1/\omega^2 L$ and $d_L$ and $d_C$ are so long that $Z_t = Z_0$* and thus the VSWR = 1. In addition to the coil and capacitor impedances, the transformed impedances $Z_{L_2}$ and $Z_{C_2}$ and their corresponding admittances $Y_{L_2} = 1/Z_{L_2}$ and $Y_{C_2} = 1/Z_{C_2}$ are given in the figures.

* note: In the text the impedances and admittances are used, while in the Smith chart the normalized ones are drawn. They differ a factor $Z_0$ and respectively $Y_0$.

The only variable parameter is the capacitance, which has to vary in such a way that the imaginary part of $Y_{L_2}$ cancels the imaginary part of $Y_{C_2}$. Thus by varying the capacitor we can make the total impedance real, which gives us the optimum power in the "resonant" loop.

The two solutions of figure 6a and 6b are given for other frequencies in the figures 7a and 7b. In these figures 7 the coaxial line length to the NMR coil $d_L$ (in $\lambda$-units) is given as function of the frequency for different VSWR values in a double logarithmic plot. The reason that $d_L$ is in $\lambda$-units is that this solution is independent of the phase velocity $u_p$ of the used coaxial line and the log-log plot was chosen to make the equi-coaxial-length lines (in meters) parallel to the hatching. In the same figures are also given the total coaxial line length $d_L+d_C$ for the resonant conditions (VSWR=1) and the capacitance values for different VSWR, where one of the two equal VSWR solutions is primed to make an unique correspondence possible between the $d_L$ and the capacitance values.

A possible combination of coaxial lines (numbered by 1,2,etc) is given in figure 7a with the limitation that the VSWR $\leq$ 2. A reasonable frequency range of 1-2 MHz with one set of coaxial lines (parallel to the hatching) is only possible for NMR frequencies of 8-30 MHz. The number of changes of the coaxial lengths is here much more then when the coil is only connected to a serial load impedance.

The NMR coil is inside the liquid helium dewar and the capacitor will be placed outside at room temperature. At this end a current probe (HP 1110A) was connected to the capacitor to optimise the resonant condition by tuning the capacitor just by hand or by a servo system described by van Ormondt [6].

In this section we described the resonant loop to get an optimum NMR $H_2$-field. The considerations in this section were based on the assumption that the real part of the coil- and capacitor impedances are negligible with respect to the imgaginary parts. For the coil and the capacitor we used, this was not always the case and therfore there was a slight deviation of the resonance frequencies and the coil current for the calculated line lengths. The gain of current in this case of a resonant loop with respect to the case of a coil with load resistance is only a factor two, because the Q-factor of the resonant loop was low. Coils of better quality might give better results for the resonant loop.

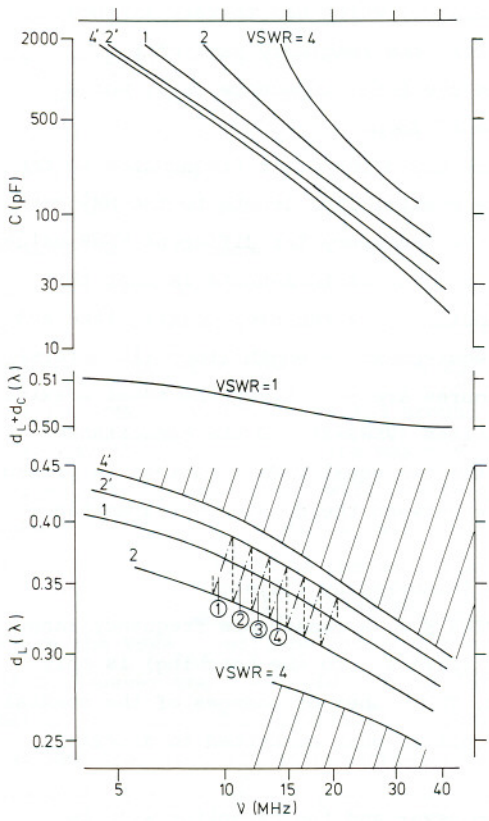


Fig. 7a.

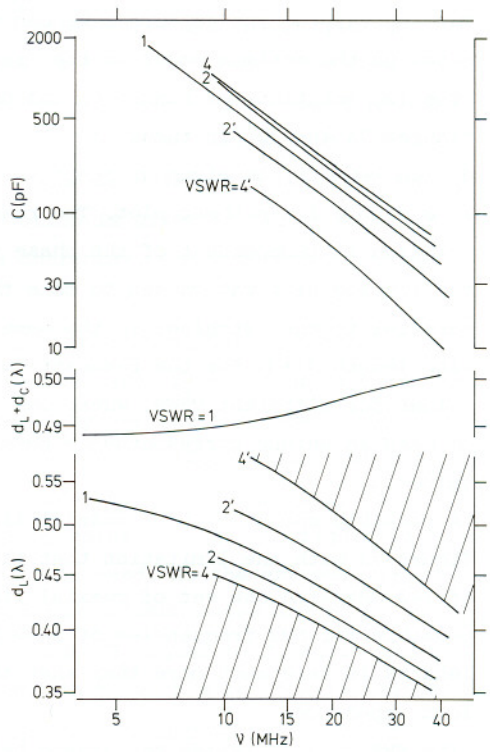


Fig. 7b.

Fig. 7a and 7b. Two *general* double logarithmic plots for two possible resonance solutions with the total impedance $Z_t$ equal to $Z_0$= 50Ω for a combination of coaxial lines with lengthes $d_L$ to the coil and $d_C$ to the capacitor. These are logarithm-logarithm plots of the coaxial line length $d_L$, the total coaxial length $d_L+d_C$ (both in λ-units) and the corresponding capacitor values *versus* the NMR frequency. The hatched areas have VSWR values greater than four and the equi-coaxial-length lines (in meters) are parallel to the hatching.

Drawn are the frequency dependences of the coaxial line numbered in the figure by 1,2,3 etc, when changing the frequency with the condition that the VSWR must be less than two to warrant an optimum NMR-$H_2$-field. As lowest frequency was chosen here $\nu_1$=10 MHz, but generally each frequency on the VSWR=1 line can be chosen as a starting frequency.

## 6. CONCLUSION

In this chapter the matching condition of the NMR coil to the NMR-amplifier and coaxial lines was described. The experimental condition of a maximum frequency range without changing anything to the setup, can be reached by an extra load impedance of 50 Ω just outside the liquid helium dewar in series with the NMR coil inside the dewar and connected by a coaxial line with each other. Over the range of 0-110 MHz the coaxial line length needs to be changed only four times.

This setup does not give us an optimum NMR $H_2$-field when this is necessary in an ENDOR experiment. An optimum NMR field is obtained by making a resonant loop of the combination of NMR coil and variable capacitor. This capacitor must be outside the dewar and will be connected to the coil by a coaxial line with length of $\approx \frac{1}{2}\lambda$. This setup will give satisfactory results in the frequency range of 8-30 MHz, where the coaxial line length has to be changed at each 1-2 MHz interval.

## 7. REFERENCES


1. H.J.Reich, P.F.Ordung, H.L.Krauss and J.G.Skalnik, Microwave theory and techniques. Boston Technical Publishers Inc., Cambridge, USA.
2. P.H.Smith, Electronics, jan. 1939.
   P.H.Smith, Electronics, jan. 1944, p 130.
3. U.Ranon and J.S.Hyde, Phys. Rev. 141 (1966) 259.
4. A.W.Hornig and J.S.Hyde, Mol. Phys. 6 (1963) 33.
5. J.H.Lichtenbelt, J.G.F.M.Fremeijer, H.Veenvliet and D.A.Wiersma, Chem. Phys. 10 (1975) 107.
6. D.van Ormondt, Thesis, T.H. Delft 1968.

"Een proefschrift over PBQ?
Geschreven ook voor U!"

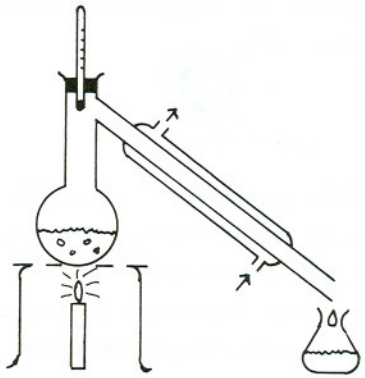


Scheikunde?
IK begrijp er niks van!
Maar leest U ook even mee?

## INLEIDING

Dit promotieonderzoek richtte zich op een stof die een sterk afwijkend karakter vertoont t.o.v. andere stoffen. Het doel was een beter inzicht te verkrijgen waarom dit zo is. In de scheikunde kunnen we de eigenschappen van de stoffen vaak voorspellen door een aantal onafhankelijke eenvoudige modellen. Voor onze stof blijkt dat dit niet meer mogelijk is en moeten we een koppeling tussen twee eenvoudige modellen veronderstellen. Dit houdt in dat als we het ene model gebruiken, we ook rekening moeten houden met een ander model. Maar daarover later meer.

## MOLEKULEN

Enkele begrippen zal ik hier nader proberen te verklaren. Als vergelijk gebruiken we aldoor Lego blokjes. We hebben daarvan een hele berg. We hebben ooit eens een aantal gelijke auto's gemaakt van het merk PBQ en op een grote hoop gegooid. Na verloop van tijd gaan we de hoop opruimen en sorteren en houden we tenslotte één auto over, van het merk PBQ.

Zo ook met zuivere stoffen. B.v. water of para-benzochinon, wat we afkorten tot PBQ (een merknaam dus). Een druppel water bevat een hoop deeltjes water. We zouden na sorteren tenslotte één deeltje water over kunnen houden. Dit noemen we een molekuul. Vergelijk met een auto. In praktijk is dit water molekuul erg klein en we kunnen hem ook niet echt los in onze handen krijgen, maar hij bestaat wel.

## ATOMEN

We zien direkt dat we nog verder kunnen gaan met het afbreken van de auto. We houden dan alleen losse steentjes over en elk steentje apart kunnen we niet meer "auto" noemen. Ze hebben wel ieder hun eigen vorm en kleur.

Ook molekulen bestaan uit bouwstenen, die we atomen noemen. Zo bestaat water uit een atoom zuurstof en twee atomen waterstof. PBQ bestaat uit zes atomen koolstof, vier atomen waterstof en twee atomen zuurstof, zoals in een figuur op de volgende bladzijde is aangegeven.

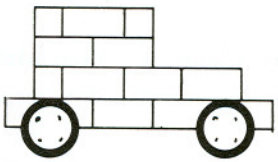

"PBQ"

één auto = één molekuul

geel wit rood

Legoblok = atoom

1 zuurstofatoom
2 waterstofatomen

= water

We gebruiken daar ook bepaalde letters voor, net zoals elk steentje zijn eigen vorm heeft, n.l. C voor koolstof, H voor waterstof en O voor zuurstof.

In de auto zijn de blokjes op een bepaalde manier gerangschikt en verbonden met elkaar.

Zo ook bij ons molekuul PBQ. De atomen zijn gerangschikt zoals in een figuur hiernaast is aangegeven en de verbindingen door streepjes.

Hoe ontstaat nu zo'n verbinding? Bij Lego blokjes erg eenvoudig door nopjes in gaatjes te plaatsen. Doordat dit strak in elkaar zit, vormt het een goede verbinding.

De verbinding tussen de atomen is ingewikkelder. Daarvoor zullen we eerst moeten kijken hoe een atoom is opgebouwd.

KERNEN EN ELEKTRONEN

Een atoom bestaat uit een kleine kern, een klein bolletje en daarom heen hele kleine en snel bewegende elektronen.

Vergelijk de zon als kern en de planeten bewegen daarom heen. En niet alleen dat, maar ze hebben elk een eigen baan. Stel nu dat we een planeet een andere baan willen geven, dan kan dat maar het kost wel (veel) energie.

Voor het atoom geldt hetzelfde. Dit is opgebouwd uit een kleine kern en daarom heen in verschillende banen de snel bewegende elektronen. De banen van de elektronen zijn verschillend van vorm. B.v. rond, maar ook acht-vormig en nog andere vormen zijn mogelijk. Echter er is een groot verschil, n.l. niet alle banen zijn mogelijk, slechts bepaalde. We kunnen wel een elektron in een andere baan brengen.

Brengen we een elektron van een kleinere, dichtbij de kern gelegen baan in een grotere, verder van de kern verwijderde baan, dan kost dat energie. We kunnen dat in bepaalde gevallen met licht doen. Licht bezit energie (lekker warm dat zonlicht he!). Als het elektron terugkeert, terugvalt in een lagere baan, dan komt er energie vrij. Dit kan o.a. ook in de vorm van licht gebeuren. Denk aan het lichtgevende knopje in het trappenhuis van een flat, maar ook de geel-oranje natriumlampen boven de autowegen.

water

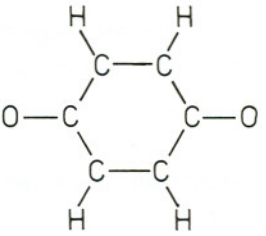

para-benzochinon
of PBQ

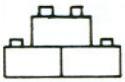
Legoblokken stapeling
in de auto = atomen in een molekuul

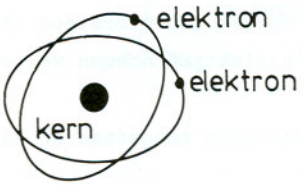


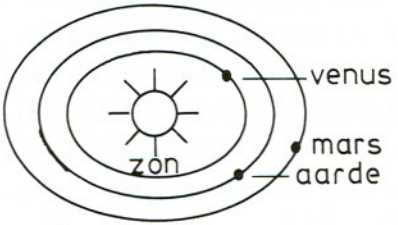


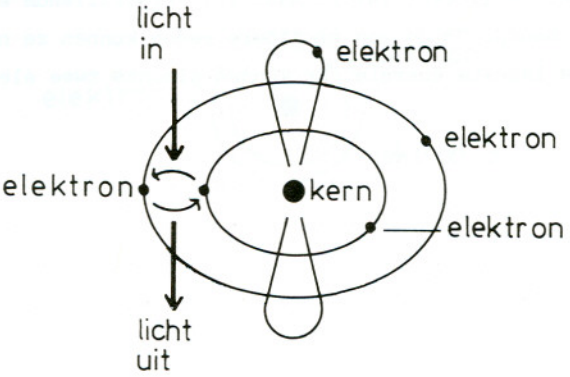

Terug naar de verschillende atomen. We kunnen nu het verschil aangeven. N.l. het zuurstofatoom, het koolstofatoom en het waterstofatoom verschillen o.a. in de groootte van de kern en het aantal elektronen.

BINDINGEN IN EEN MOLEKUUL

Hoe onstaat nu de binding tussen die atomen, zodat er een molekuul gevormd kan worden? Want meerdere atomen samen met bindingen ertussen vormen een molekuul. Het blijkt dat de banen van de elektronen vervormen en zo kan het zijn dat een elektron niet om één atoom beweegt, maar om twee. We hebben dan een binding gekregen, die stabiel is omdat het blijkt dat dit elektron liever zit in zo'n baan om twee atomen i.p.v. een. Een ander elektron kan dan weer een ander atoom erbij binden, enz., zodat een geheel molekuul wordt gevormd.

Andere banen zijn echter ook mogelijk, b.v. waarbij het elektron zich over het gehele molekuul beweegt. Niet door de kernen, maar er boven en er onder. Deze laatste baan heeft een naam gekregen, die we aangeven m.b.v. een Griekse letter $\pi$ (spreek uit "pi"). Er blijven echter ook elektronen in de oorspronkelijke atoombanen zitten. Ze doen dus niet mee aan de verbindingen van het molekuul. Zo zitten er op het zuurstofatoom in PBQ twee elektronen in een achtvormige baan. Zo'n elektron noemen we een n-elektron en het zit in een n-baan.

Ook voor molekulen geldt dat niet alle banen zijn toegstaan en dat elke baan meer of minder energie bezit.
Meestal vinden we het molekuul met zijn atomen en elektronen in banen met de minste energie (lekker lui!). Maar wel verschillende elektronen in verschillende banen. Om de een of andere reden kunnen ze niet allemaal in de baan met de laagste energie. Er kunnen slechts twee elektronen in een baan.

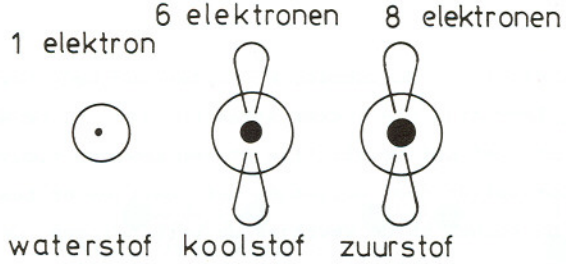
1 elektron
6 elektronen
8 elektronen
waterstof
koolstof
zuurstof


elektron
atoomkernen

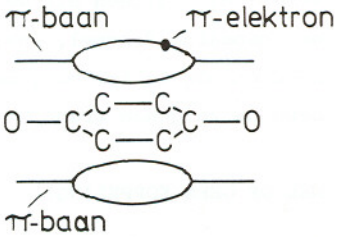
π-baan
π-elektron
O—C
C—C
C—C
C—O
π-baan

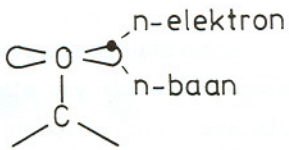
n-elektron
O
n-baan
C

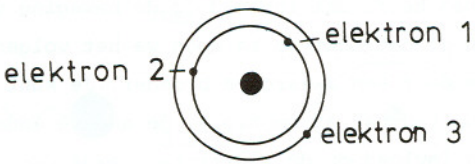
elektron 1
elektron 2
elektron 3

KERN BEWEGINGEN

Zo dit is de start van de chemie. We moeten nog even terug naar de verbindingen. Bij Lego zijn die lekker strak en star. Ze bewegen niet. Bij molekulen is dat niet het geval. Alle atomen bewegen t.o.v. elkaar. Je kunt je dat voorstellen door bolletjes met veertjes er tussen. De bolletjes zijn dan de kernen en de veertjes de verbindingen. De veertjes kunnen ingedrukt worden, uitgerekt, maar ook gebogen, opzij en naar boven en naar onderen. Alles is mogelijk. Als we er wat extra energie in stoppen, gaan ze harder bewegen. Maar ook hier geldt dat niet alles is toegestaan. Stoppen we er meer energie in dan zullen ze niet steeds sneller gaan bewegen, maar alleen als we er meer in stoppen dan een bepaald minimum, een bepaalde drempel, enz. Net zoals op een trap. Het kost energie om een been omhoog te krijgen, maar we kunnen de energie pas gebruiken als het been de volgende trede bereikt heeft.

WEL OF GEEN KOPPELING?

In de scheikunde worden in het algemeen molekulen beschreven met de beweging van de kernen en de elektronen onafhankelijk van elkaar. De gemeten energieën blijken goed overeen te komen met de boven beschreven modellen.

Het molekuul PBQ echter niet. Het blijkt dat als we een elektron uit de n-baan van het zuurstofatoom in een andere baan ($\pi$-baan van het molekuul) brengen, dat de atomen dan opeens anders t.o.v. elkaar gaan bewegen. We hebben dus een koppeling gekregen. Als we het elektron in een andere baan stoppen, dan heeft dat invloed op de beweging van de atomen.

Om nu te kontroleren of dat echt zo is doen we het volgende proefje. We vervangen een atoom door een zwaardere broeder. Je kunt je dan voorstellen dat de beweging van dat atoom t.o.v. de andere anders zal worden. Normaal heeft dat geen invloed op de elektronen, maar door de koppeling blijkt dat voor de door ons onderzochte stof PBQ wel het geval te zijn. N.l. de energie van de elektronen verandert als we de beweging van de kernen veranderen.

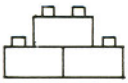

Lego verbinding

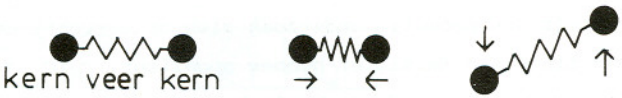


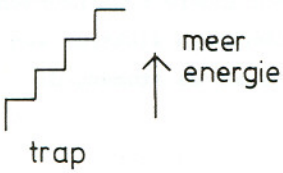


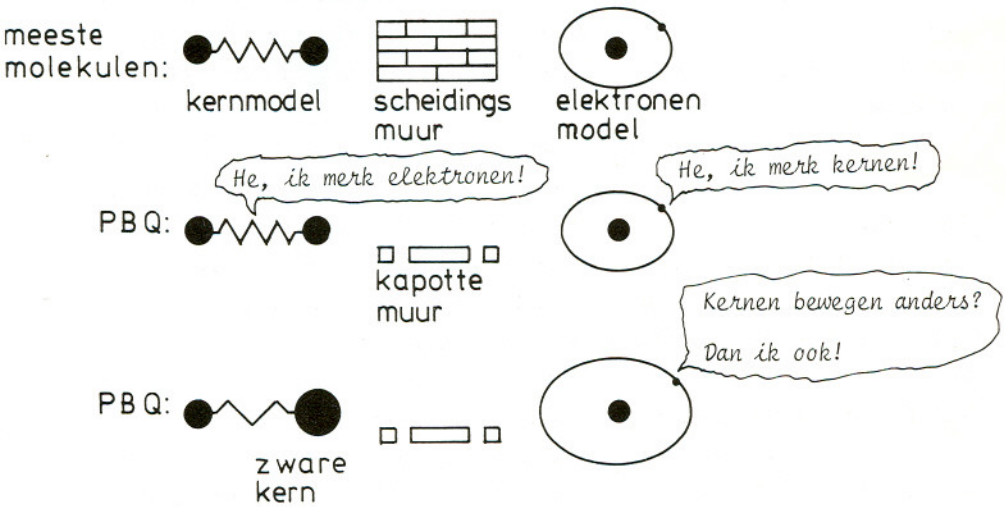

KONKLUSIE

Het model van aparte elektron banen met hun eigen energieën en de kernen met hun aparte kernbewegingen blijkt voor het molekuul PBQ (para-benzochinon) niet altijd op te gaan. Erg interessant en de vraag is waarom? Daar heeft ons promotie onderzoek zich op gericht. Het lijkt er op dat we een tipje van de sluier hebben opgelicht.

Uit ons promotie onderzoek bleek dat een mogelijke oorzaak van dit afwijkende gedrag van PBQ is dat sommige elektronen zich zeer thuis voelen bij het zuurstofatoom. Ga je deze elektronen naar een andere baan brengen, dan probeert het zuurstofatoom met alle middelen elders een elektron weg te willen halen. Dit resulteert in grote beroering onder de atomen, die daardoor anders gaan bewegen.

Wilt U het onderzoek nu voortzetten?

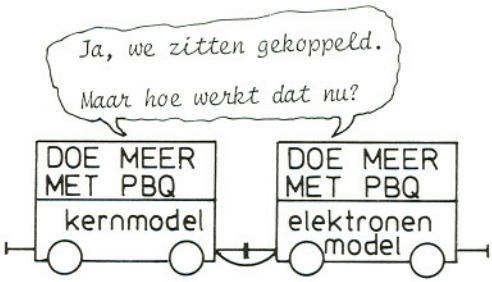
Ja, we zitten gekoppeld.
Maar hoe werkt dat nu?
DOE MEER MET PBQ
kernmodel
DOE MEER MET PBQ
elektronen model

"Wetenschap beoefenen is net zo iets als een
n-dimensionale kruiswoordpuzzel oplossen.
Het lukt je niet hem geheel op te lossen,
of als je denkt dat het je wel gelukt is
blijken er nog meer dimensies te bestaan."

JHL.